Republic of Iraq
Ministry of Higher Education And
Scientific Research
University of Babylon-College of
Engineering
Materials Engineering

HIGH TEMPERATURE PROPERTIES OF CERTAIN AEROSPACE LIGHT ALLOYS AND COMPOSIT MATERIALS

A Thesis

Submitted to the Department of Engineering Materials-College of Engineering-University of Babylon in a Partial Fulfillment of the Requirements for the Degree of Doctor of Philosophy in Materials Engineering

By

Nabil L. K. Al-Saffar

Supervision

Prof. Dr. Abdul-Wahid Kadhim Rajih

May 2008

جمهورية العراق
وزارة التعليم العالي والبحث العلمي
جامعة بابل/ كلية الهندسة
قسم هندسة المواد

خواص بعض سبائك الفضاء الخفيفة والمواد المركبة بدرجات الحرارة العالية

أطروحة مقدمة إلى قسم هندسة المواد/ كلية الهندسة ـ جامعة بابل وهي جزء من متطلبات نيل درجة دكتوراه فلسفة في هندسة المواد

من قبل

نبيل لطيف الصفار

بإشراف

أ.د. عبد الواحد كاظم راجح البكري

1429هـ

بسم الله الرحمن الرحيم

يَـا مَعْشَـرَ الْجِـنِّ وَالإِنـسِ إِنْ اسْتَطَعْتُمْ أَنْ تَنفُذُوا مِـنْ أَقْطَـارِ السَّـمَاوَاتِ وَالأَرْضِ فَانفُـــذُوا لاَ تَنفُـــذُونَ إِلاَّ بِسُـلْطَانٍ (33) فَبِـأَيِّ آلاَءِ رَبِّكُمَا تُكَذِّبَانِ (34)

صدق الله العلي العظيم
سورة الرحمن

الخلاصة

بات معروفاً من ديناميك الحرارة ان التشغيل بدرجات حرارة عالية يرافقه زيادة في الكفاءة. هذا السبب تحديداً يكمن خلف تطبيقات في درجات حرارة عالية. للأسف ان التشغيل بدرجات حرارة العالية يزيد من مهاجمة اوساط التشغيل المعادية ويسبب نقصان كبير في الخواص الميكانيكية .

يهدف البحث الحالي لدراسة تأثير عناصر السبك ومتغيرات اخرى على سلوك سبائك ذات اساس **(Al-Cu-Mg)** بدرجات الحرارة العالية.

كما تم استخدام التحليل النظري للتنبؤ بانفعال الزحف. ان دراسة الانفعال المعتمد على الزمن يمثل عملية طويلة ومكلفة وتستهلك اختباراتها وقتاً طويلاً لذا تم تصميم وبناء خمس اجهزة لاختبار الزحف تضمنت تحضير **(100)** نموذج.

كما تم استخدام تقنية السباكة التي هي الاخرى تضمنت تصميم وبناء فرن غازي ذوسعة أكثرمن **(10)** كغم تقريبا ويعمل حتى **(1000)** درجة مئوية. وجرت السباكة بقالب فولاذي خاص يوفر امكانية التجمد الاتجاهي.

كما تم تصميم وبناء فرن كهربائي يعمل حتى **(1000)** درجة مئوية وذلك باستمرارية في التعاملات الحرارية للنماذج المحضرة .

تم استخدام ماكنة **(CNC)** لتشغيل النماذج بالابعاد القياسية كما جرى استعمال المجهر الالكتروني الماسح في الاختبارات الميتالورجية . وكدلك تم ادخال تحويرات محددة لاجراء اختبار الشد بدرجات حرارة مختلفة لقياس معامل المرونة **(E_m)** ومقاومة الشد القصوى **(UTs).**

اظهرت النتائج ان معامل المرونة **(E_m)** للنماذج يعتمد على درجة الحرارة التي يجري عندها الاختبار والتي يتحكم بها البنية البلورية.

اما مقاومة الشد القصوى فقد اظهرت سلوكاً مشابهاً ، كما اظهرت السبائك التي تحتوي على **(SiC)** زيادة في قيم معامل المرونة ومقاومة الشد القصوى بلغت 32% و 30% على التتابع مقارنة بالسبيكة **(A).**

ان تأثير كربيد السيلكون **(SiC)** على منحنيات **الزمن- ألانفعال** كان واضحاً اذ ان منحنيات **الزحف** للسبائك الخالية من **(SiC)** بلغت نقطة الكسر بينما السبائك المناظرة الحاوية على هذا المركب **(A_c)** لازالت منحنيات الزحف لها في بداية الاختبار كذلك فان اضافة الليثيوم**(Li)** وحده او الليثيوم + الزركونيوم **(Zr+Li)**

للسبيكة **(A)** سببت تحسناً في منحنيات الزحف وذلك للتأثير على عملية الترسيب وحجم الحبيبات ومعدل التشكيل وخاصة في المراحل الاولى.

البحث الحالي اظهر وجود نماذج فشلت بالكسر السريع سواء بدرجات الاختبار العالية او الافراط في التحميل ، اما قيم الانفعال المحسوبة من التحليل النظري فكانت اقل مما اظهرته الاختبارات العملية.

Acknowledgement

Praise, thank, and gratitude to the benefactor and Single handed ALLAH, Lord of all creation who enabled and helped me to achieve this work.

I wish to express my sincere gratitude, deep thanks, and great appreciation to my Sir, Imam, and great teacher Al-Hujja Al-Montadher (peace is upon him) for all his support, throughout my study.

I am grateful to the department of material, college of engineering assistance, and benefaction throughout the various stages of the present work.

I would like to thank my supervisor Prof. Dr. Abdul-Wahid Kadhim Rajih for his helpful advice and suggestions University of Babylon especially to the head of the department of Engineering materials and mechanical Engineering department.

I would like to thank the staff of the workshop, materials lab. In Babylon University.

I record my deep thanks and gratitude to the single hearted and single-minded my sisters and my family for their encouragement, kindness, and support during the entire period of this work.

Finally, I would like to thank everyone help me in anyway for obtaining the present work.

Appendix

```
/BATCH
/COM,ANSYS RELEASE  5.4    UP19970828       12:26:43    12/03/2007
/input,menust,tmp     ,,,,,,,,,,,,,,,,1
/GRA,POWER
/GST,ON
RESUME
/COM,ANSYS RELEASE  5.4    UP19970828       12:26:46    12/03/2007
EPLOT
MPLIST,ALL,,,EVLT
/FILNAM,f400
/PREP7
MPDELE,ALL,1,1,1,
!*
UIMP,1,EX, , ,75e9,
UIMP,1,DENS, , , ,
UIMP,1,ALPX, , , ,
UIMP,1,REFT, , , ,
UIMP,1,NUXY, , , ,
UIMP,1,PRXY, , , ,
UIMP,1,GXY, , , ,
UIMP,1,MU, , , ,
UIMP,1,DAMP, , , ,
UIMP,1,KXX, , , ,
UIMP,1,C, , , ,
UIMP,1,ENTH, , , ,
UIMP,1,HF, , , ,
UIMP,1,EMIS, , , ,
UIMP,1,QRATE, , , ,
UIMP,1,MURX, , , ,
UIMP,1,MGXX, , , ,
UIMP,1,RSVX, , , ,
UIMP,1,PERX, , , ,
UIMP,1,VISC, , , ,
UIMP,1,SONC, , , ,
!*
SAVE
MPLIST,ALL,,,EVLT
FINISH
/SOLU
LSCLEAR,ALL
FLST,2,6,1,ORDE,4
FITEM,2,1
FITEM,2,52
FITEM,2,57
FITEM,2,-60
D,P51X, ,0, , , ,ALL
```

```
LSCLEAR,ALL
EPLOT
!*
/PSF,DEFA, ,1
/PBF,DEFA, ,1
/PSYMB,CS,0
/PSYMB,NDIR,0
/PSYMB,ESYS,0
/PSYMB,LDIR,0
/PSYMB,ECON,0
/PSYMB,DOT,1
/PSYMB,PCONV,
/PSYMB,LAYR,0
!*
/PBC,ALL, ,0
/REP
!*
FLST,2,6,1,ORDE,4
FITEM,2,1
FITEM,2,52
FITEM,2,57
FITEM,2,-60
D,P51X, ,0, , , ,ALL
SAVE
FLST,2,6,1,ORDE,3
FITEM,2,22
FITEM,2,27
FITEM,2,-31
F,P51X,FY,-250,
SAVE
TUNIF,175,
SAVE
FLST,2,16,1,ORDE,10
FITEM,2,7
FITEM,2,-8
FITEM,2,12
FITEM,2,-16
FITEM,2,18
FITEM,2,37
FITEM,2,-38
FITEM,2,42
FITEM,2,-46
FITEM,2,51
BF,P51X,TEMP,175,
SAVE
!*
```

```
OUTRES,ALL,ALL,
!*
TIME,200
AUTOTS,0
NSUBST,400,0,0,0
KBC,1
!*
/STAT,SOLU
SOLVE
/POST1
FINISH
/POST1
SET,FIRST
AVPRIN,0,0,
!*
PLNSOL,S,EQV,2,1
AVPRIN,0,0,
!*
PLNSOL,EPTO,EQV,2,1
SET,LAST
AVPRIN,0,0,
!*
PLNSOL,EPTO,EQV,2,1
SET,NEXT
SET,FIRST
SET,NEXT
AVPRIN,0,0,
!*
PLNSOL,EPTO,EQV,2,1
SET,1,4,1,
AVPRIN,0,0,
!*
PLNSOL,EPTO,EQV,2,1
SET,1,8,1,
AVPRIN,0,0,
!*
PLNSOL,EPTO,EQV,2,1
SET,1,16,1,
AVPRIN,0,0,
!*
PLNSOL,EPTO,EQV,2,1
SET,1,8,1,
AVPRIN,0,0,
!*
PLNSOL,EPTO,EQV,2,1
SET,1,10,1,
```

```
AVPRIN,0,0,
!*
PLNSOL,EPTO,EQV,2,1
SET,1,12,1,
AVPRIN,0,0,
!*
PLNSOL,EPTO,EQV,2,1
SET,1,14,1,
AVPRIN,0,0,
!*
PLNSOL,EPTO,EQV,2,1
SET,1,16,1,
AVPRIN,0,0,
!*
PLNSOL,EPTO,EQV,2,1
SET,1,20,1,
AVPRIN,0,0,
!*
PLNSOL,EPTO,EQV,2,1
SET,1,30,1,
AVPRIN,0,0,
!*
PLNSOL,EPTO,EQV,2,1
SET,1,40,1,
AVPRIN,0,0,
!*
PLNSOL,EPTO,EQV,2,1
SET,1,50,1,
AVPRIN,0,0,
!*
PLNSOL,EPTO,EQV,2,1
SET,1,60,1,
AVPRIN,0,0,
!*
PLNSOL,EPTO,EQV,2,1
SET,1,80,1,
AVPRIN,0,0,
!*
PLNSOL,EPTO,EQV,2,1
SET,1,100,1,
AVPRIN,0,0,
!*
PLNSOL,EPTO,EQV,2,1
SET,1,120,1,
AVPRIN,0,0,
!*
```

```
PLNSOL,EPTO,EQV,2,1
SET,1,160,1,
AVPRIN,0,0,
!*
PLNSOL,EPTO,EQV,2,1
SET,1,200,1,
AVPRIN,0,0,
!*
PLNSOL,EPTO,EQV,2,1
SET,1,240,1,
AVPRIN,0,0,
!*
PLNSOL,EPTO,EQV,2,1
SET,1,280,1,
AVPRIN,0,0,
!*
PLNSOL,EPTO,EQV,2,1
SET,1,320,1,
AVPRIN,0,0,
!*
PLNSOL,EPTO,EQV,2,1
SET,1,360,1,
AVPRIN,0,0,
!*
PLNSOL,EPTO,EQV,2,1
SAVE
EPLOT
!*
!*
FINISH
/FILNAM,f500
!*
/PREP7
MPDELE,ALL,1,1,1,
!*
UIMP,1,EX, , ,80e9,
UIMP,1,DENS, , , ,
UIMP,1,ALPX, , , ,
UIMP,1,REFT, , , ,
UIMP,1,NUXY, , , ,
UIMP,1,PRXY, , , ,
UIMP,1,GXY, , , ,
UIMP,1,MU, , , ,
UIMP,1,DAMP, , , ,
UIMP,1,KXX, , , ,
UIMP,1,C, , , ,
```

```
UIMP,1,ENTH, , , ,
UIMP,1,HF, , , ,
UIMP,1,EMIS, , , ,
UIMP,1,QRATE, , , ,
UIMP,1,MURX, , , ,
UIMP,1,MGXX, , , ,
UIMP,1,RSVX, , , ,
UIMP,1,PERX, , , ,
UIMP,1,VISC, , , ,
UIMP,1,SONC, , , ,
!*
SAVE
/SOLU
FINISH
/SOLU
LSCLEAR,ALL
FLST,2,6,1,ORDE,4
FITEM,2,1
FITEM,2,52
FITEM,2,57
FITEM,2,-60
D,P51X, ,0, , , ,ALL
SAVE
FLST,2,6,1,ORDE,3
FITEM,2,22
FITEM,2,27
FITEM,2,-31
F,P51X,FY,-250,
SAVE
TUNIF,175,
FLST,2,16,1,ORDE,10
FITEM,2,7
FITEM,2,-8
FITEM,2,12
FITEM,2,-16
FITEM,2,18
FITEM,2,37
FITEM,2,-38
FITEM,2,42
FITEM,2,-46
FITEM,2,51
BF,P51X,TEMP,175,
SAVE
MPLIST,ALL,,,EVLT
SAVE
!*
```

```
OUTRES,ALL,ALL,
!*
TIME,200
AUTOTS,0
NSUBST,400,0,0,0
KBC,1
!*
SAVE
/STAT,SOLU
SOLVE
/POST1
FINISH
/POST1
SET,FIRST
AVPRIN,0,0,
!*
PLNSOL,EPTO,EQV,2,1
SET,LAST
AVPRIN,0,0,
!*
PLNSOL,EPTO,EQV,2,1
SET,1,2,1,
AVPRIN,0,0,
!*
PLNSOL,EPTO,EQV,2,1
SET,1,4,1,
AVPRIN,0,0,
!*
PLNSOL,EPTO,EQV,2,1
SET,1,8,1,
AVPRIN,0,0,
!*
PLNSOL,EPTO,EQV,2,1
SET,1,10,1,
AVPRIN,0,0,
!*
PLNSOL,EPTO,EQV,2,1
SET,1,12,1,
AVPRIN,0,0,
!*
PLNSOL,EPTO,EQV,2,1
SET,1,14,1,
AVPRIN,0,0,
!*
PLNSOL,EPTO,EQV,2,1
SET,1,16,1,
```

```
AVPRIN,0,0,
!*
PLNSOL,EPTO,EQV,2,1
SET,1,20,1,
AVPRIN,0,0,
!*
PLNSOL,EPTO,EQV,2,1
SET,1,30,1,
AVPRIN,0,0,
!*
PLNSOL,EPTO,EQV,2,1
SET,1,40,1,
AVPRIN,0,0,
!*
PLNSOL,EPTO,EQV,2,1
SET,1,50,1,
AVPRIN,0,0,
!*
PLNSOL,EPTO,EQV,2,1
SET,1,60,1,
AVPRIN,0,0,
!*
PLNSOL,EPTO,EQV,2,1
SET,1,80,1,
AVPRIN,0,0,
!*
PLNSOL,EPTO,EQV,2,1
SET,1,100,1,
AVPRIN,0,0,
!*
PLNSOL,EPTO,EQV,2,1
SET,1,120,1,
AVPRIN,0,0,
!*
PLNSOL,EPTO,EQV,2,1
SET,1,160,1,
AVPRIN,0,0,
!*
PLNSOL,EPTO,EQV,2,1
SET,1,200,1,
AVPRIN,0,0,
!*
PLNSOL,EPTO,EQV,2,1
SET,1,240,1,
AVPRIN,0,0,
!*
```

```
PLNSOL,EPTO,EQV,2,1
SET,1,280,1,
AVPRIN,0,0,
!*
PLNSOL,EPTO,EQV,2,1
SET,1,320,1,
AVPRIN,0,0,
!*
PLNSOL,EPTO,EQV,2,1
SET,1,360,1,
AVPRIN,0,0,
!*
PLNSOL,EPTO,EQV,2,1
SAVE
FINISH
! /EXIT,ALL
```

Contents

Chapter Three: Experimental Work

Chapter four: Results and Discussion

Dedication

*To **********

*Spirit of My father****

*Spirit of My mother**

Specially My sisters

*My family *****

With love and respect

Chapter One
Theoretical Development of Light Metals for Aerospace Industries

1.1. Introduction:

The development of new materials is becoming essential to meet the every rising demand in modern age of scientific and industrial achievement. In aerospace industries, the thrust for achieving higher and higher speed, larger payload capacity, improved fuel economy and better landing capacities of aircrafts, has led to remarkable research and development output in material's field. Such demand of materials has led to a revival of interest in development and fabrication of Al-light alloys since the seventies [Ekvall et al., 1982].

Recently, considerable progress has been made in the development of some light materials, but many difficulties have been encountered in their subsequent processing. Those difficulties usually arise due to the lack of knowledge of the behavior and properties of the material under the conditions encountered in the processing operation and heat treatment [Gragali & Aksakal, 1998].

Lights metals are the materials of choice for technical applications where low specific weight combined with high specific stiffness is demand. The term "light metals" has traditionally been given to both aluminum (2.7 g/cm^3) and magnesium (1.7 g/cm^3) because they are frequently used to reduce the weight of components and structure. On this basis, titanium (4.5 g/cm^3) also qualities and beryllium (1.8 g/cm^3) should be included although it is little used, which compare with density of copper (8.9 g/cm^3) iron (7.9 g/cm^3) and osmium (22.6 g/cm^3) the heaviest

of all metals, the alkali metals lithium, potassium, sodium, rubidium and cesesium, and the alkaline earth metals calcium and strontium are too reactive, whereas yttrium and scandium are comparatively rare. [Van Vlack, 1970].

The property of lightness has led to the association of the light metals with transportation and, more especially, with aerospace applications which has provided great stimulus to the development of alloys during the last years. Strength weight ratios have thus been a dominant consideration these are particularly important in engineering design when parameters such as stiffness or resistant buckling are involved. Concern with aspects of weight saving should not obscure the fact that light metals possess other properties of considerable technological importance, e.g. the high corrosion resistance and high electrical and thermal conductivities of aluminum, the machinability of magnesium and extreme corrosion resistance at titanium [Polmear & Chester, 1989]. Reinforcing aluminum with powders, short or continuous fibers provides components with high strengths, improved wear & creep resistance and low densities. The relatively new technology of metal matrix composites and the expense of manufacturing metal matrix composites (MMCs) limit their use to high performance aerospace and automotive applications [Polmear, 2006].

1.2. Al-alloys:

Aluminum and its alloys are used in many aspects of modern life, from soda cans and household foil to the automobiles and aircraft in which we travel. Aluminum alloys have numerous technical advantages that have made them one of the most useful alloy systems. Although many aluminum alloys have typically low to intermediate strength, alloys

containing precipitation-hardening element such as copper (2XXX) or zinc and magnesium (7 XXX) can have mechanical properties equivalent to some steels such as in the manufacturing of auto bodies, robotics, machine tools because of the significant weight saving, corrosion resistance and good weld ability [Romhanji et al., 2001; Yic et al., 1998]. The combination of high strength and low density make these alloys particularly attractive when structural weight is critical property. In addition to high strength, aluminum alloys have a strong resistance to corrosion, which is a result of a tenacious oxide surface that forms quickly in air. This hard microscopic oxide coating protects aluminum from many chemical and weathering conditions. Aluminum and its alloys also characterized by good workability that enables them to be economically rolled, extruded, or forged into useful shapes. Cold working, annealing, and in some alloys, precipitation-hardening and heat treatments are used to control strength [Dmstry et al., 2001; Murayame, 1999].

Aluminum alloys are separated into two major classes-cast and wrought this designation was standardized by the aluminum association (AA) in Washington (1954) [Avner, 1983]. Cast-aluminum alloys are produced in hundred of compositions by all commercial casting processes. Because cast alloys are poured into their final shape, they may be strengthened by heat-treatment but are not work-hardened. Wrought alloys can be shaped by deformation. Aluminum alloys may be strength by thermal treatments (heat-treatable alloys) and by work- hardening (work-harden able). Wrought aluminum alloys are further separated into heat-treatable (2XXX, 6XXX and, 7XXX) and non-heat-treatable (1XXX, 3XXX, and 5XXX) series alloys, and thus are work hardened by cold-working processes, usually by cold rolling [Aluminum Federation, 1998].

Heat-treatable aluminum alloys contain one or more soluble constituents such as copper, lithium, magnesium, silicon and that individually, or with other elements, can form phase that strengthen the alloy. Also aluminum alloys may contain impurities such as iron and silicon. Because of limited solubility, the morphology of phases formed by the combination of these impurities with major solute additions can not be affected by heat treatment. In aluminum alloys, the percentage of alloying elements and impurities must be controlled carefully. If they are not, properties such as strength, toughness formability, and corrosion resistance, for example, may be affected adversely. However, while certain mechanical properties are improved, it may be often be at the expense of other properties. For example, tensile and yield strength can be increased but this often results in lower elongation and fracture toughness. Thus, heat treatments are designed to optimize properties [Avner, 1983].

Heat-treating improve the strength of aluminum alloys through a process known as precipitation hardening which occurs during the heating and cooling of an aluminum alloy in which precipitates are formed in the aluminum matrix. These second-phase particles affect dislocation motion which in turn affects strength. The composition of particular alloy determines the heat treatment temperature. When an aluminum alloy is heated above the solves temperature of the secondary phases in the matrix, the alloying elements dissolve into the aluminum matrix to form solid solution. Following a quench (or rapid cooling), the alloying elements precipitate out of solution. This step, known as aging, occurs at room temperature (natural aging); however, an alloy can be artificially aged at an elevated temperature in order to increase the kinetics of the process [William, 1981].

Annealing in precipitation-hardening alloy is a process that imparts the most ductile condition. During annealing, the alloy is heated to above its solution temperature and then slowly cooled to room temperature. During the cooling process, the alloying elements precipitate out of solution and form coarsely distributed phases, which are not effective barriers to slip. The result is a low-strength alloy [Avner, 1983].

The important micro structural features, as for as toughness is concerned, are second phase particles and grain structure. The second-phase particles of concern are:

1. Coarse, insoluble particles formed during casting, or coarse particles of normally soluble phases formed during casting or subsequent processing.
2. Smaller intermediate particles formed during homogenization.
3. Aging precipitates.

The as-cast microstructure is highly segregated as a result of coring during solidification in which soluble element concentration and secondary phases are distributed an evenly throughout the microstructure [Polmear, 2006].

The first stage in alloy processing is, therefore, homogenization, the high temperature step is necessary to eliminate, (or reduce) the coating by dissolving soluble phases and precipitating equilibrium phases. Although the precipitate dissolution is not the only metallurgical process that is occurring during homogenization temperature can be determined from a thermodynamic analysis of the phases that are present. The homogenization time at a given temperature is dependent upon the types of precipitates present, their shape, size, distribution, and chemical composition [Rometsch et al., 2002].

Subsequent processing steps for wrought alloys include cold working, during which an alloy is simultaneously deformed and

strengthened; hot working, during which an alloy is deformed at high temperatures without strengthening; and annealing during which the effects of strengthening caused by cold working are modified. By controlling these processes, the material is processed into a usable shape while material properties are improved and controlled.

Microstructure development depends heavily on all of the processing steps the alloy experiences. Ultimately, the properties of the alloy depend strongly on the microstructure so it is particularly useful to gain a quantitative understanding of the micro structural changes that occur during thermal and mechanical processing. During thermal treatments, the microstructure becomes more homogeneous and secondary phases are dissolved, hence, any modeling efforts directed towards understanding these processes is important [Rometsch et al., 2002]. There are different aluminum alloys which are:

1.3. Al-Cu Based Alloys:

The most widely studied age-hardening alloy system is Al-Cu, and several commercial alloys based on this system remain in use in the 2xxx alloy series. Although the alloy is composed of only two elements, the micro structural evolution is complex, and the precipitation sequence varies depending on the degree of super saturation and the aging temperature, Fig. (1.1) shows the Al-rich comer of the equilibrium Al-Cu phase diagram, and includes the metastable solves boundaries for GP zones, θ^{n} and $\theta^{'}$. Over many studies [Abe et al., 1982; Karlik & Jouffrey, 1997], it has been proposed that the decomposition sequence in this system contains one or more of the following processes:

Supersaturated Solid Solution (SSSS) $\rightarrow$ GP zones $\rightarrow \theta^{''} \rightarrow \theta^{'} \rightarrow \theta$

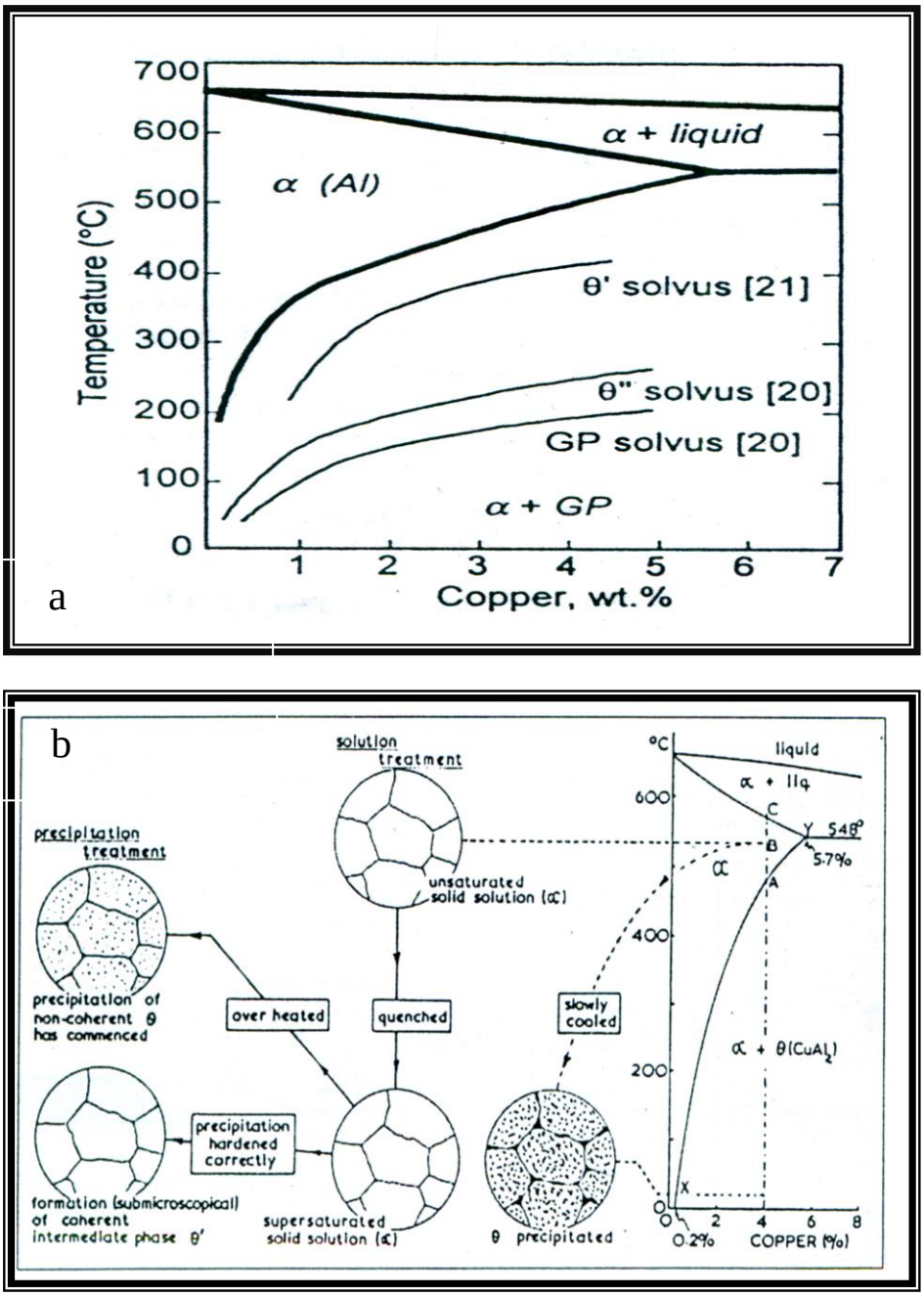

Fig. (1.1): a. Al-rich corner of the Al-Cu phase diagram showing the metastable solves boundaries for GP zones, θn and θ'., together with the equilibrium solves line for the θ phase. [Beton & Rollason, 1957; Murray, 1985].

b. The aluminum-rich end of the Al-Cu equilibrium diagram. Observable micro structural changes due to slow cooling, solution and precipitation treatment are indicated [John, 1983].

The complete precipitation sequence can only occur when the alloy is aged at temperatures below the GP zone solves (Fig.1.1). Various steps

in this process may be suppressed by aging at temperatures close to or above the intermediate solves temperatures. Fig. (1.2) shows a hardness-time plot for Al-1.7Cu aged at 130 and 190°C, which represents temperatures below and above the GP zone solves temperature, respectively. The first stage of hardening at 130°C is attributed to the formation of GP zones. After reaching a critical diameter of between 5 and 10nm, an incubation period commences, during which the zone size and the hardness remain constant [Hardy, 1953; Silcock et al., 1985].

Further aging results in a second rise in hardness, attributed to θ^n precipitation. The formation of $\theta^{"}$ is also followed by a shorter incubation period and the subsequent formation of the metastable θ phase. Prolonged aging results in the formation of the equilibrium θ phase. Each precipitation stage does not necessarily correspond to the stages observed in the hardness curve, and more than two phases can coexist at a given stage of the aging process. The mechanism of the transformation sequence from one phase to another usually involves heterogeneous nucleation at the sites of earlier products, resulting in fine and uniform precipitate dispersions. However, under a suitable degree of super saturation, the products in the above evolutionary sequence nucleate directly into the matrix [Silcock et al., 1985].

This is precisely what occurs when the alloy is aged at 190°C Fig.(1. 2). Single-stage hardening occurs here because the temperature is above the solves for the GP zones and θ^n nucleates directly. However, the smaller driving force for precipitation together with the lower volume fraction of θ^n at 190°C Fig. (1.1), results in a coarser dispersion and lower peak hardness. The kinetics of the aging process are faster at this temperature due to the higher solute diffusivity, and this produces a

shorter time to peak hardness than that at 130°C. the nucleation of θ' at θ" sites is similarly accelerated at 190°C.

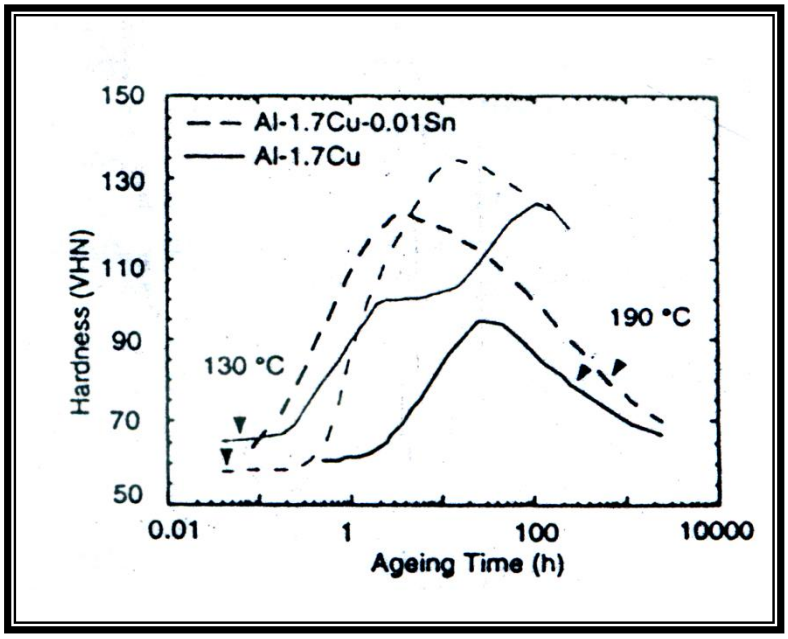

Fig. (1.2): Hardness–time plot for Al-1.7Cu aged at 130 and 190°C, showing the effect of a 0.01 Sn addition. [Hardy, 1951].

To understand the mechanism of the increase in hardness that accompanies aging it is useful to examine the individual stages of the micro structural evolution described above. By the early 1960s, X-ray diffraction and resistivity measurements suggested that solute atoms may spontaneously cluster in certain Al alloys after quenching to temperatures below the metastable GP zone solves line [Matsubara & Cohen, 1983].

The formation of these clusters precedes the formation of GP zones. In the Al-Cu system, Rioja and Laughlin [Rioja & Laughlin, 1977] interpreted the observation of diffuse satellites in selected area electron diffraction (SAED) pattems as evidence for spinodal decomposition. Moreover, Matsubara and Cohen [Matsubara & Cohen, 1983] have reported absolute X-ray intensity measurements that indicate that the Cu atoms are in a nonrandom distribution even at the solution treatment temperature and in the as-quenched (AQ) state. Despite the high election

scattering amplitude of Cu, Nicholson et al. have pointed out that these clusters are difficult to observe by TEM, due to the need for very thin foils so as to improve the average scattering from the clusters [Nicholson et al, 1985]. These clusters have been observed in FIM studies of AQ Al-1.7Cu alloys, and the concentration fluctuations that they cause are readily detected in corresponding 1DAP analyses [Hono et al., 1986].

Following the X-ray diffraction (XRD) work by Guinier [Guinier,1938] and Preston [Preston, 1938], there have been numerous studies of GP zones, involving XRD [Silcock et al., 1985], small-angle X-ray scattering [Osamura et al., 1983], resistivity [Desorb et al.,1958], CTEM [Nicholson et al.,1958]. HRTEM [Karlik & Jouffrey, 1997], and APFIM [Hono et al., 1986]. There is now general agreement that GP zones are single – atom layers of Cu on $[001]_\alpha$ planes. However, multilayer GP zones have also been observed [Hono et al., 1986].

Fig. (1.3 a) provides a series of Ne FIM images from a field-evaporation sequence of four $(022)_\alpha$ planes. The sections of the zone observed in the $[100]_\alpha$ direction are always observed as a two-layer atomic row, providing direct evidence for a two-layer thickness of Cu atoms. Models for the single-layer and multilayer GP zones are provided in Fig. (1.3b-c) the single and multilayer models for GP zones are distinct from that of the θ^n phase, which is considered as two layers of Cu separated by three $[001]_\alpha$ layers of Al Fig.(1.3 d) [Silcock et al.,1985; Hono et al., 1986]. While the disc or planer shaped GP zones exhibit a rod-like shape effect normal to their $[100]_\alpha$ habit planes, giving rise to continuous streaking in $<010>_\alpha$ directions in SAED patterns, the θ^n phase is distinguished in $<100>_\alpha$ SAED patterns by the occurrence of intensity maxima at the $[010]_\alpha$ directions [Philips, 1973].

Atom probe studies on GP zones and the θ^n phase are consistent with the structural features described above. The results of 1DAP suggest that the Cu composition of GP zones is approximately 33 atomic percent

9at. %). Which is the same as that of the equilibrium phase [Hono et al., 1986]. In the case of the θ" phase, two peaks in the Cu concentration, separated by three Al layers, were detected. The concentration change near the GP zones appeared to be somewhat more diffuse, and it is uncertain whether this is due to irregular evaporation behavior of Cu near the GP zones. More recent work using a 3DAP [Bigot, 1998] succeeded in analyzing both GP zones and θ" with a near-atomic resolution. Similar concentration-depth profiles were obtained. However, in that work, the diffuse character of the atom-probe concentration-depth profiles was attributed to evaporation artifacts, and it was suggested that the actual concentration of GP zones is close to 100 atomic percent (at.%) Cu.

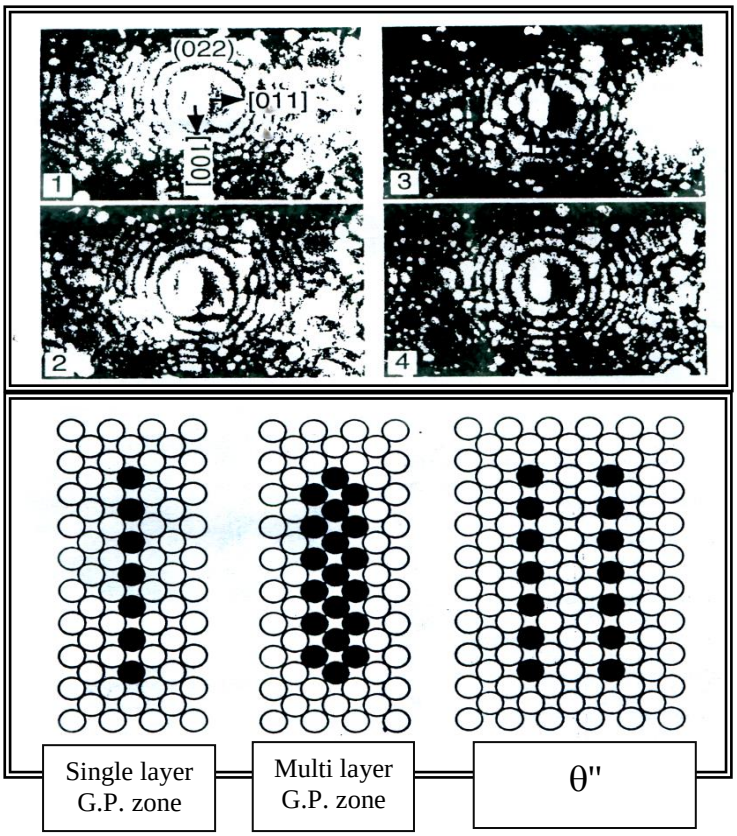

Fig. (1.3): (a) Field ion micrograph (Ne) sequence produced by field evaporation of four (1-4) successive $(022)_{\alpha}$. Planes of an Al-1.7Cu alloy aged at 100°C for 300 min. (b)-(d) These represent schematic diagrams of the structure of single-layer GP zones, multilayer GP zones, and θ'' precipitation, respectively. [Hono et al, 1986].

The crystal structure of θ' phase is well established [Silcock et al., 1985] as a body-centered tetragonal (14/mcm, a=0.404nm and c=0.580 nm), and occurs as octagonal-shaped platelets oriented such that $[011]_{\alpha}//[001]'_{\alpha}$ and $[010]_{\alpha}$ //<010>'$_{\alpha}$ the morphology of these precipitates is accounted for using intersection point group symmetry analysis [Philips, 1973].

Because the above orientation relationship requires that all of the symmetry elements of the θ^{n} phase are common to those of the m3m α-inatrix, the intersection point group is the same as that of θ' phase: 4/mcm. Because the point group of the matrix phase contains 48 symmetry elements and the intersection point group contains 16, the index of the intersection point group in the α-inatrix is 48/16=3. Symmetry thus requires three crystallographic alloys compatible with this point group include pinacoide normal to the fourfold axis, and tetragonal prisms parallel to twofold axes possessing the required mirror symmetry, which is consistent with observation [Phillips, 1960].

The tetragonal θphase (14/mcm, a=0.6066nm, c=0.4874 nm) [Bradley & Jones, 1933] occurs in a variety of orientations and morphologies. These have been systematically examined by Vaughan and Silcok, who showed that there are 159 known orientations for a θ particle relative to the α-Al matrix [Vaughan & Silcock, 1967].

1.4. Al-Cu-Mg Based Alloys:

The range of microstructures, phases formed and the response to micro alloying in Al-Cu-Mg alloys is highly dependent on alloy composition Fig.(1.4). The following discussion summarizes the results of recent studies on the micro structural mechanisms and evolution during aging these alloys [Brook, 1963].

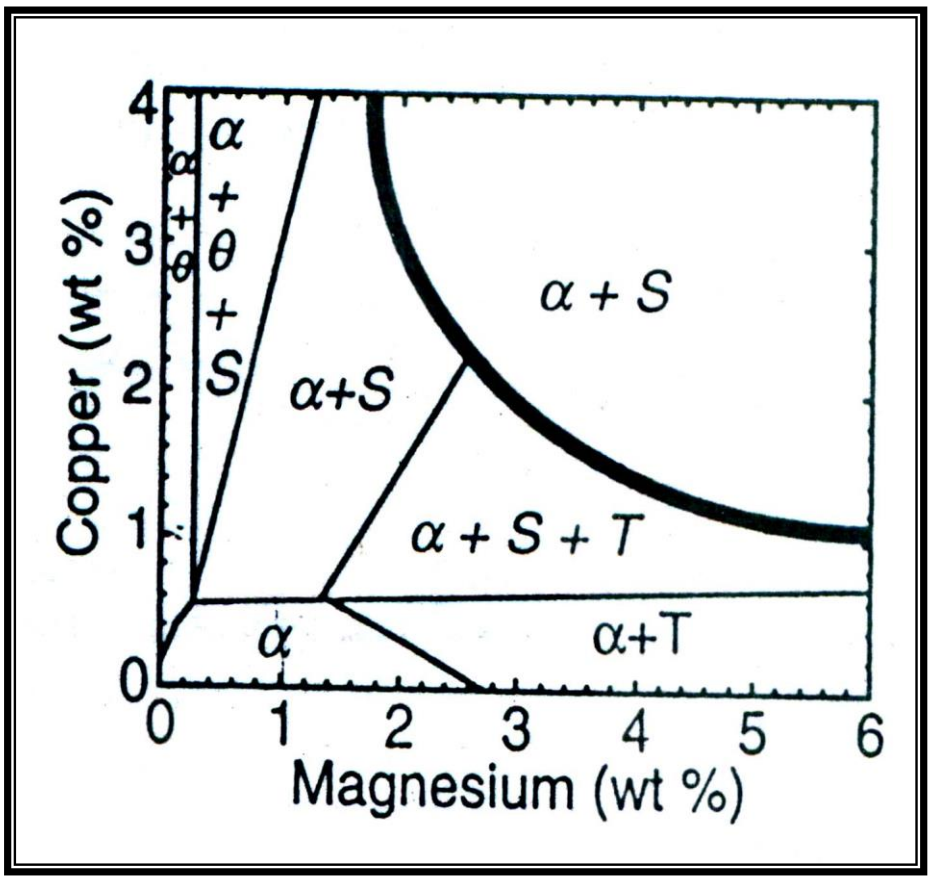

Fig.(1.4): Al-Cu-Mg phase diagram showing phase boundaries at 190°C. The thick solid line defines the α / α+S phase boundary at 500°C. after Brook [Brook, 1963].

1.4.1. Alloys In the α + θ Phase Field:

Fig. (1.5) is a hardness-time plot for the Al-1.7Cu-0.3Mg ternary alloy at 200°C, and includes curves for Ag and Ag and Li containing alloys [Polmear & Chester, 1989]. The data show that micro alloying on both Al-Cu-Mg-Ag and Al-Cu-Li-Mg-Ag- based alloys is highly effective in enhancing the age hardening response. Indeed high- strength Li-containing alloys possessing ultimate tensile strength exceeding 600 MPa have recently been developed [Polmear & Couper, 1988; Pickens et al., 1989].

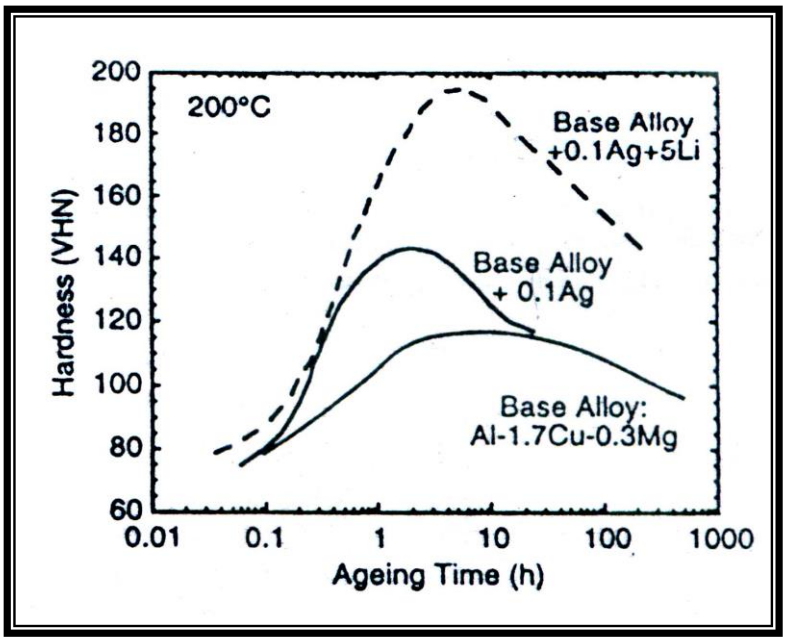

Fig.(1.5): Hardness-time plot for Al-1.7Cu-0.3Mg at 200°C showing the effects of additions of Ag and Li After [Polmear & Chester, 1989].

1.4.2. Micro structural analysis :

Micro structural analysis using APFIM in conjunction with TEM is particularly useful in examining the very early stages of the precipitation process and for understanding the effects of microalloying. Fig. (1.6 a) is a 1DAP-integrated concentration-depth profile of the ternary base alloy after aging 30s at 180°C [Ringer et al., 1996]. The data indicate a preferred interaction between Cu and Mg, in contrast to the AQ alloy samples, which indicated that the Cu and Mg were, distributed independently [Silcock. 1960-61].

These results were supported by contingency table analysis, which indicated that there was no preferred interaction between Mg and Cu at the 99.6% confidence level. As suggested by the data in Fig.(1.6 b), the tendency of co-clustering of Mg and Cu atoms was observed after aging for 30 s at 180°C. independent Cu-rich clusters were also detected at this early stage of aging. The microstructure evolved after 2.5 hr. at 180°C consists of a fine and uniform dispersion of θ' precipitation on the $[001]_{\alpha}$

planes together with GPB zones, which occur as rod-like features elongated along the cube directions of the matrix Fig.(1.7) [Silcock.1960].

The term GPB zones was introduced by Silcock in recognition of the XRD work on these rod-shaped zones by Bagaryatsky, who considered the zones to be associated with short-range ordering along the $[100]_{\alpha}$ places[Bagrayatsky, 1952].

Silcock proposed that the zones formed along the $<100>_{\alpha}$ directions s small cylinders estimated to be 1 to 2nm in diameter, and with lengths ranging from 4 to more than 8nm, depending on quenching rate, [Silcock. 1960-61]. At 180°C, the microstructural evolution of the Al-1.7Cu-0.3Mg alloy is similar to that of binary Al-Cu. In addition, the Mg-Cu interaction results in the formation of GPB zones and prolonged aging at this temperature induces precipitation of the equilibrium S phase (Cmcm; a = 0.400nm, b=0.923nm, c=0,714nm)[45].

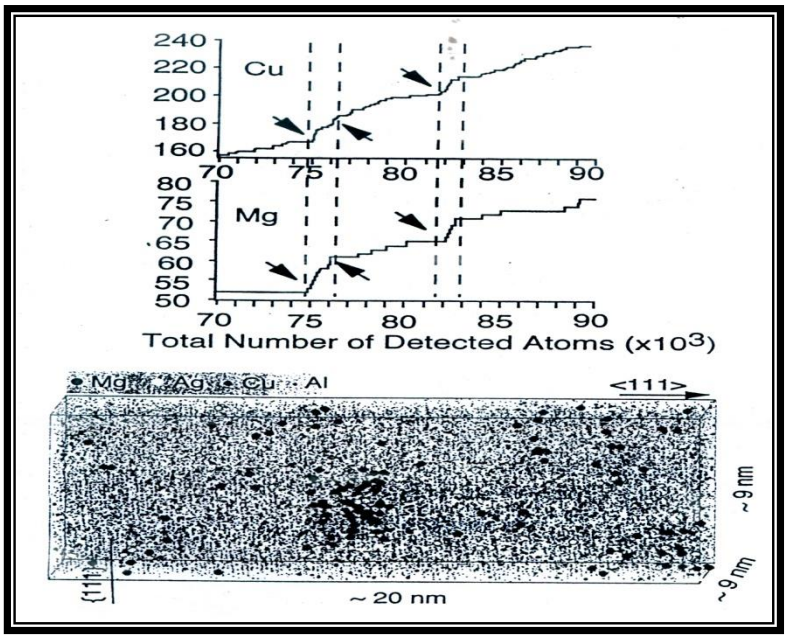

Fig.(1.6): (a) Integrated concentration-depth profiles (IDAP) from the ternary Al-1.7Cu-0.3Mg alloy after aging 30s at 180°C. After Ringer et al.,[54].

(b) Atomic reconstruction (3DAP) from the quaternary Al-1.7Cu-0.3Mg-0.2Ag alloy after aging 30s at 180°C [Reich et al., 1998].

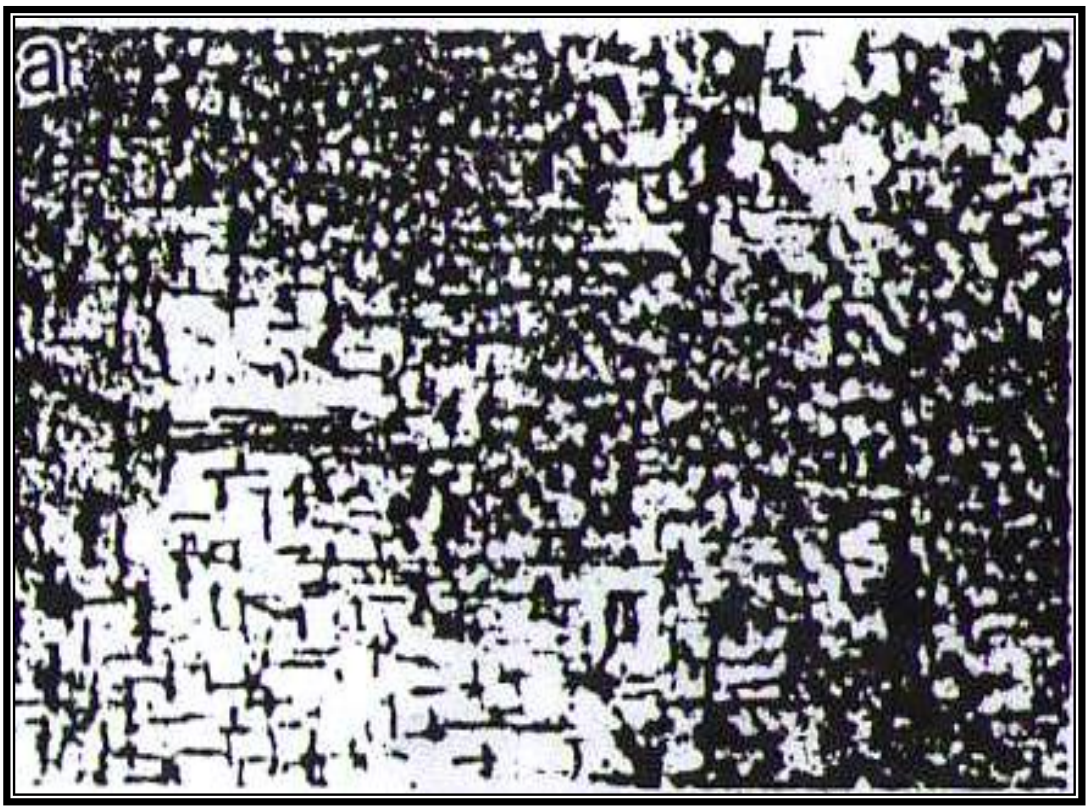

Fig.(1.7) Bright –field TEM showing the microstructure in the ternary Al-1.7 Cu -0.3 Mg. The electron beam is parallel to <001> α and <011> α respectively, after Ringer [Ringer et al, 1996].

1.4.3. Alloys In The α + S Phase Field:

These material remain as one of the two major classes of aluminum alloys (200series) used for aircraft construction world wide [Polmear, 1998;Polmear, 1995].

Fig.(1.8) is a hardness-time plot for the Al-1.1Cu1.7Mg alloys at 150 ^{o}C showing the effect of a 0.1 Ag addition .Isothermal aging of these alloys and their commercial counterparts such as AA2618 and AA2024 reveals several interesting features Fig.(1.8):

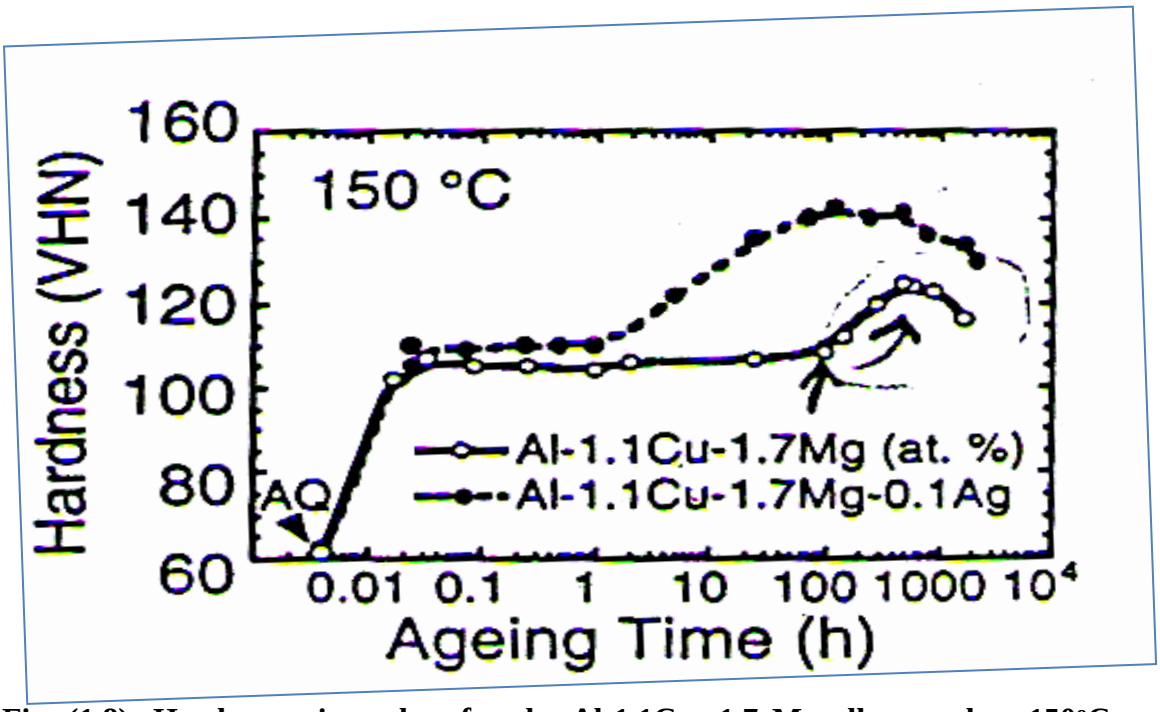

Fig. (1.8): Hardness- time plots for the Al-1.1Cu -1.7 Mg alloy aged at 150°C showing the effect Ag additions.[Ringer et al., 1997].

(i) hardening occurs in two distinct stages separated by a plateau during which time the hardness remains constant for many hours[Vietz & Polmear, 1966] ; (ii) the first stage of hardening occurs very rapidly ,and is largely complete within 60s ; and (iii) some 60 % of the total hardening during aging (peak hardness minus the AQ hardness value) occurs during this rapid first stage the Last two feature are not widely realized , particularly in commercially heat treated alloys , because accurate values of AQ hardness are often not determined. The first stage of hardening in Al-Cu-Mg alloys has generally been attributed to the formation of GPB zones, while the second stage of hardening has generally been at stage of hardening has generally been attributed to the formation of the S' of S phase [Silcock, 1990-61] .

Recent work proposed a different interpretation of the origins of hardening in this alloy [Ringer et al., 1997]. The microstrutural evolution during aging after solution treatment is considered to involve the following processes:

1. Quenching a rapid coalescence of quenched- in vacancies occurs, resulting in vacancy condenses occurs, resulting in vacancy condensation and the formation of a large number of dislocation

loops. The loops lie on the {110}α planes and possess a/ 2 <110> α Burgers vectors [Nicholson, 1965].

2. Within seconds of aging at elevated temperature, a rapid hardening reaction occurs. This is thought to be related to a subtle redistribution of the solute through a preferred interaction between Mg, Cu, and dislocations. The terms cluster hardening was recently introduced to describe this phenomenon [Ringer, 1997].
3. The diffusion of Mg and Cu atoms to the dislocation loops and helices which leads to heterogeneous precipitation of the S phase at these defects [Ratchev et al., 1998]. Once formed, these precipitates persist throughout the subsequent aging sequence.
4. towards the end of the hardness plateau, a fine and uniform precipitation of GPB zones occurs [Ringer et al., 1997] Figs. (1.9 & 1.10) causes as second increase in hardness which reaches a maximum when the zones occur in a critical dispersion [Ringer et al., 1998].
5. Over aging occurs as the GPB zones are gradually replaced by matrix precipitation of the S phase which grows progressively coarser [Ringer et al., 1997]

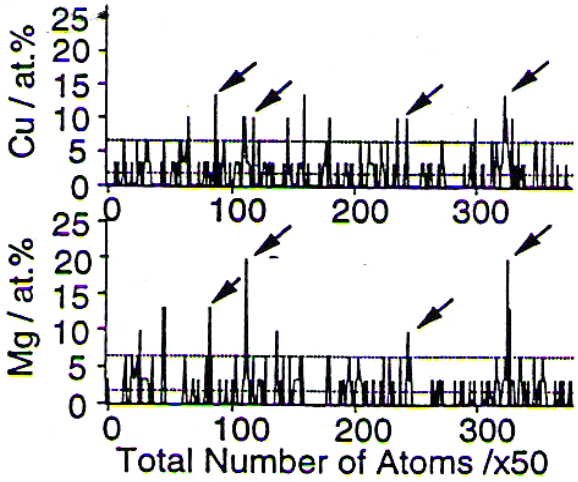

Fig. (1.9) Concentration-depth profiles (1DAP) the temry Al-1.1Cu – 1.7 Mg alloy aged to the end of the hardness plateau (150 °C, 100 h),showing co enrichment of Cu and Mg at GPB zone [Ringer et al., 1997].

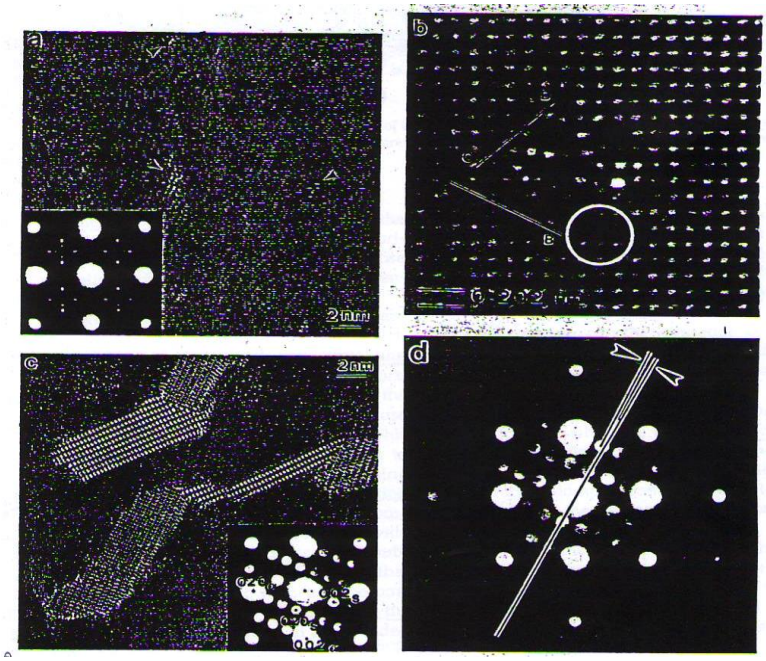

Fig.(1.10) Higher-resolution transmission electron micrographs form the hardness microstructure of the Al-1.1Cu-1.7 Mg alloy (aged 500 h at 150 ºC) . (a) GPB zone and a general SAED pattern (inset),(b) digitized and enlarged view of a typical zone showing the development of facets labels AB and CD, approximately parallel to $\{210\}_{\alpha}$ and $\{110\}_{\alpha}$,respectively; some elastic distortion of the α matrix is also circled ,(c) S precipitates ,as viewed in the <001>α orientation together with a typical micro beam electron diffraction patterns (inset) .(d) Micro beam electron diffraction pattern showing the α / S lattice rotation [Ringer et al.,1997].

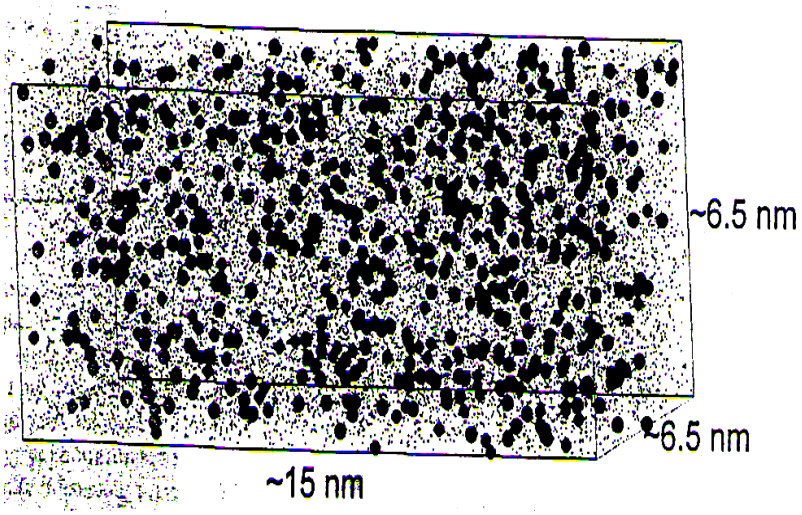

Fig. (1.11) Three dimensional reconstruction (3DAP) of the solute distribution in the ternary Al-1.1Cu-1.7 Mg alloy following aging for 5 min at 350 ºC. Dark spheres represent Mg, and the fine dots represent Al atoms After [Ringer et al., 1997].

Observation using CTEM and HRTEM show no evidence of matrix precipitation in an (Al- 1.1Cu- 1.7Mg) alloy in either the AQ condition or after aging at 150 ^{o}C for 5 min that is, just before and after the rapid hardening reaction. Similarly, APFIM of the alloy in the AQ condition detected independent Mg clusters and Cu clusters with no evidence of precipitation. Fig (1.11) provides 3DAP data [Ringer, 1998] from the (Al- 1.1Cu- 1.7Mg) alloy after aging for 5 min. at 150 ^{o}C , and maps the spatial distribution of Cu and Mg atoms and confirms that the formation of Zones or precipitates has not occurred within this short aging time [Ratchev et al., 1998]. However, in contrast to earlier reports, based on 1DAP data [Ringer et al., 1997], the 3DAP results reveal little or no evidence of a uniform distribution of (Cu-Mg) co clusters throughout the matrix. This illustrates how the larger volume of sample acquired in 3DAP provides a unique and critical insight into alloy microstructure. Random area 1DAP analyses [Ringer et al., 1997] reported slight difference in the Cu-Mg distribution between samples in the AQ condition and samples aged 5 min at 150 ^{o}C.

Whereas this was interpreted as evidence of a uniform distribution of (Cu-Mg) co clusters, the 3DAP results suggest that a preferred (Cu-Mg interaction is clearly not an effect that is observed uniformly throughout the matrix, suggesting that there is another, previously unconsidered, aspect to these is another, previously unconsidered, aspect to these interactions. Recent work suggests that the disparity between the previous 1DAP results and recent 3DAP data Fig. (1.9), arises because the Cu and Mg atoms cluster at the sites of the quenched in defect structure and so occurs in a distinctly non-uniform dispersion. This eventually leads to the

heterogeneous precipitation of the S phase at this dislocation [Zahra et al., 1998] .The rapidity of this heterogeneous precipitation increase with increasing aging temperature and supersaturating [Ratchev et al., 1998]. Significantly, the heterogeneous precipitation of the S phase proceeds after the rapid hardening [Ringer et al., 1997] .This suggests that the mobile dislocations that were available in the AQ specimens are pinned or locked by solute forming a sessile dislocation network. Therefore, the rapid hardening effect appears to have origins that are distinctly different form those usually attributed to precipitation hardening effects.

Recent results indicate that this hardening is also stimulated by deformation such that a thermo mechanical cycle involving short-term aging after initially quenching form the solution treatment temperature can cause hardening at both aging steps [Nicholson, 1965]. This thermo mechanical sequence is thought to evolve as follows; the initial age-hardening derives from the (Mg-Cu) solute interaction with dislocations, which rapidly become locked by solute atoms and form a sessile dislocation network. The deformation subsequently generates new dislocations that are thought to interact with and become locked by (Cu-Mg) solute atom during the second aging step, resulting in an extended sessile dislocation network and, therefore a second hardening increment.

Near the end of the hardness plateau, uniform precipitation of GPB zones was observed [Ringer et al., 1997] and Fig. (1.10). provides typical concentration- depth profile , which suggest that the zones contain approximately equal number of Cu and Mg atoms .It should be noted that the kinetics for the GPB zone formation are extremely slow compared to those for other GP zones observed in most other aluminum alloys. This

suggests that most of the quenched-in vacancies were condensed before or during the rapid hardening process, and it is this process that leads to the formation of numerous dislocation loops in the AQ microstructure. It is thought that rapid condensation of quenched-in vacancies also provides a mechanism for the transport of solute to these sites due to a preferred interaction involving Cu, Mg and vacancies. The localized vacancy condensation at the start of the decomposition sequence retards the kinetics of the subsequent precipitation of GP zones.

Regarding the precipitation of the S phase, it is noteworthy that MBED analysis provided result that was consistent with the Perlitz-Westgren structural model and the following orientation relationship has been observed [Ringer et al., 1996].

$[100]_s // [100]_\alpha$

$[100]_s // [0\,\bar{2}\,1]_\alpha$

$[100]_s // [012]_\alpha$

These results suggest a slightly different particle morphology t that deduced by [Wilson & Partridge, 1965], who proposed that the broad of the lath was the $(010)_s$ plane, based on matching of periodicity of the two lattices. Inspection of Fig.(1.11) shows that the broad facet of the lath is , in fact , (001)s ,and similar conclusion were drawn from HRTEM studies [Chang, 1992]. Recently, it was also reported that the habit plane of the lath arrowed at the right of Fig. (1.11) can be rotated several degrees form $\{210\}_\alpha$ [Ringer et al., 1996]. A slight rotation between the $S_{-\alpha}$ lattices has been recorded in many MBED patterns, implying an irrational orientation relationship where $(001)_s$ is rotated between 2 and 3 degree form $(0\,\bar{2}\,1)_\alpha$

around $[100]_{\alpha}$ Fig. (1.11) .This effect is not exclusive to precipitates with certain sizes or nucleation sites ,and seems to be a feature of equilibrium precipitation in Al-based alloys , because it is consistent with occurrence of multiple orientation relationships and morphologies for the θ phase in (Al-Cu) alloys and the η phase in (Al-Zn-Mg) alloys.

Finally, it may be noted that the evidence for the existence of intermediate phase that warrant the introduction of nomenclature such as S'' of S' does not appear to be conclusive. Recent MBED [Ringer et al., 1996] and SAED [Gupta et al., 1987] studies suggest that there is no justification for differentiating these precipitates form the equilibrium S. Here it may be noted that the reflections attributed s″ by [Ratchev et al., 1998] are coincident with the oxide film refections known to from in Al alloys [Park & Ardell, 1983].

1.5. Al-Li Alloy:

The earliest study on aluminum-lithium always might have been conducted in Germany in 1924 [Silcock, 1959-60]. However, interest in Al- Li alloys and accelerated development of these alloys occurred in the seventies. The development work on Al-Li alloys was concerned with properties such as strength modulus of elasticity, corrosion and density … etc. A number of review papers and conference proceeding on Al-Li alloys have been published [Lavernia et al., 1990]. Six international conferences on Al-Li alloys have been held. The first one was held in 1980 in OSA [Sanders & Starke, 1980] and the sixth one was in Germany in 1992 [Peters & Winkler, 1992]. After the sixth conference, the subject

of Al-Li alloy was merged into international conferences on Al-Li alloys [Sanders & Starke, 1994]. The development work led to the introduction of several commercial Al-Li alloys. These alloys rely on additions of copper, zirconium, and magnesium as essential alloying elements to obtain the desired combination of properties [Sanders & Starke, 1989], as shown in Table (1-1).

Al-Li based alloy are precipitation harden able. The phase equilibrium and precipitation reaction, that control the microstructure and hence the properties, are sgnificaly different from these of conventional alloy [Willams & Howell, 1989]. The effect of different alloying additions is to alter the phase equilibrium and to modify the precipitation sequence. These alloys may possess moderate to high strength levels and contains recrystallized or unrecrystallized grain structures, depending upon the type of temper used during heat treatment [Grims et al., 1986].

As shown in the Table (1-1), the Al-Li alloy that contains Li, Cu, Mg and Zr. The presence of these alloying elements lends to the formation of various precipitates which are listed in Table (1-2) along with their crystal structures.

Chapter two

Creep

2.1. Introduction:

Creep is the term given to the material deformation that occurs as a result of long term exposure to level of stress that are below the yield or ultimate strength, often in combination with temperatures near its melting point. An easily produced example of creep is the sagging of a chocolate bar under its own weight on a hot day. The high temperature material problem has been mentioned that the strength of materials decreases with increasing temperature, because of:-

1. The mobility of atoms increases rabidly with temperature also result-in greater mobility of dislocations by the mechanism of climb.
2. The diffusion – controlled process can have a very significant effect on high temperature mechanical properties.
3. The equilibrium concentration of vacancies likewise increases with temperature.
4. The slip system changes, or additional slip systems are introduced.
5. Deformation of grain boundaries becomes and added possibility in the high temperature deformation of metals.
6. The effect of prolonged exposure at elevated temperature on the metallurgical stability of metals and alloy.
7. Another important consideration is the interaction of the metal with its environment [Dieter, 1986].

The degradation undergone by materials in these extreme conditions can be classified into two groups:-

1)-Mechanical degradation: In spite of initially resisting the applied loads the material undergoes, an elastic deformations change with time.

2)-Chemical degradation: this is due to the reaction of the material with the chemical environment and to the diffusion of external element into the materials. Chlorination and internal oxidation are example of

chemical degradation. The anelastic or time dependent deformation material is known as creep. [Meyers and Chawla, 1999]

So, a metal subjected to a constant tensile load at an elevated temperature will creep and undergo a time-dependent increase in length or we can say that, "creep is time-dependant plasticity occurring at stresses below the flow stress in a material over along duration of time", and the creep strain of engineering significance is typically not encounter until the temperature in excess about **0.4** of the melting temperature in degree Kelvin (^{o}k) of an alloy [Dieter, 1986; Collines, 1981].

Creep occurs by a number of mechanisms, some well characterized others not, but all of which have an element of thermal activation which enables plastic deformation at stresses below those needed to deform the lattice without thermal activation [Garafalo, 1965].

Creep is critical in a number of applications: steels used in power and chemical plants where the service temperatures high, turbine components, ice and lead at ambient temperatures[Evans &Wilshir, 1993]

When loaded with, for example, a constant load a material will stretch elastically but will also gradually extend plastically. The main concern in applications is dimensional stability, although prolonged creep will also lead to rupture. Creep extension plotted against time produces a graph with a characteristic shape consisting of three distinct regions. [Smallman, 1999; Chan & Haasen, 1996]. This division into stages was made by [Andrade, 1911], one of the pioneers in the study of creep.

Creep tests are carried out on a specimen loads e.g. in tension or compression, usually at constant load, inside a furnace which is maintained a constant temperature. The extension of the specimen is measured as a function of time. A typical creep curve for metals polymers and ceramics is represented in Fig. (2.1a). The temperature at which materials begin to creep depends on their melting point T_m for instance, $\mathbf{T > 0.4T_m}$ for metals and $\mathbf{T > 0.5T_m}$ for ceramics. The general procedure for creep testing is covered in **ASTM** specif. **E139-83**(1990).

The response of the specimen loaded by σ_0 at time t=0 can be divided into an elastic and a plastic part as:

$$\varepsilon_o = \sigma_o / E(T) + \varepsilon_p(\sigma_o, T) \ldots\ldots\ldots\ldots\ldots (2.1)$$

Where E (T) is the modulus of Elasticity. The creep strain in Fig (2.1a) can then be expressed according to: $\varepsilon_c = \varepsilon(t) - \varepsilon_0 \propto t^k$ …… (2.2)

Where k<1 in the primary, k =1 in the secondary, and k>1 in the tertiary creep stage. These terms correspond to a decreasing, constant and increasing strain rate respectively and were introduced by[Andrade,1910] . These three creep stages are often called transient creep, and accelerating creep respectively [Josef Betten, 2005].

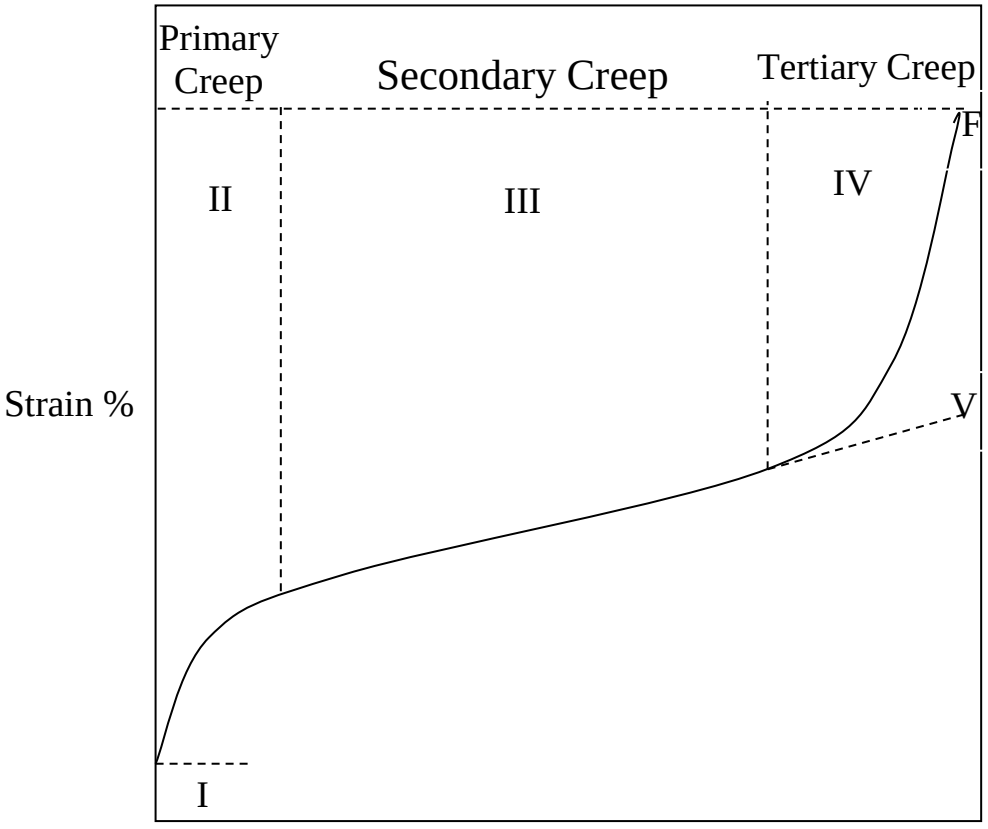

Figure (2.1a) The strain, time curve showing the three stages of creep: - I, elastic extension; II, decreasing creep rate; III, minimum creep rate; IV, increasing creep rate; V, constant stress test; F, fracture.

As shown in Fig.(2.1a), the slope of the curve is called creep rate ($\dot{\varepsilon}$) and the end point of the curve **F** is the time for rupture. The creep rate is not ordinarily constant and can be divided into three phase. The region **II** is commonly considered as primary or transient creep stage, and it starts at a rapid rate and slows with time. The region **III** stands as secondary or steady state creep, which has a relatively uniform rate. **IV** as tertiary creep has an accelerating creep-rate and terminates at the point **F** by failure of material at time for rupture [Murugananth, 2002].

The results of eq. (2.1) and eq. (2.2) form the creep test justify a classification of material behavior in three disciplines: elasticity, plasticity, and creep mechanics [Haupt, 2000]. Due to a proposal of HAUPT one can also distinguish four theories of material behavior as follows:

- The theory of elasticity is concerned with the rate-independent behavior without hysteresis.
- The theory of plasticity specifies the rate- independent behavior with hysteresis.
- The theory of viscoelasticity describes the rate-dependent behavior without equilibrium hysteresis.
- The theory of viscoplasticity is devoted to the rate dependent behavior with equilibrium hysteresis.

. The creep behavior exists in two of the above listed categories, namely in the theories of viscoelasticity and viscoplasticity [Josef Betten, 2005].

Primary creep: During primary creep, the strain rate decreases with time until a constant rate is reached, and this tends to occur over a short period [Martin & Oettel, 1997]. Primary creep strain is usually less than one percent of the sum of the elastic, steady state, and primary strains. The mechanism in the primary region is the climb of dislocations that are not

pinned in the matrix [J.I.Rhoads, INT.]. Since the amount of initial strain of a material is due to the number of dislocations initially present, decreasing creep rate as dislocation microstructure develops to reduce strain rate [Reed Hill, 1973]. The primary region is strongly dependent on the history of the material. If the material has been heavily worked before the creep test, there would be many more dislocations present and the characteristics of the primary creep region would be much different.

Secondary creep: Steady-state creep is so named because of the strain rate is constant. In this region, the rate of strain hardening by dislocations is balanced by the rate of recovery. Steady-state creep is roughly centred at the minimum in the plot of creep rate versus time. The minimum rate is empirically found to be inversely proportional to the time to rupture. This is often called the Monkman-Grant relationship [Monkman&Grant, 1956] in which the product of the minimum creep rate and rupture time is found to be constant for a given mechanism. Equilibrium is established between deformation and recovery mechanisms to maintain a steady state strain rate [Hertzberg, 1989]. Minimum creep rate may not be entirely constant but occurs in this region.

Tertiary creep: In the tertiary region, the high strains start to cause necking of the material just as in the uniaxial tensile test. This necking causes an increase in the local stress of the component, which further accelerates the strain [J.I.Rhoads,INT.]. Eventually the material will pull apart in a ductile fracture around defects in the solid. These defects could be precipitates at high temperatures or grain boundaries at lower temperatures [Phaniraj et al., 2003]. In any case the importance of the tertiary region to normal operation and creep design criteria is minimal. In Fig.(2.1a) above, the time scale of the tertiary region is greatly expanded for the purpose of clarity. Considering the small amount of time in addition to the fact that the tertiary region develops a plastic instability

similar to necking, operating in the tertiary region is not feasible. Therefore, it is a conservative estimate to approximate the end of serviceable life of any component to coincide with the end of the steady state creep region. Only under accidental conditions may the extra time in the tertiary region be useful to consider.

. The primary creep could be described as the work-hardening stage for the material in which the resistance to creep is built up by virtue of its own deformation: during steady-state creep there is a state of balance between work-hardening and thermal softening; tertiary creep precedes fracture through cavitations, inter-crystalline cracking or some other damage mechanism [Evans &Wilshire, 1985]. The studies on the primary and steady stages of creep are usually more interesting for engineering analysis. Tertiary creep is usually associated with the onset of failure (necking, damage) and is short-lived [Evans, 1984].

Although there are a great number of fundamental theories describing the process of creep deformation and rupture life in different regimes of stress, temperature and strain rate, the theories have not been applied with effect in useful materials of the type used in engineering. This is because practical materials tend to be complex.

Increasing creep rate as the effective cross section reduces leading to failure typically logarithmic curve. (Note tertiary creep can refer to both the final failure stage of creep or to whole curve where this has a logarithmic curve) [Sharby & Burke, 1967].

2.2. Creep data and it's use:-

Creep tests are conducted at constant load or at constant stress. In the latter the creep rig is designed to reduce the load on the test-piece in proportion to the extension, this keeps the load constant provided the

strain is homogenous. Three tests are represented as shown in Fig. (2.1b), three constant loads corresponding to three engineering stresses σ_a , σ_b **and** σ_c **,** where used at constant temperature. It can be seen that $\varepsilon_a > \varepsilon_b > \varepsilon_c$ as a consequence of the relationship $\sigma_a > \sigma_b > \sigma_c$, the rupture time t_{ra} , t_{rb}, t_{rc} increases with decreasing stress.

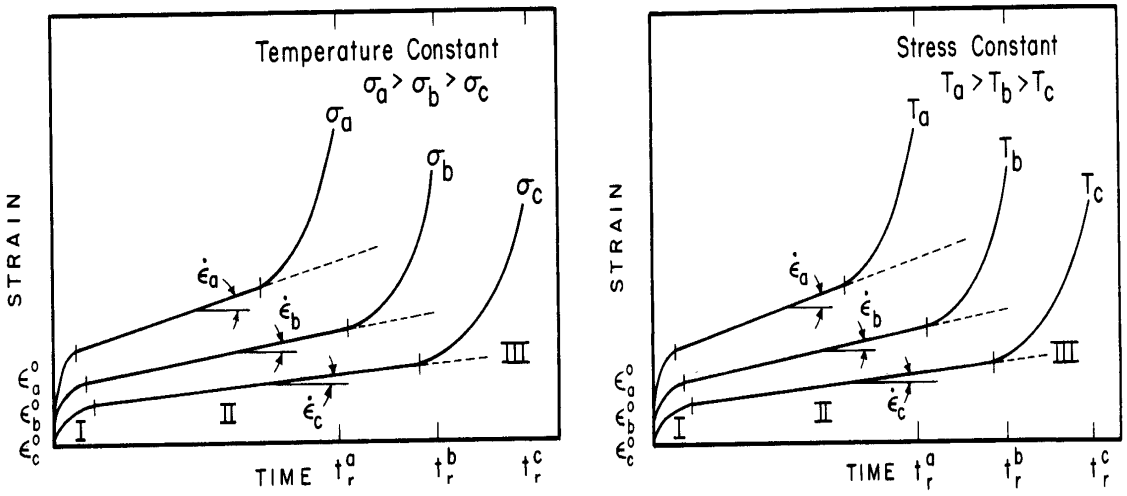

Fig. (2.1b, c) Creep strain vs time at: - b- Difference constant stress levels and temperature. c- A constant engineering stress and different temperatures. [Meyers & Chawla, 1999].

In Fig. (2.1c) the engineering stress was kept constant and the temperature was varied. Since the test are conducted in tension, the stress rises as the length of the specimen increases, because of the reduction in area. The dashed line (III) in Fig. (2.1b, c) represent the constant stress curve. Initially they are identical, because ε_e=0. As specimen increasing in length, the stress increases and so does the creep rate, at a constant load. The failure times under constant stress and constant load can be drastically different. The curve shown in Fig.(2.1a) have been expressed mathematically as $\varepsilon_t=\varepsilon_o+\varepsilon[1-\exp(-mt)]+\varepsilon_s t$, where ε_o is the instantaneous strain (the strain at the instant of application of load), $\varepsilon_s t$ is a linear function of time, depicting S.S creep and the term $\varepsilon[1-\exp(-mt)]$ represent primary stage in which m is the exponential time parameter and ε is the strain that stage [Meyers & Chawla, 1999].

Creep strength: stress to produce nominal strain (normally 1.0%) in given time typically 10,000 h (1 year), for aeronautical industry and 100,000 h ($11^1/_2$) years, for power plant. Ideally timescale of tests should be comparable with the timescale of service exposure.

Creep life: Time to nominal 1% or 2% stress at given stress and temperature.

Minimum creep rate: Measured as a function of stress and temperature. . Tests expensive focus on accurate value for the minimum creep rate need to maintain constant stress and temperature over very long periods of time. Tests can last 100,000 h. [Dieter, 1986].

Stress Rupture life: The time to break the specimen at a particular stress and temperature. Use of the word 'rupture' implies tests done at high stress-these are quick and cheap but the strain is not measured accurately [Van Vlack, 1970].

2.3. Monkman-Grant Relationship:

For many materials the steady state regime dominates the creep life and the creep life is thus mainly dependent on the minimum creep rate $\dot{\varepsilon}$. . This relationship is expressed as the Monkman-Grant relati-onship: [Monkman & Grant, 1956].

$\dot{\varepsilon}_{\min} \times t_R = C$ Where *C* is a constant and t_R is the life to rupture.

Temperature and stress dependence:

Empirically the minimum creep rate is well described by the expression:-

$$\dot{\varepsilon} = \dot{\varepsilon}_o \left(\frac{\sigma}{\sigma_o} \right)^n \exp - \left(\frac{E_a}{RT} \right) \text{..... (2-3)}$$

Where σ_o and $\dot{\varepsilon}_o$, are creep constants, n takes values from **3-8** at high stress and **1** at low stress, and E_a is the activation energy for creep

which is usually the same as the diffusive process by which the creep occurs, e.g. self diffusion, as shown in Fig. (2.2).

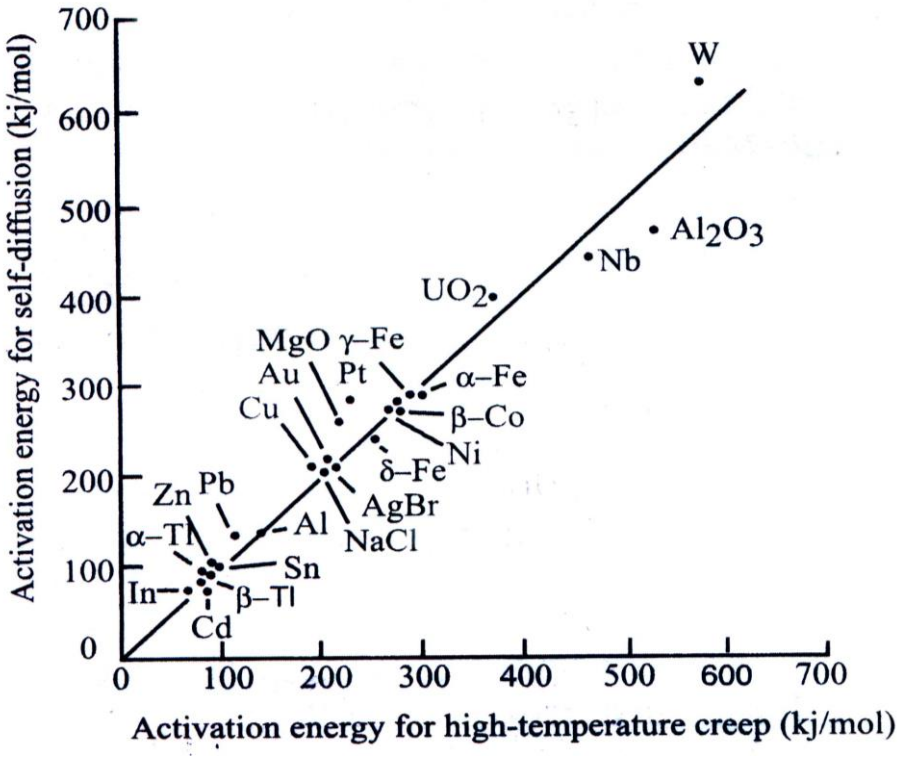

Fig. (2.2) Correlation between Activation energy at high temperature creep and self diffusion for a number of metals [Sherby & Miller, 1979]

The temperature dependence can be explored experimentally using temperature dip tests. Once the steady state regime has been reached and the creep rate is stable, the temperature is changed by a small amount **(10-20°)** and the creep rate re-measured once this has reached a new steady-state. The activation energy is found in the normal way taking logs of both sides of equation (2.3) above:

$$E_A = R \frac{\ln(\dot{\varepsilon}_1 / \dot{\varepsilon}_2)}{\left(\frac{1}{T_2} - \frac{1}{T_2}\right)} \quad \ldots\ldots\ldots\ldots\ldots\ldots (2.4)$$

The value for E_A correlates well with the self-diffusion coefficient for the bulk material. At lower temperatures it correlates with the lower

value of the self-diffusion coefficient for grain boundary diffusion [Mishra & Pandey 1990].

2.4. The Functional Forms of the Creep Relations:-

The shapes of creep curves, their various time laws, and the dependence of the strain-rate on imposed external parameters have received much attention. The varity of empirical function forms which have been proposed have been reviewed by TAKEUCHI and ARGON (1976b), while some of these forms have been proposed purely for empirical operational conveniences, other have been guided by under-lying mechanisms.

The portion of the creep curve of greatest interest is the S.S. part which will be considered to have the potential to produce limitless strain at a constant structure under a constant applied stress. A variety of function form has been proposed for the S.S. creep rate. These and their individual merits have been reviewed by (Takeuchi and Argon).

--Mukherjee-Bird-Dorn Equation:-

At 1964 they proposed an empirical equation of the form $\dot{\varepsilon} = \frac{AGb}{KT} D_0 \exp[-\frac{Q_c}{RT}][\frac{b}{d}]^p[\frac{\sigma}{G}]^n$ Where A is a dimensionless constant , $\mathbf{D_o}$ is a frequency factor , **G** is the shear modulus , **b** is the Burgers vector , **K** is Boltzmann's constant , **T** is the absolute temperature, **σ** is the applied stress, **d** is the grain-size , **P** is the inverse grain-size exponent , **n** is the stress exponent, $\mathbf{Q_c}$ is the appropriate activation energy, and **R** is the gas constant [Mukherjec et al., 1964].

And because of that, the activation energy for diffusion is often equal to the activation energy for creep $\mathbf{(Q_c=Q_D)}$. The diffusion coefficient is.

$$D = D_o \exp[\exp -\frac{Q_D}{RT}] \text{ and then } \dot{\varepsilon}_s = \frac{AGbD}{KT}[\frac{b}{d}]^b[\frac{\sigma}{G}]^n .$$

Essentially, these applied stress, temperature and the grain size. Fig. (2.3a, b) illustrates the application of the Dron-Mukherjee-Bird equation to metal (Aluminum and Al-alloys) and ceramics [K.T. Park et al., 1990].

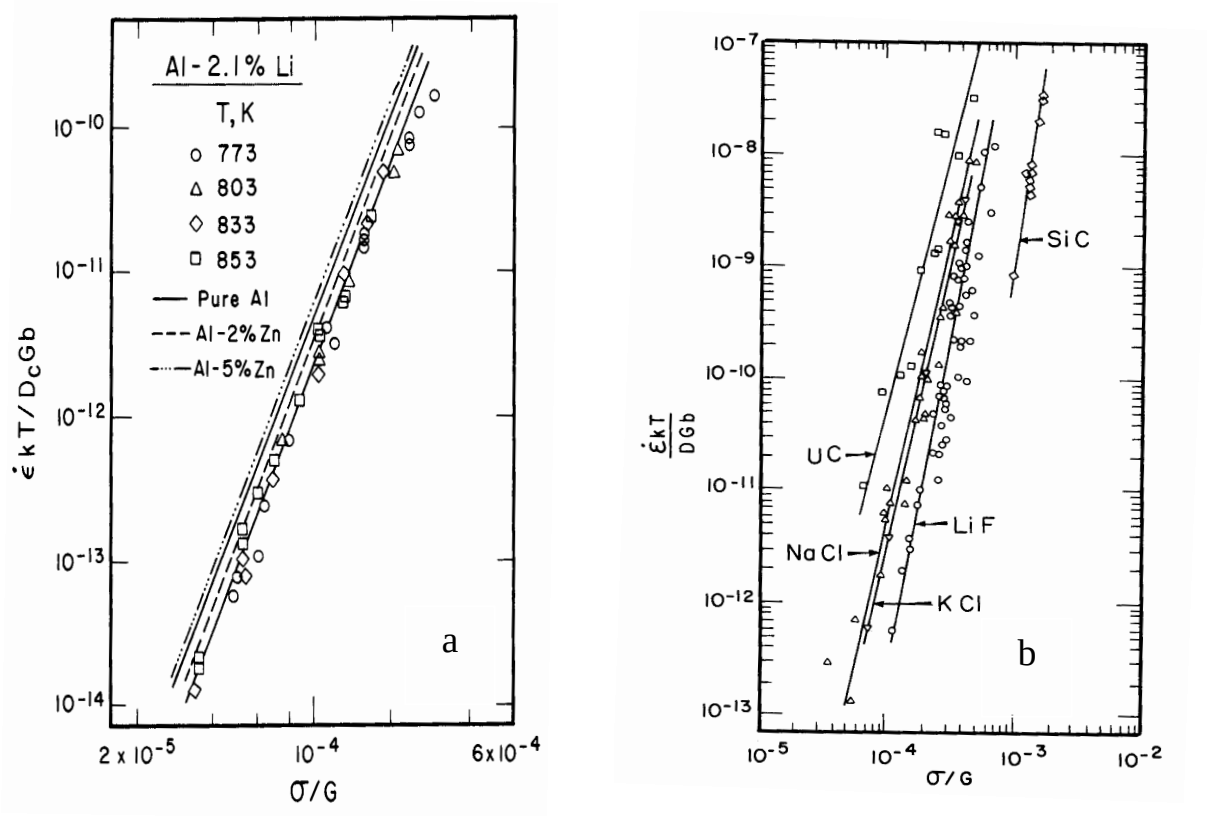

Fig.(2.3a,b) Normalized creep rate vs normalized stress, according to Mukherjee-Bird-Dorn,equation,for: a- aluminum, Al-Zn & Al-Li, solid-solution. [Park et al., 1990]; b- Various ceramics [Chokshi & Langdon, 1991].

---Dorn Equation:

One that has received wide acceptance in that formulated by McLean (1962), and by Dorn & Co-Workers (1964), Mukherjee et al. (1962) and by Dorn and Co-workers (1964) ,Mukherjee et al. (1969), and Bird et al. (1969), and amended by Barrett and sherby (1965).

$$\varepsilon_{ss}^{\bullet} = A_o \nu_D \left(\frac{\chi}{\mu b}\right)^3 \left(\frac{\mu\Omega}{KT}\right)\left(\frac{\sigma}{\mu}\right) \exp\left(\frac{-Q_c}{KT}\right) \ldots\ldots\ldots (2.5)$$

Where $\mathbf{Q_c}$ is the activation energy of power law creep σ is the applied tensile stress , μ is the shear modulus , Ω is the atomic volume, x is the stacking fault energy, b the magnitude at the Burgers displacement , V_D the atomic frequency , m & A_o material constants. A more compact form was proposed by (Bird et al., 1969).

$\varepsilon_{ss}^{\bullet} = A_o \nu_d \left(\frac{\chi}{\mu b}\right)^3 \left(\frac{\mu b D}{KT}\right)\left(\frac{\sigma}{\mu}\right)^m$ this equation Know as the **Dorn Equation**

Where D is self diffusion constant which obey, $D = D_o \exp\left(-\frac{Q_D}{KT}\right)$

Dorn equation has a wide range of applicability to BCC and CPH metals and solid solution alloys. This broad correlation is shown in Fig. (2.4a, b). [Bird et al., 1969].

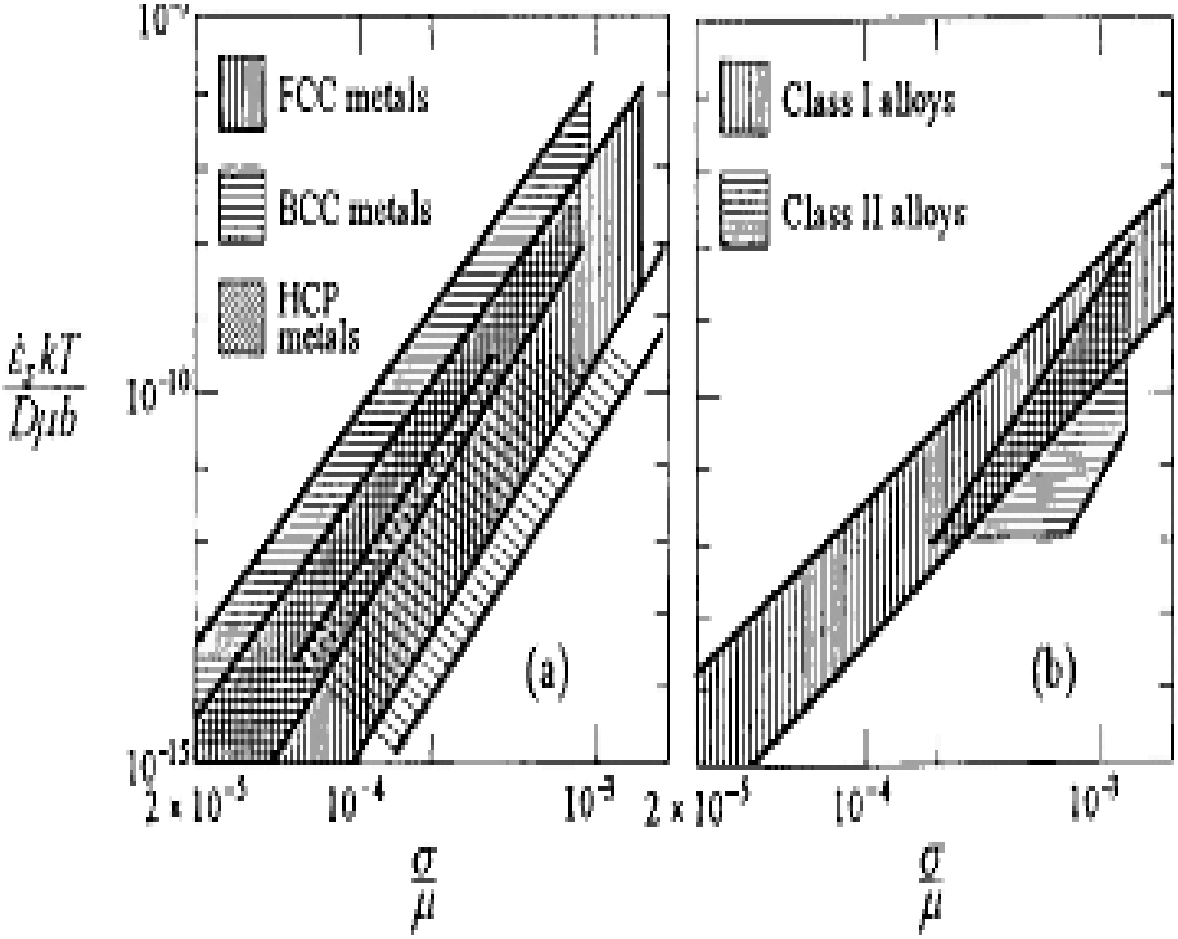

Fig. (2.4) Dependence of steady state creep rate on stress: (a) - In pure metals; (b) - In diluted solid solution alloys [Bird et al., 1969].

2.5. Larson Miller Parameter:-

If new materials are to be brought into service within a reasonable timescale it is necessary to estimate the creep life by extrapolating higher temperature data to much longer times at lower temperatures.

Essentially, the creep test is accelerated by raising the temperature, and the time difference is accounted for by using the activation energy, assuming this to be the same as at the service temperature. To do this a considerable amount of data at a range of stresses and temperatures are required. To plot this data on a single graph a number of parameters combining time to failure and temperature have been proposed.

In 1952, Larson and Miller proposed a method, that correlates the temperature T, with the time to failure t, at a constant engineering strees σ. The Larson-Miller equation has the form:

$$P = T(\ln t + C) = Q/R \quad \text{.....} \quad (2.6)$$

Where **P** is the **L.M**. **P**arameter, **t** is the time to rupture (or to some defined strain e.g. 1%), **Q** is the activation energy for creep, **R** is the gas constant and **C** is a constant for a particular material and has a value typically between **30-65**. A value of **46** can be used for most metals where a specific value is not determined, (a value of **20** will be quoted if $\log_{10}$ are used). If the Larson Miller parameter P is plotted (as shown in Fig.(2.3) against the stress for all the tests and the results should lie on a single line reflecting the effect of the stress of lowering the activation energy for the creep process. (Details of the derivation are discussed in **D**ieter, 1976, section 13-13 p.483.) Tests conducted at the same stress but at different temperatures should give similar L.M Parameters within the experimental spread. From this plot, can obtain the time to rupture at any time and stress.

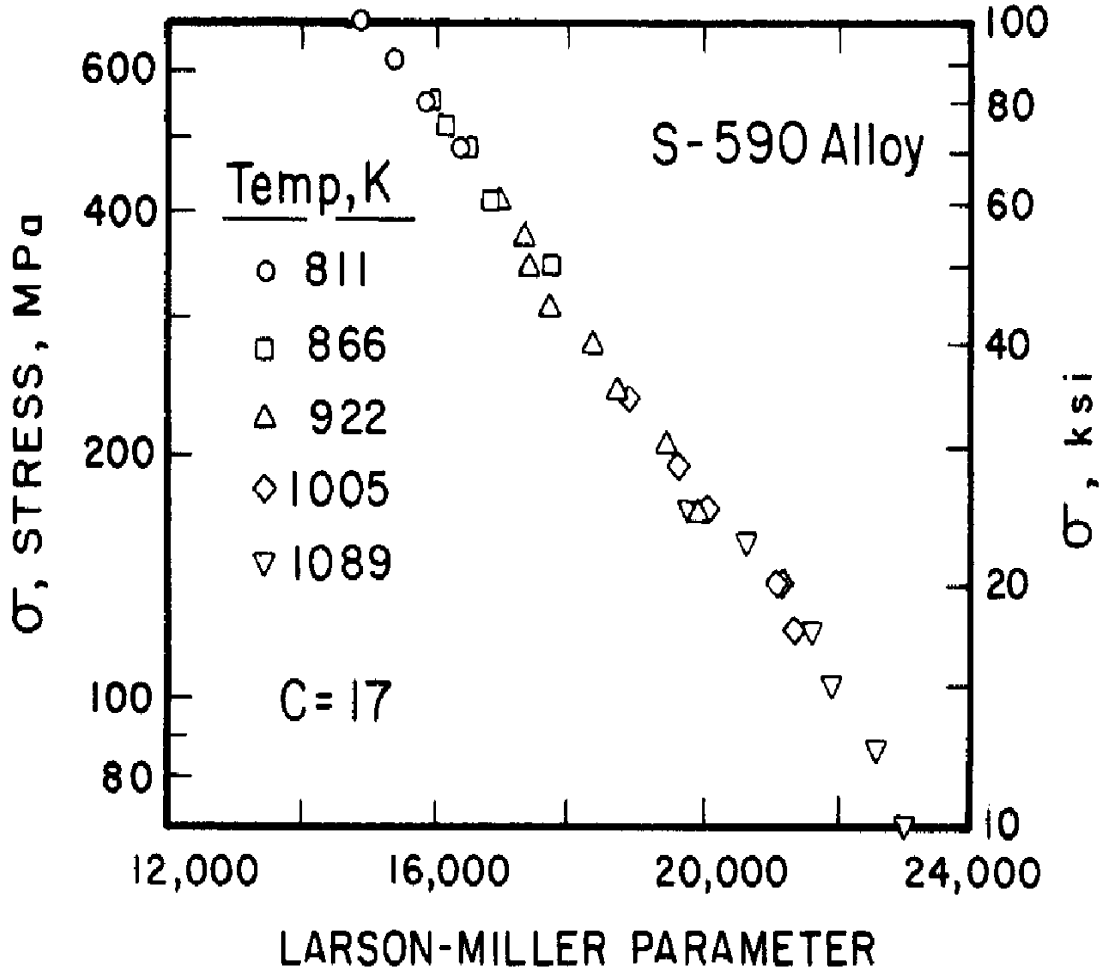

Fig (2.5) Master plot for Larson-Miller parameter for S-590 alloy[Goldhoff,1959]

2.6. Mechanisms for Creep:

Remember that creep is essentially plastic deformation at stresses below the flow stress. The key is that thermal activation processes allow the physical barrier to deformation (work-hardening, precipitates etc.) to be overcome. For this to happen takes time; the higher the temperature and the closer to the flow stress the more rapid this process will be, hence the increase in creep rate with stress and temperature mentioned above. The details of the creep mechanism Fig.(2.6), are as variable as the microstructure of the material and the nature of the dislocations, nevertheless strong patterns emerge which are common to many materials. Creep deformation occurs by the activated movement of

dislocations or directly by the diffusion of atoms to change the shape of individual grains and thus the macroscopic material (diffusion creep).

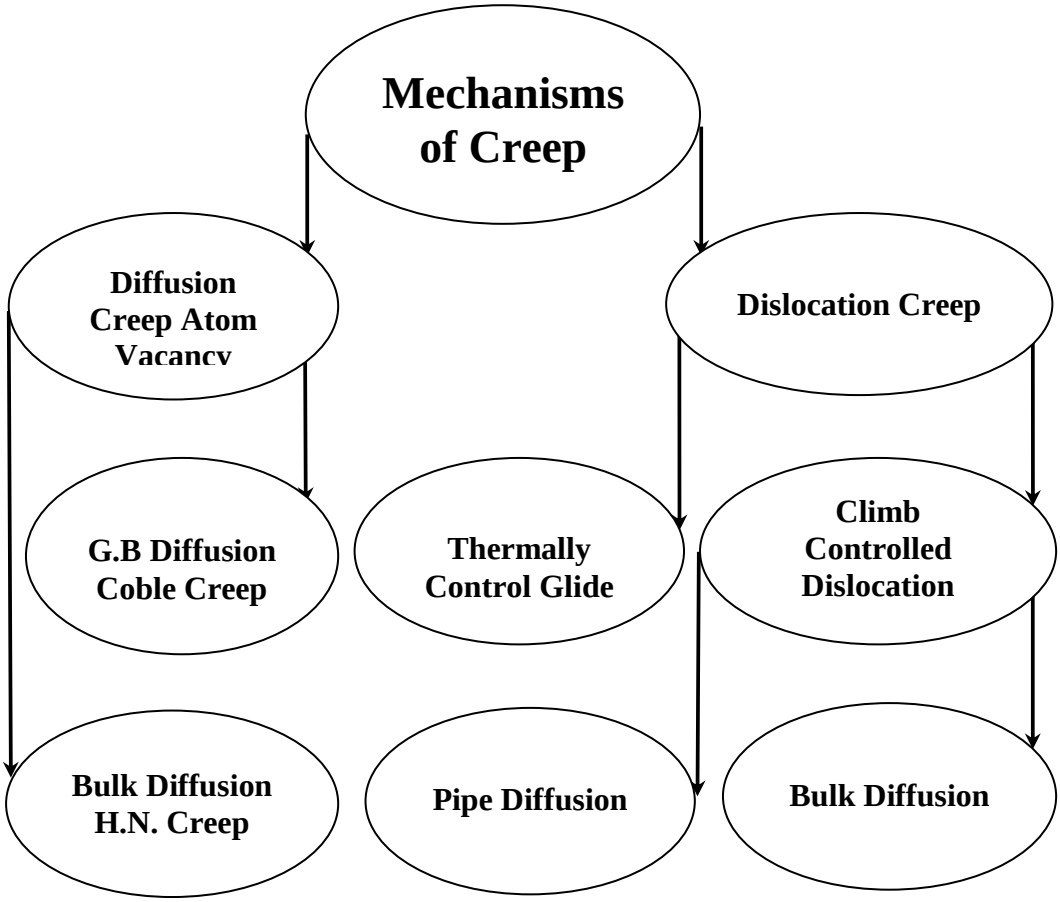

Fig. (2.6) Creep Mechanisms

2.6.1. Diffusion Creep:

2.6.1.1. Herring-Nabarro Creep:

Deformation occurs by the movement of atoms between differently oriented interfaces under the influence of an imposed stress to produce a macroscopic shape change. It is intrinsically a very slow process but comes into its own at stresses too low for dislocation motion to be activated and at relatively high temperatures where the diffusion is fast enough to produce a measurable creep rate.

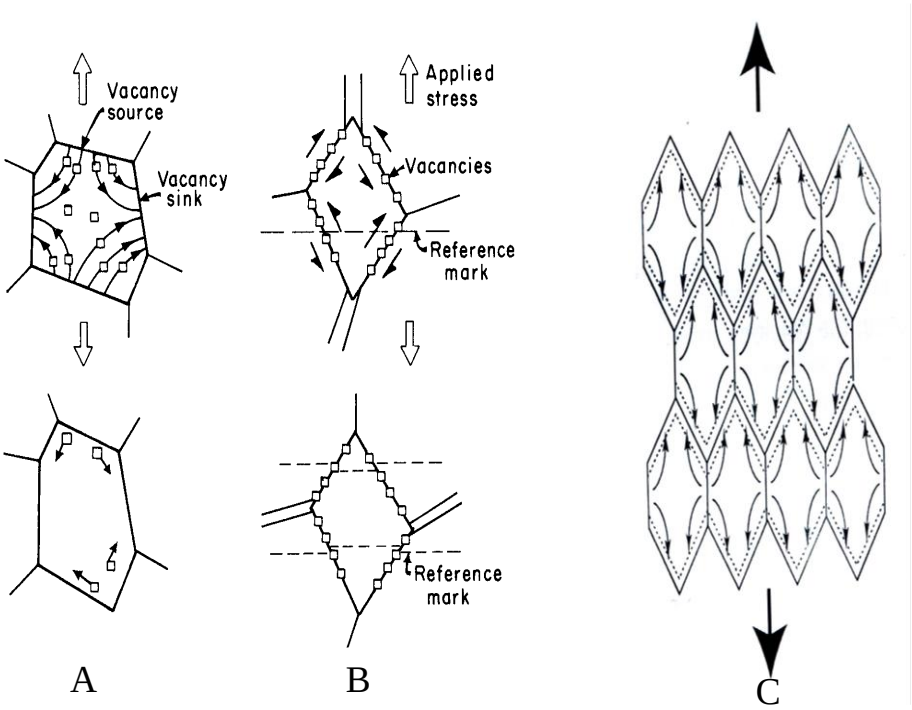

Fig.(2.7) Flow of vacancies according to (A) Naborra-Herring and (B) Coble mechanisms. (C) Resulting in an increase in the length of the specimen.

The creep rate can be derived without resorting to arbitrary constants as . follows:

The equilibrium concentration of vacancies C_o depends on the energy to form a vacancy E_v: $C_o = \exp\left(\frac{-E_v}{kT}\right)$ the effect of a tensile stress is to reduce the energy for the formation of a vacancy by σb^3 hence:

$$C = \exp-\left(\frac{E_v - \sigma b^3}{kT}\right) = \exp\left(\frac{-E_v}{kT}\right) \times \exp\left(\frac{\sigma b^3}{kT}\right) = C_o \exp\left(\frac{\sigma b^3}{kT}\right) \ldots\ldots (2.7)$$

The excess volume fraction of vacancies at the horizontal boundaries is given by:

$$C - C_o = C_o\left[\exp\left(\frac{\sigma b^3}{kT}\right) - 1\right] \text{ Which for } \sigma b^3 \langle\langle kT \quad C - C_o = \frac{C_o \sigma b^3}{kT} \quad ...(2.8)$$

(The concentrations C and C_o are dimensionless).

The flux of vacancies from the horizontal to the vertical interfaces

is given by Ficks 1st law $J = -D\frac{\partial C}{\partial x}$ hence: $J = -\frac{D_v C_o \sigma b^3}{kTL}$ ..(2.9)

Where L is the diffusion distance approximated to the grain size L. this gives the thickness of matter removed from the vertical boundaries and plated out on the horizontal boundaries per second as a result of the stress. Hence, the resulting strain rate is give by dividing this flux by the distance between the boundaries, L, and replacing D_vC_o by the self-diffusion coefficient D: $\dot{\varepsilon} = \frac{D\sigma b^3}{kTL^2}$ ..... (2.10)

The strain rate is proportional to the applied stress and inversely proportional to the grain size squared. A more careful analysis of the diffusion paths leads to an expression where the strain rate is 12 times that of equation (2.10), this makes sense because L represents the maximum distance any vacancy would have to travel and the equation estimates the minimum concentration gradient that would be achieved. The agreement between this expression and the data is extraordinarily good considering the expression is derived from first principles and contains no 'fitted' parameters.

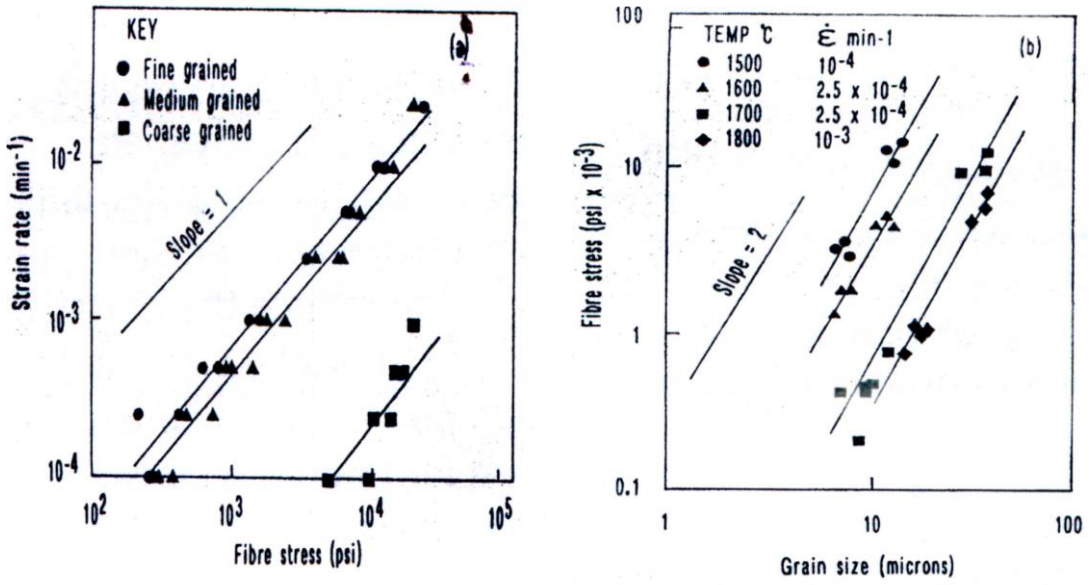

Fig.(2.8):Linear dependence on stress and inverse square dependence on grain size for creep in alumina fibers tested at 1700°C. Note: second graph plots stress for constant strain at each temp.

2.6.1.2. Coble Creep:

As diffusion is very sensitive to temperature, at lower temperatures the main diffusion path is along the grain boundaries since the activation energy for grain boundary diffusion is considerably less than that for bulk diffusion. The effect on the expression is to replace the self-diffusion coefficient by that for grain boundary diffusion and to reduce the cross-sectional area through which diffusion occurs from L^2 to αbL where αb is the 'thickness' of the grain boundary for diffusion purposes, and α is a dimensionless constant ≈ 1. Hence the creep rate for Coble Creep is:

$$\dot{\varepsilon} = \frac{\alpha D_{GB} \sigma b^4}{kTL^3} \quad \ldots\ldots\ldots\ldots\ldots\ldots\ldots\ldots\ldots\ldots\ldots\ldots(2.11)$$

Both these mechanisms of creep occur simultaneously at all temperatures but, as E_A reaches $\approx kT$, the high sensitivity of the diffusion rate to the activation energy means that there is an abrupt change from Coble creep to Herring-Nabarro creep kinetics.

Apart from the evidence of the kinetics of creep in both metals and ceramics, very direct evidence of the mechanism comes from the formation of precipitate-free material on the horizontal boundaries and the accumulation of precipitates on vertical boundaries as a result of the process as shown in Fig,(2.9).

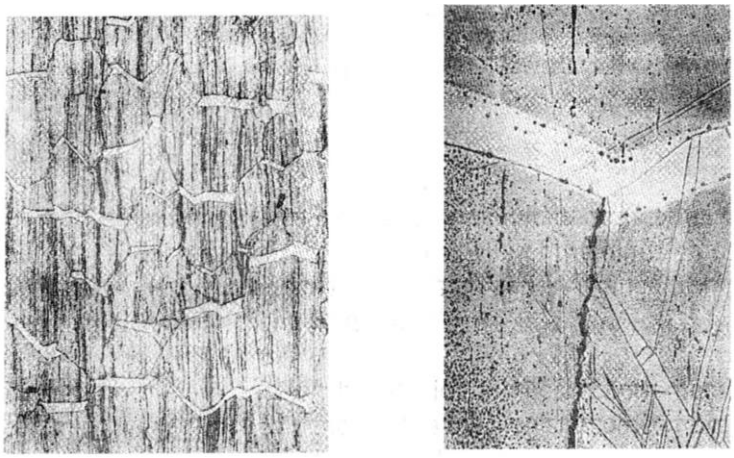

Fig. (2.9) Herring- Nabarro creep of Mg 0.55% Zr alloy showing precipitate-free horizontal boundaries and precipitate enrichment on vertical boundaries.

2.6.2. Dislocation Mechanisms:

2.6.2.1. Power Law Creep:

For a very important range of higher stress and at temperatures in excess of 0.5 T_m the strain rate is related to the stress by an equation of the form:

$$\dot{\varepsilon} \alpha \left(\frac{\sigma}{\mu} \right)^n \quad \text{.....(2.12)}$$

Where the exponent n takes values between **3** and **10** and thus the creep rate is very sensitive to the stress. (Taken together with the Arhenius equation, this gives rise to the equation (2.3).

Power law creep essentially describes deformation produced by the movement (glide) of dislocations which is itself limited by the climb of those same dislocations around obstacles substantial enough to prevent plastic flow, as shown in Fig,(2.10). The obstacles are precipitates or dislocation locks; in creep resistant alloys precipitates or dispersions coherent or incoherent are added to prevent dislocation glide. At temperatures in excess of $\mathbf{0.5T_m}$ the dislocations can escape from the obstacles by climbing out of the slip plane and thus can continue to glide. The rate-determining step is the climb process, but the strain is produced during the glide to the next obstacle.

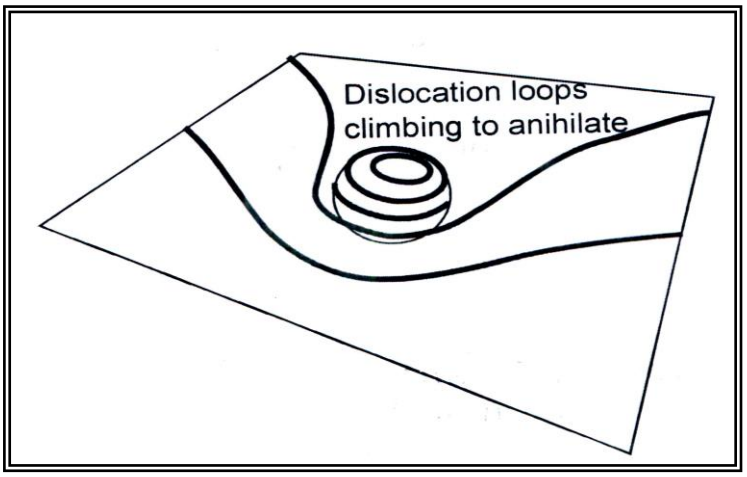

Fig. (2.10) Dislocations climbing around obstacles: the kinetics is governed by climb, the strain is achieved by glide.

The rate of creep is thus determined by the rate at which the dislocations move and the density of dislocations, expressed as the **O**rowan **e**quation [Orowan, 1947]:

$$\dot{\gamma} = \rho b \upsilon \quad \text{..... (2.13)}$$

Where υ is the average dislocation velocity and ρ the dislocation density. In the plastic region the density of dislocations in a metal is generally assumed to be proportional to the stress squared. The rationale for this is that where the dislocations are pinned by interactions with other dislocations of average spacing r, the bypass stress is $\sim \mu b/r$. Hence the dislocation density which, is inversely proportional to r^2, is proportional to the applied stress squared.

$$\sigma = \frac{\mu b}{r} \; ; \; \rho = \frac{1}{r^2} \; ; \qquad \therefore \rho = \left(\frac{\sigma}{\mu b} \right)^2 \quad \text{.....(2.14)}$$

The velocity of a dislocation, which requires repeated activation processes in order to continue moving, is proportional to the applied stress. These processes could be the nucleation of kinks or jogs for activated glide or climb respectively. The applied force σb, reduces the activation barrier in the direction of the stress by σbx where x is the distance moved, and increases it in the reverse direction by a similar amount. Under these circumstances the Einstein equation applies:

$$\upsilon_c = \frac{D}{kT} F = \frac{D_v \sigma_n b^2}{kT} \quad \text{.....(2.15)}$$

Where D_v is the vacancy diffusion coefficient, σ_n is the stress component normal to the slip plane and υ_c is the climb velocity. The creep strain rate can thus be derived from Equations 2.13, 2.14 & 2.15.

$$\dot{\gamma} = \alpha \left(\frac{\sigma}{\mu b} \right)^2 \frac{D_v \sigma_n b^3}{kT} \quad \Rightarrow \quad \dot{\gamma} = A \frac{D_v \mu b}{kT} \left(\frac{\sigma}{\mu} \right)^3 \quad \text{.....(2.16)}$$

The dimensionless constant A taking into account that the stress causing climb is proportional to the applied stress, $\sigma_n \propto \sigma$, and that the

average velocity of the dislocation although determined by the climb rate will be larger as some glide between obstacles will occur, $\upsilon_{av} \propto \upsilon_c$.

Equation (2.16) suggests that the stress exponent for steady state creep should be **3**, in fact this applies only to a very few materials including some ceramics and ice, the more general value of the exponent is **5** (applies well to pure metals) but values as high as **10** are found. The reasons will depend on the particular nature of the dislocations and the barriers to motion in each materent. For instance in a super alloy containing a high density of coherent precipitations the dislocation density may not depend on the stress as above, also dislocations may move cooperatively effectively raising the stress dependence.

2.6.2.2. Pipe diffusion at low temperatures:

At low temperatures it is found that the measured activation energy for creep can fall and that the stress exponent rises. The explanation for this is that as lattice diffusion is frozen out, diffusion along the dislocation cores, or pipe diffusion, becomes the dominant mechanism. The activation energy for pipe diffusion is pretty difficult to measure although some values have been determined and the value is close to that for grain boundary diffusion. The effective relative cross section through which diffusion can occur is reduced from one, for lattice diffusion, to the dislocation density times the cross- sectional area of the dislocation core. Since we are assuming that the dislocation density is proportional to the stress squared, this will raise the stress exponent by **2** for pipe diffusion.

$$\dot{\gamma} = A_2 \frac{D_{DC}\mu b}{kT}\left(\frac{\sigma}{\mu}\right)^{n+2} \qquad \text{..…….. (2-17)}$$

Where D_{DC} is the diffusion coefficient for pipe diffusion. On the Ashby diagrams this is labeled 'LT creep' to distinguish it from the 'HT creep' controlled by lattice diffusion.

2.6.2.3. Grain boundary sliding:

As the grains change shape relative movement of the grain centers is geometrically necessary to maintain continuity at the grain boundaries. This has been demonstrated by looking at displacements of scratches and fiduical grids following creep. It can be inhibited by precipitates at the grain boundaries and this may become rate limiting.

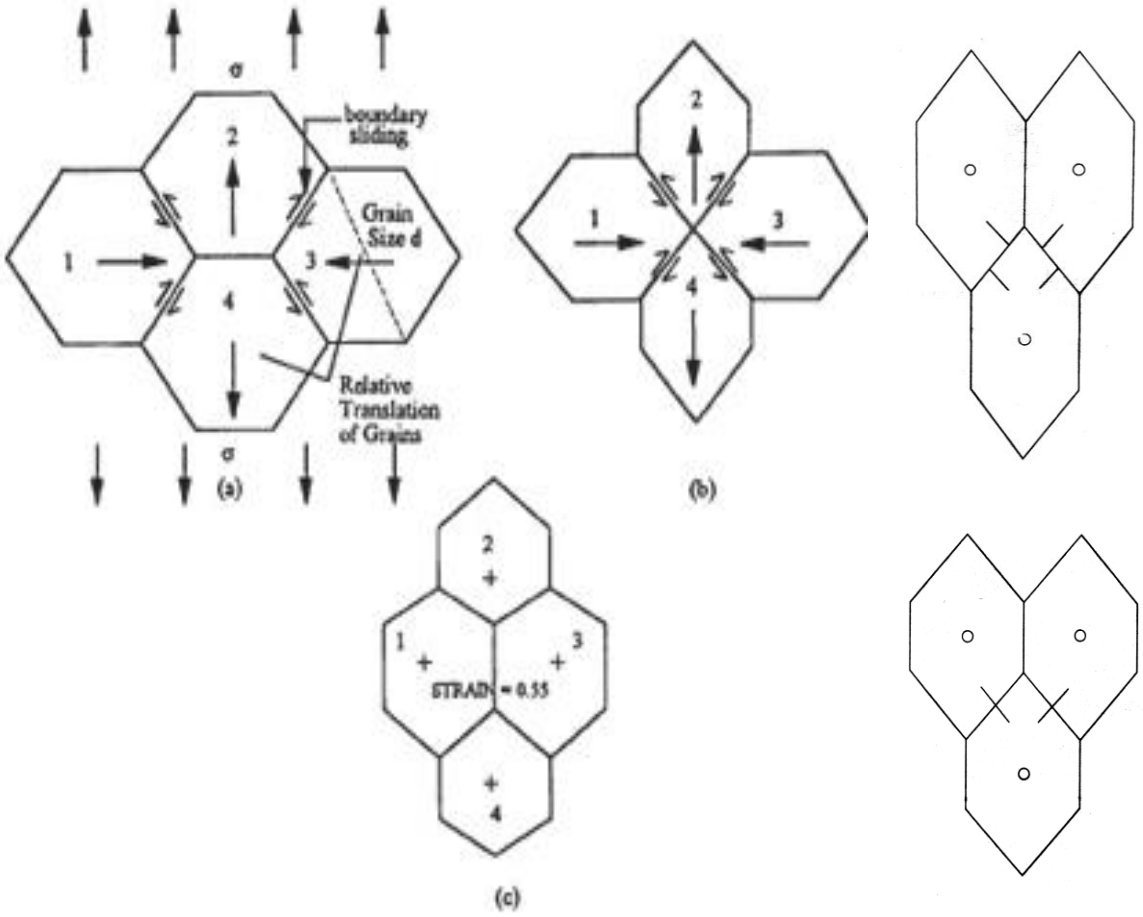

Fig.(2.11) Grain boundary sliding assisted by diffusion in Ashby verral model.[Ashby & Verall, 1973].

2.7. Designing Creep Resistant Materials:

- Use FCC alloys.
- High melting point material.
- Increase grain size or elongate grains in direction of principle tensile stress.
- Add grain boundary precipitates to prevent sliding
- Dispersion hardening.

Chapter Three

Experimental Work

3.1. Introduction:

This chapter deals with the experimental work which was required to study the different parameters for the creep behavior of the prepared Al-alloys and to verify the model results .This experimental work is conducted according to the following steps:

1. Designing and building the test rig.
2. Preparation of creep samples by casting and CNC machining with different alloying elements in slandered conditions.
3. Examining the effect of alloying elements.
4. Creep tests under different parameters.
5. Heat treatment of samples.
6. Metallography.
7. To verify the creep tests and alloying elements, another test was conducted to examine the microstructure, hardness and yield stress by tension. A certain properties were selected as initial properties for modeling analysis process.

3.2. Used Alloys:

The AL-based alloys used in this research are shown in table (3-1):

Table (3-1): AL-base alloys used in this work

Alloy	% Cu	%Mg	%SiC	%Li	%Zr	%Al
A	**4**	**1.5**	-	-	-	BAL
A_c	**4**	**1.5**	**15**	-	-	BAL
B	**2**	**1**	-	**2**	-	BAL
C	**2**	**1**	-	**2**	**0.12**	BAL

As can be seen that the base alloy is **(AL-Cu-Mg)** and the alloying elements are **SiC** powder, **Li**-metal and **Zr** powder. The used materials in this study are shown in the Fig. (3-1).

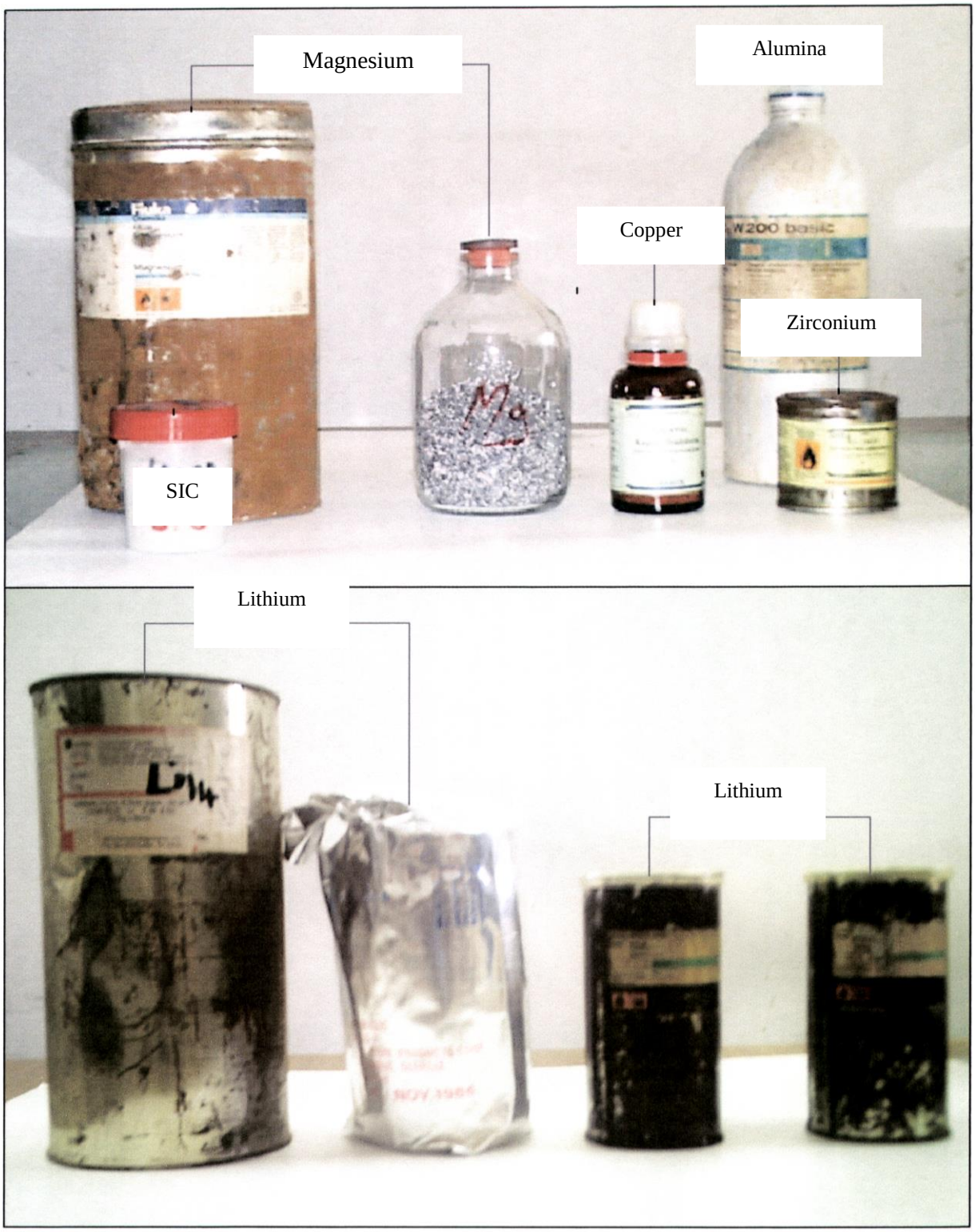

Fig. (3-1) used materials

3.2.1. Sample Preparation:

All specimens were prepared firstly, by casting process and then machined to the required dimensions. These ingots were prepared as follows [Karl B. Rundman].

A- Casting Process:

Casting process includes that, die designing and manufacturing.. The furnace was also, designed and manufactured for ingot production as shown in Fig.(3.2).These ingots were prepared by melting in **(alumina)** crucible under controlled environment **(argon)** and then cast in especially design die Fig.(3.2) Steel die is designed and manufactured with dimension and tolerance with respect to the required ingot as shown in Fig. (3.2).The die was directly quenching in ice cooled water.

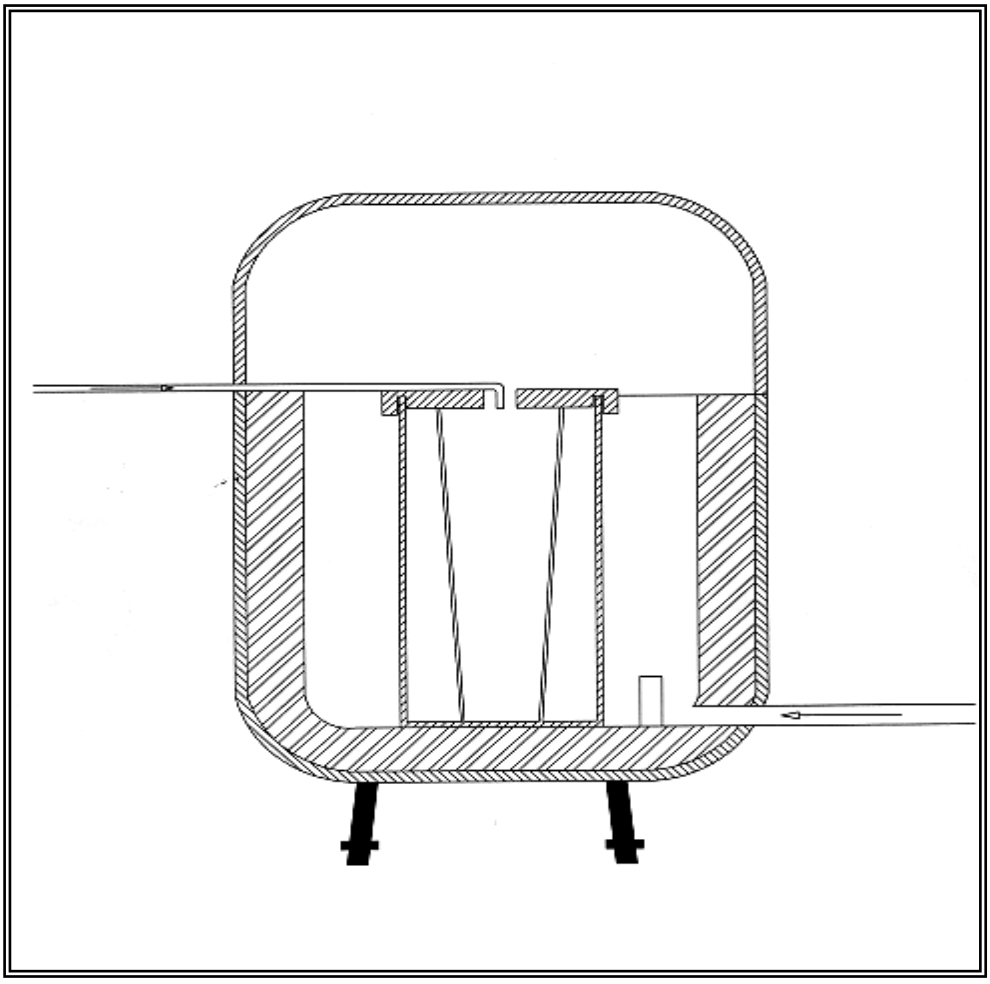

Fig. (3.2): Gas furnace

The design of the mold, however, enhance the **directional** solidifications since it built of **double** layers, and almost the only direction of heat flows from the bottom of the die.

A number of specimens were produced to obtain the same property for samples in the same time Fig. (3.3).

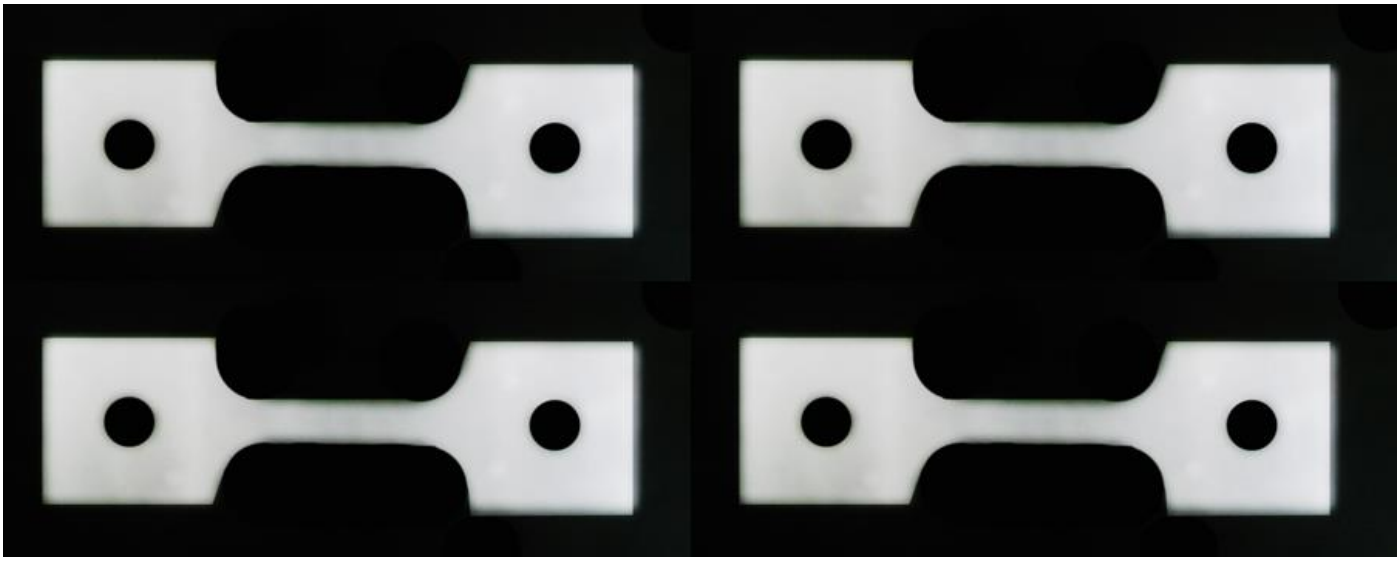

Fig. (3.3): Prepared samples

B- Furnace Design and Manufacture:

LPG. Gas furnace was made to melt aluminum and alloying elements with capacity of about **(10 kg)** max., and temperature range up to about **(1000 C^{o})** when it is closed, as shown in the Fig. (3.1) and (3.4), with **argon** bottle and its accessories,

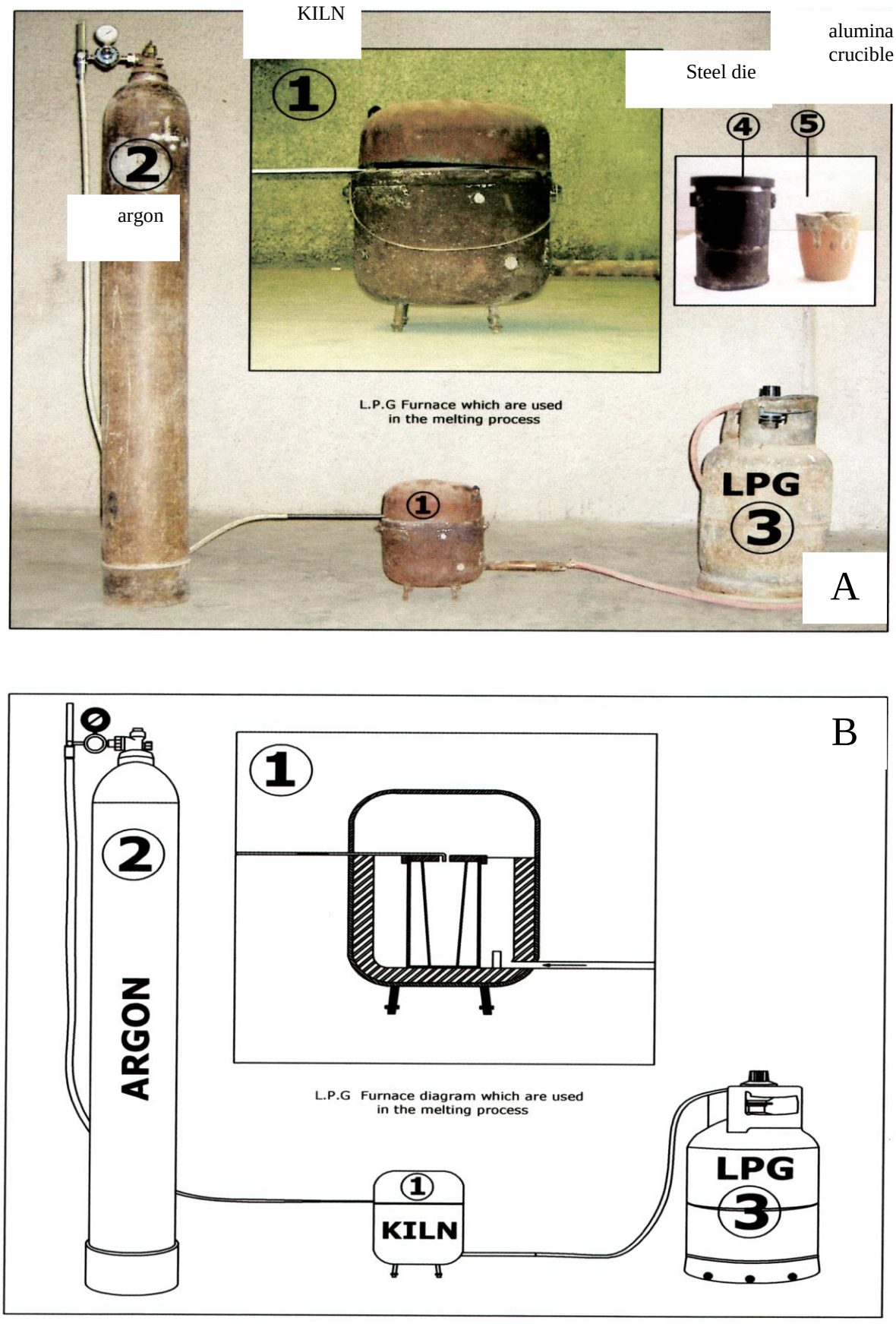

Fig. (3.4): Gas furnace.

A- Photograph B- Schematic

Electric furnace was also built during this work to homogenize and solutionize the aluminum alloy ingots and the samples before creep testing respectively. Its capacity was **(2 kg)** max., and temperature range **(25-1000)°C**, as shown in Fig. (3.5).The ingots were **homogenized** at **500°C** for **ten** hours. The samples were **aged** at **190°C** for **ten** hours.

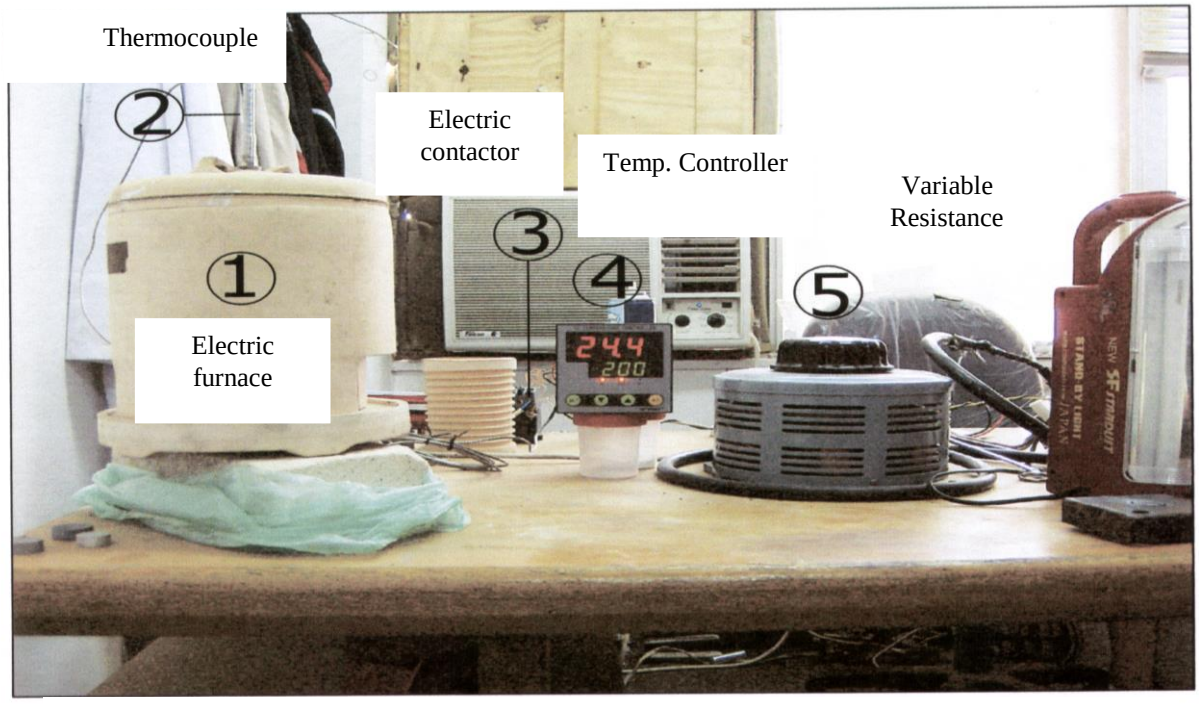

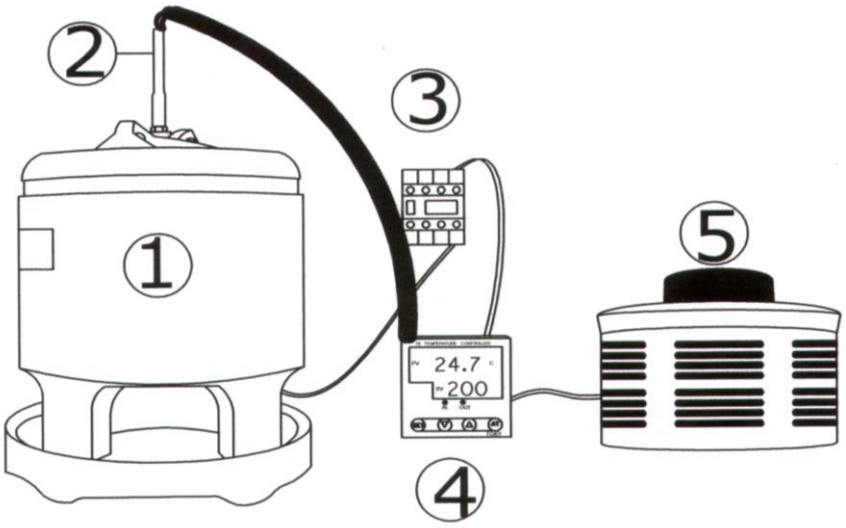

Fig. (3.5): Electrical furnace

A- Photograph B- Schematic

C- Samples Machining:

Samples machining involves the following steps:

1. This process includes the milling process for obtaining sheets of aluminum with **2.25 mm** thickness.
2. Grinding Process: to obtain the final thickness of the sheet **(2mm)** according to the standard sample thickness as shown in Fig. (3.7).
3. CNC vertical milling process: in order to obtain the standard profile of the standard sample, the CNC milling process type (TRIAC/DENFORED) is used as shown in Fig. (3.6).

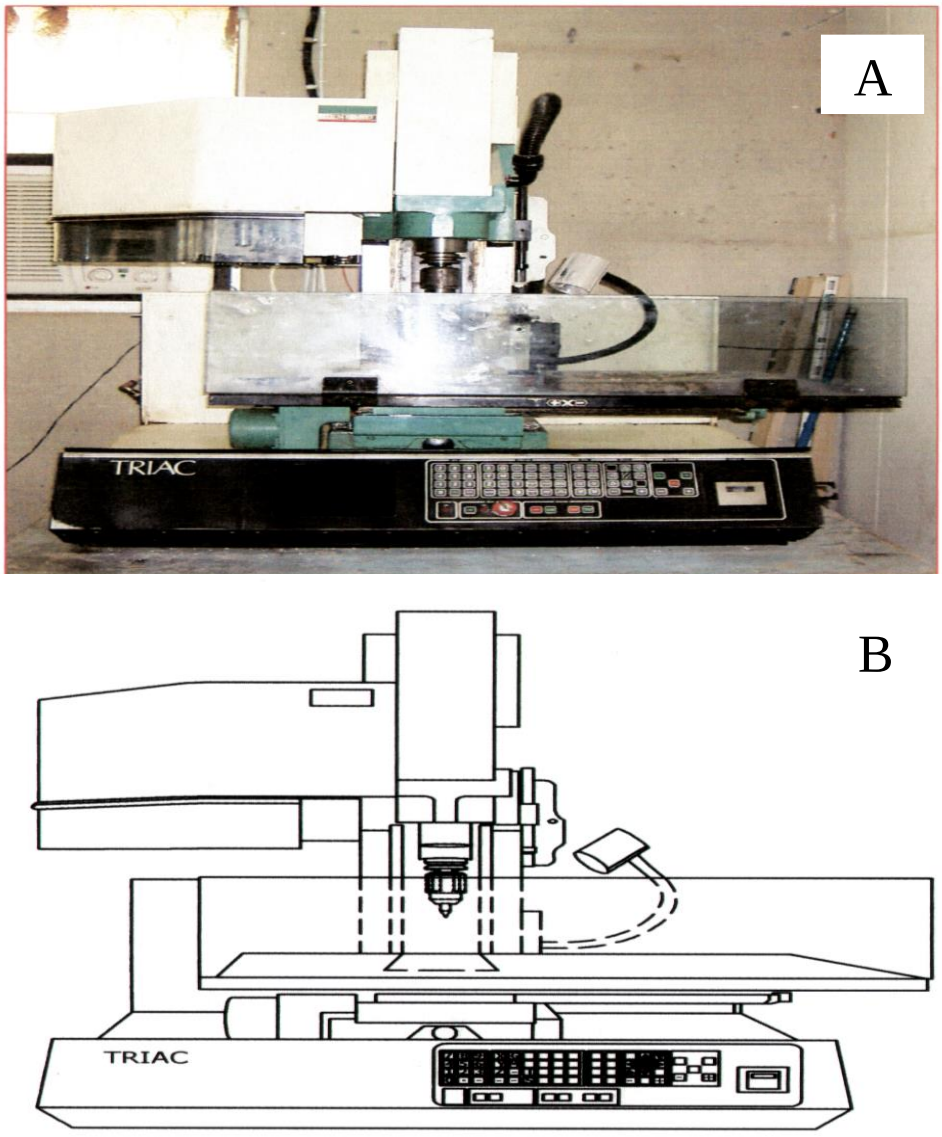

Fig. (3.6) The CNC milling machine

A- Photograph B- Schematic

Fig. (3.7) Grinding machine

3.3. Testing procedure:

3.3.1. Creep test:

After preparing the standard samples which were homogenized, heat treated and was ready for testing, unfortunately, the main test rig was not available in Babylon University and other universities and therefore, it is required to design and built the Test Rig.

A-Creep Test Rig:

Five creep tests Rigs were carefully designed and built with respect to creep sample standard **(E139-83)** as shown in Fig. (3.8A, B, C, D). This rig consists different new components for giving more flexibility to carry out the creep test under different conditions (Temp., Stress, time), these components are:

1. Frame.
2. Heating system (electric heater, controller, variable resistance).
3. Strain measurement system (dial gauge, fixture).
4. Loading (loads, holders, initial load system).

B

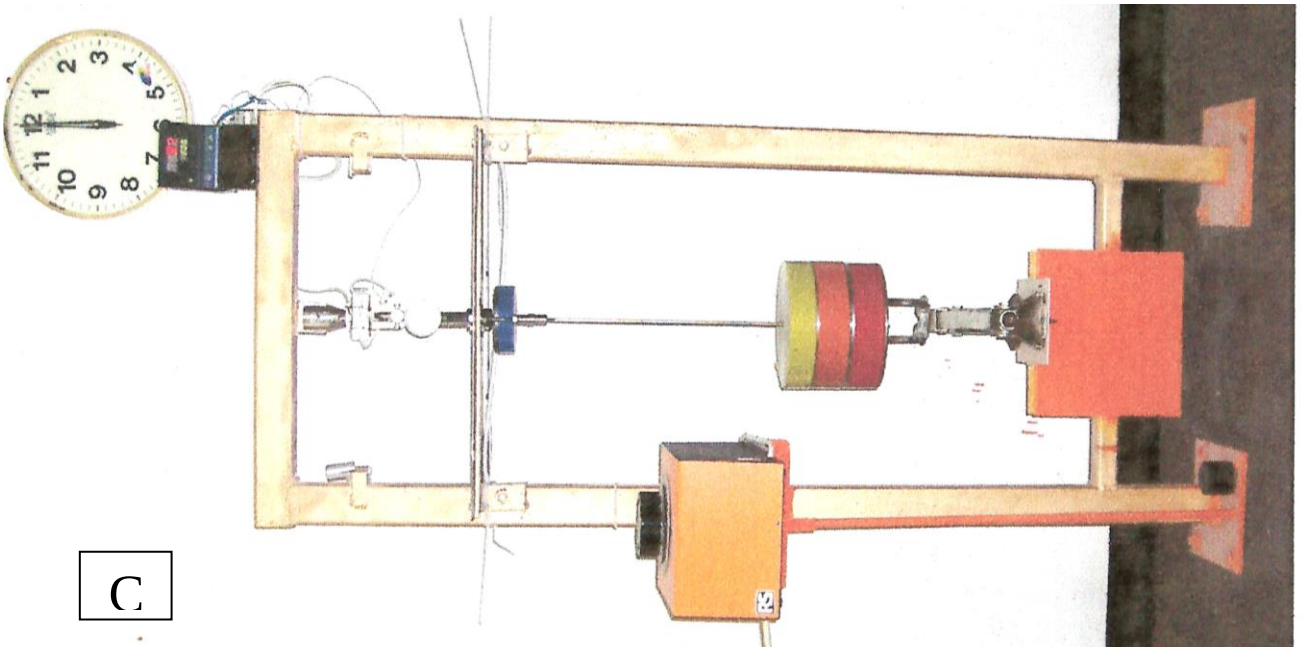

C

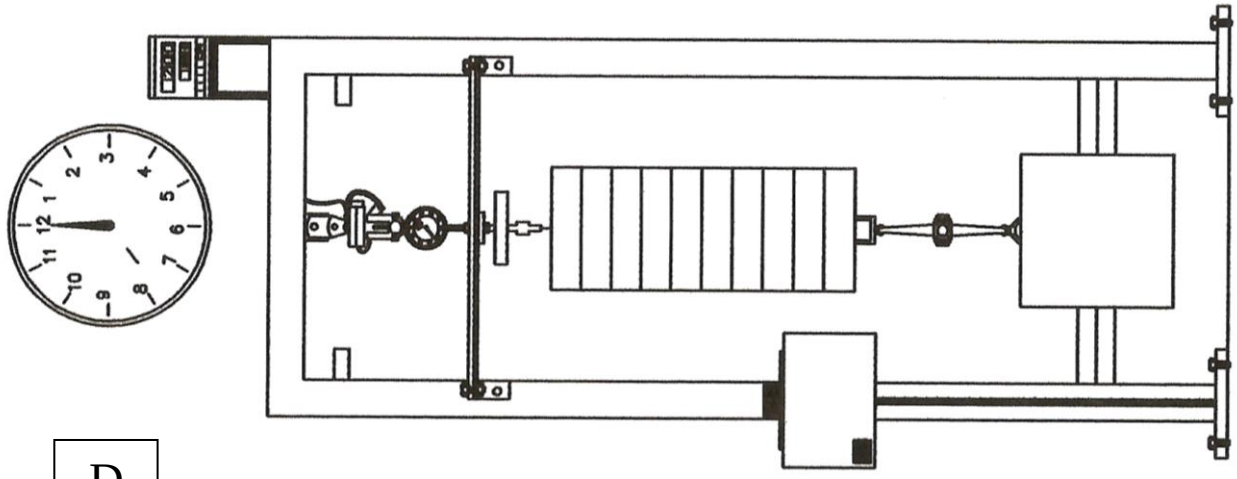

D

Fig. (3.8 A, B, C, D): Creep test rig

A,C- Photograph B,D- Schematic

The temperature on t he sample is adjusted by a control system , with **± 1ºC** Fig. (3.9). The heat source is designed for giving a constant heat flux on the creep affected samples by using a variac of a current rate **(0.2-0.5) Amp.** and **(80-100) AC Volts**.

This Varity in temperature was **± 1°C** and the sensor (thermocouple) was placed near the center of the sample to give the accurate temperatures readings. Others parts of the creep rig are shown in Figs. (3.9), (3.10), (3.11), (3.12).

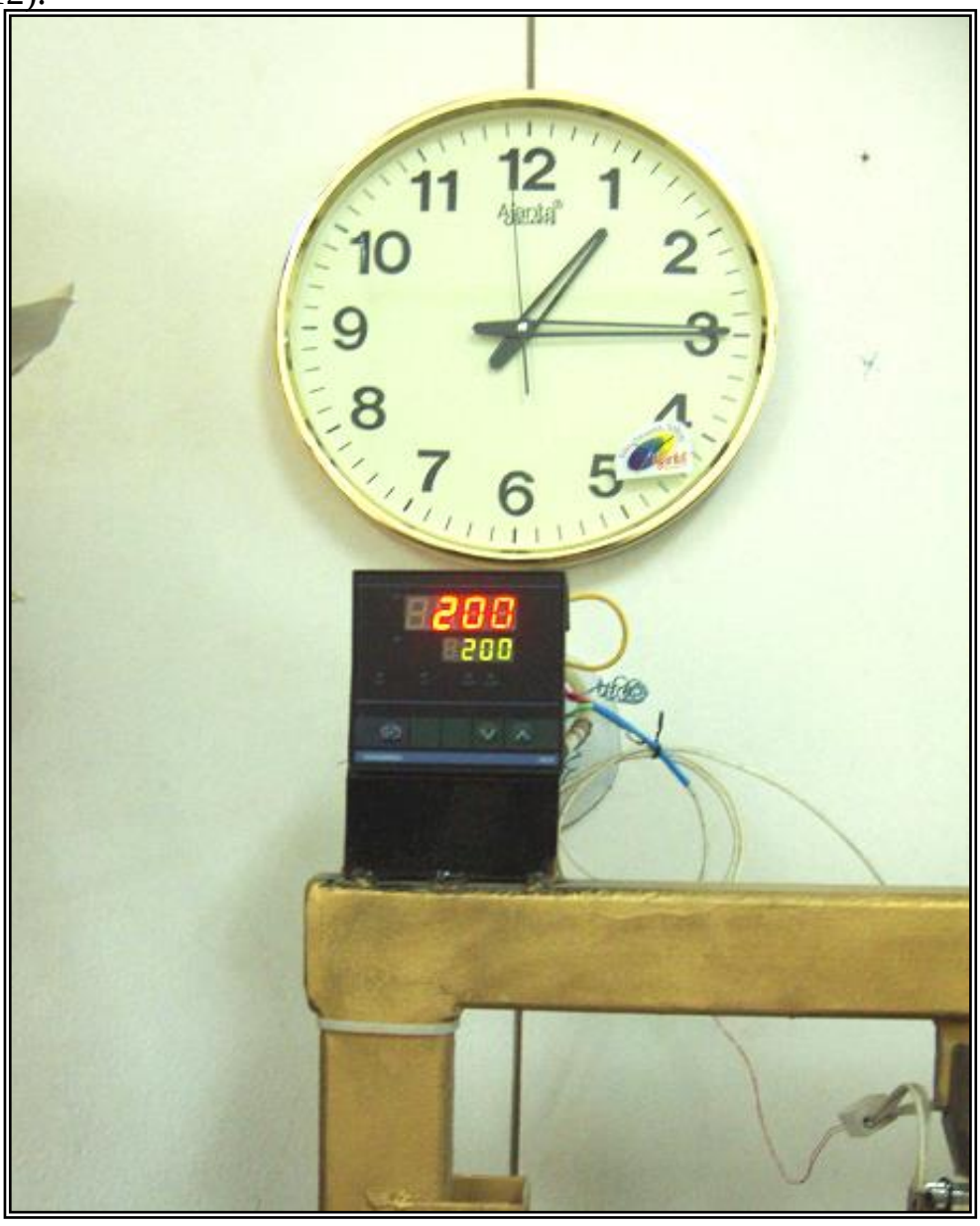

Fig. (3.9): Control system

The stress on the sample applied as a uniaxial stress by using a load weight, which are carrying by the initial loading system as shown in the Fig. (3.10).

Fig. (3.10): The loading system.

The strain was measured by measurements system which consists of dial gauge with **(10^{-3})** mm accuracy fixed on the rigid frame and attached to the transmitted bar which is fixed at the lower sample holder as shown in the Fig. (3.11A, B).

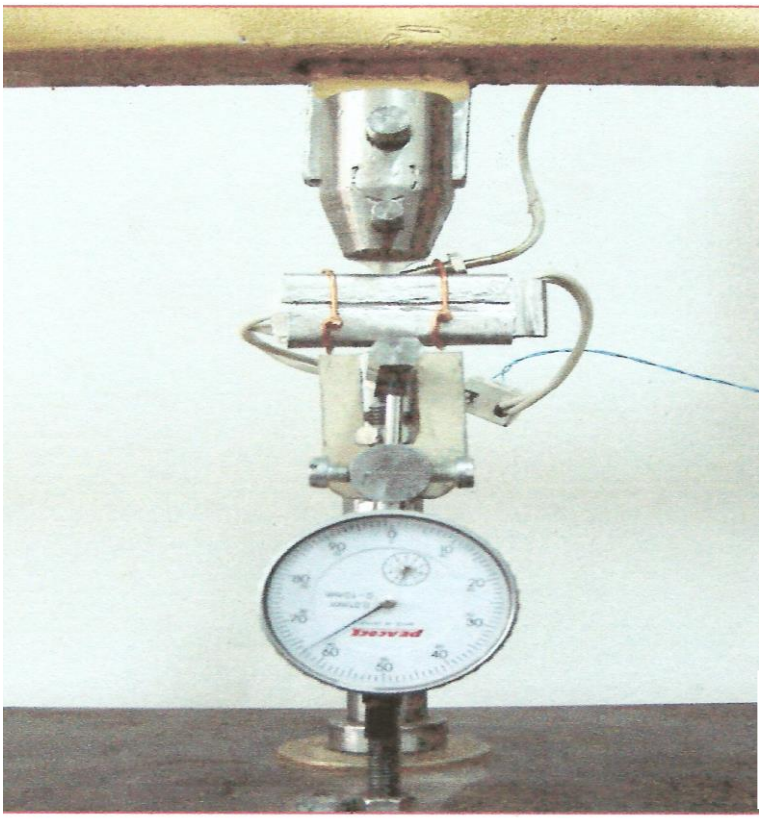

A

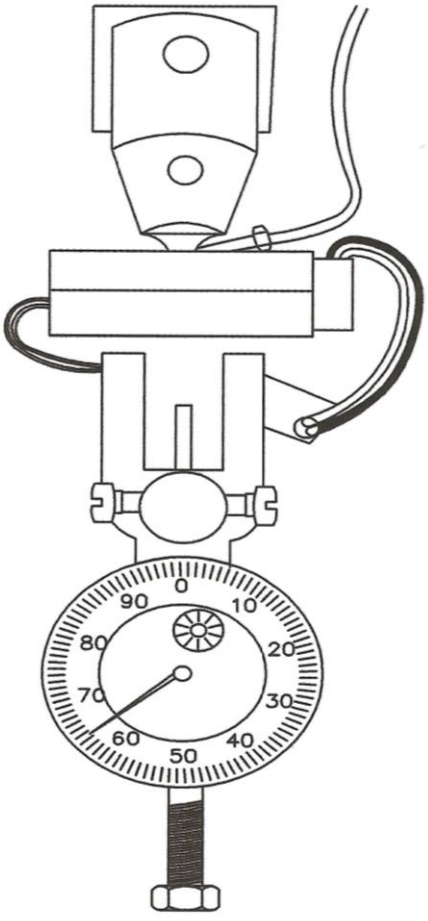

B

Fig.(3.11A, B): Measurements system

A- Photograph B- Schematic

B- Testing Procedure:

The creep test includes the following steps:

1. Clamping the sample from upper end by the holder which is fixed on the frame and the load was applied by stainless steel hang.
2. Heat is supplied to the specimen by electric contact furnace up to the constant condition this was achieved within **(5)** minutes.
3. After that time, the applied load is supplied on the specimen by relieving the reaction force which supports the weight i.e. manual (Jack).
4. The strain and time were recorded until the end of the test.
5. All the previous steps were repeated for different types of alloy.
6. The load and temperatures were changed.

3.3.2. Tensile Test:

The tensile test was carried out by using the (Instron / PHYWE - AG / W. Germany) after introducing modification to determine the Modules of Elasticity **(E_m)** and the Ultimate Tensile Strength **(UTS)** for different aluminum alloys with temperature up to **260°C** as shown in Fig.(3.12A, B). These properties were used in the modeling process for creep phenomenon analysis by using ANSYS software.

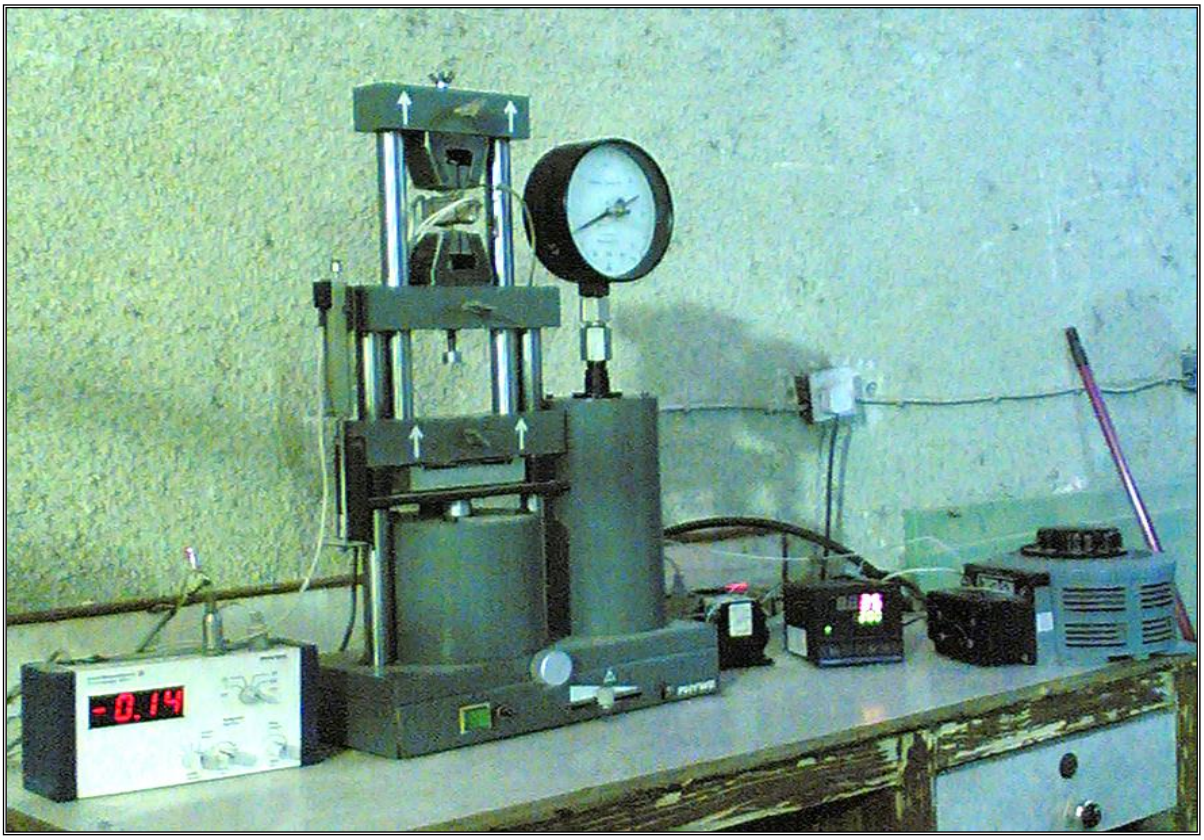

Fig. (3.12A): Tensile Test Rig

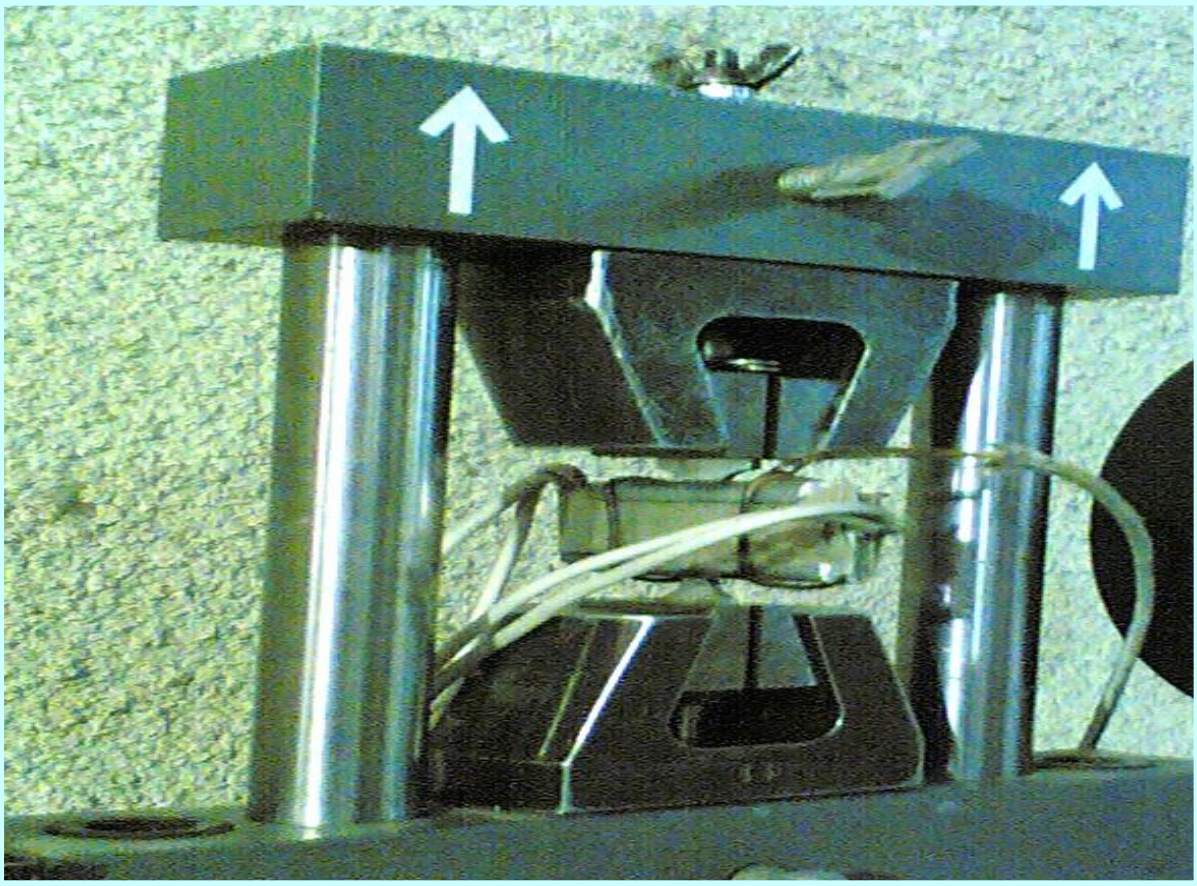

Fig. (3.12B): Modified High Temperatures Tensile Test Rig

3.4. Microstructure Inspection:

Different techniques are used to inspect the alloys microstructure with different alloying elements to insure the existence of the second phase particles and its volumetric the fraction in the (Aluminum) matrix. These techniques are:

1. X-Ray diffraction:
2. The scanning microscope:

   The (SEM) is used to scan the surface texture for the specimen to capture the microstructure images shown in Fig.(3.13A).This test is conducted on the specimen after surface treatment by polishing and etching with (killer) etching solution.

A

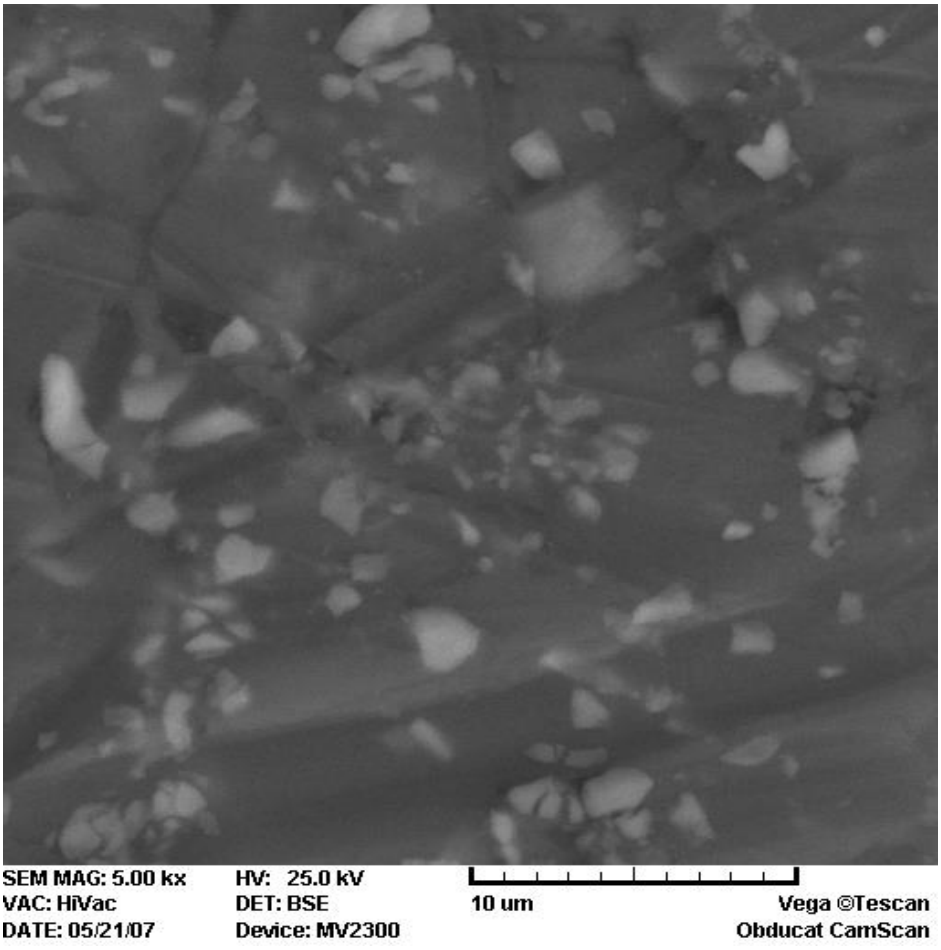

Fig. (3.13A**): Scanning microscope analysis of C alloy.**

3.5. Modeling and Theoretical Analysis of Creep

Phenomenon:-

Two types of models were used the first is micromechanics model to evaluate the affect of alloying elements on alloys modulus of elasticity. The second one was to describe the creep test (micromechanics) according to the first model results.

3.5.1. Modeling Process:

3.5.1.1. Modeling process assumptions:

To simplify the modeling process for creep phenomenon in Al-alloy, there are multi assumptions which are depended on as follows:

1. The creep model was described for uniaxial creep.
2. The materials properties which are used in the model for the different Al-alloys are isotropic property.
3. The applied temperature was uniform and the heat flux is study state.
4. The affected zone is applied to constant temperature.
5. Two dimensional models was used to describe the creep phenomenon.
6. The micro- mechanic model depends on rule of mixture in the defined of the matrix and strengthening partical phase.

The strengthening partical phase property is taken from literature review according to previous expected.

3.5.2. Models Constituents:

Two dimensional models are built the firs one describe the effects of alloying elements on the creep phenomenon in aluminum alloys depends on the micro mechanics approach and the second model is used to simulate the creep test of aluminum alloy under heat and local condition and depends on macro mechanic approach the stage of the model building is as follows:

3.5.3. Micro mechanics Approach:

Two dimensional model was created consists of the Aluminum matrix and second phase particle with unit cell as shown in Fig. (3.14)
The procedure to create this model is described as follows:

1- Image processing: includes three steps which:

A- read the image and input it as variables in the matlab by using the following statement.

```
I = imread('c:\d2.jpg');
```

B- remove the second phase color and convert the image variable to the matrix: by using the following statement.

```
level = graythresh(I);
```

C- create a matrix of the points which have the (1) value by using the following statement.

```
BW = im2bw (I, level);
```

2- convert the matrix to the ANSYS file:

A- read the points which have the (1) value. By using the following statement.

```
num1=0
for y=1:512
for x=1:512
if (BW(y,x) == 1)
num1 = num1 +1;
```

```
End;
End;
End
```

B- Rearrangement the ANSYS file. by using the following statement.

```
fid = fopen('c:\f2temp.txt','w+');
fprintf(fid,'/BATCH  \n');
fprintf(fid,'/COM,ANSYS RELEASE  5.4    UP19970828        19:52:52
10/30/2007\n');
fprintf(fid,'/input,menust,tmp     ,,,,,,,,,,,,,,,,1\n');
fprintf(fid,'/GRA,POWER\n');
fprintf(fid,'/GST,ON\n');
fprintf(fid,'/PREP7\n');
fprintf(fid,'FLST,3,%u,8\n',num1);
for x=1:512
for y=1:512
if (BW(y,x) == 1)
fprintf(fid,'FITEM,3,%u,%u,0\n',x,y);
end;
end;
end
fprintf(fid,'K, ,P51X\n');
fclose(fid);
```

the result of image processing are as shown in Figs. (4.15, 4.17)

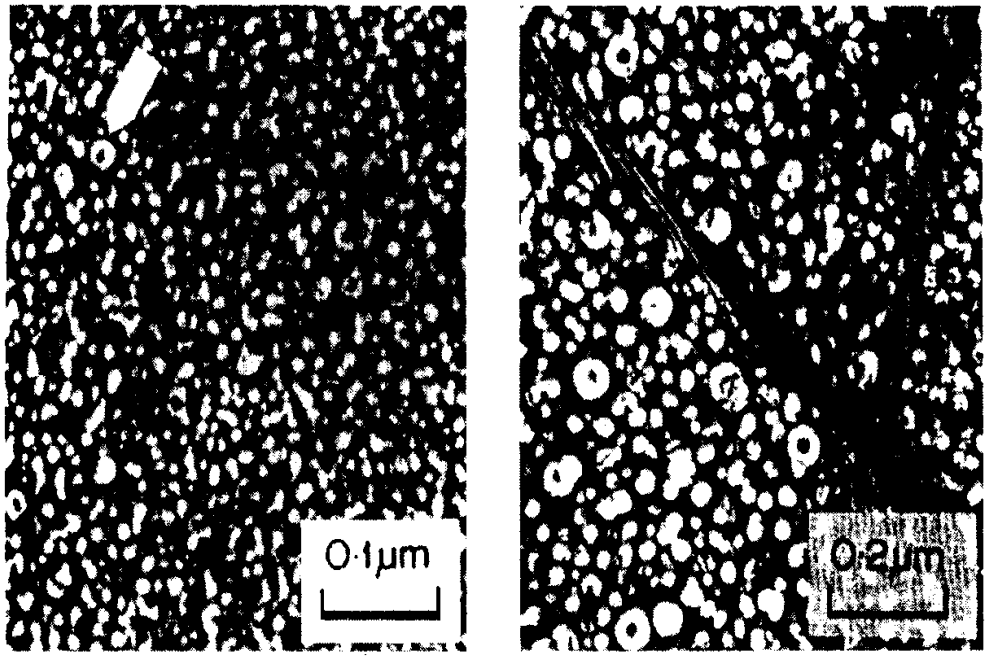

Fig.(3.13B) a- Particles of [δ'] precipitate in an Al-Li-Mg-Zr alloy at 190°C.The arrow indicates a[δ']precipitate that has, . nucleated on an Al_3Zr particle [Grgson, 2002]. . b-Shearing of[δ']precipitates leading to strain location in . a deformed Al-Li-Zr alloy [Lloyd, 1985].

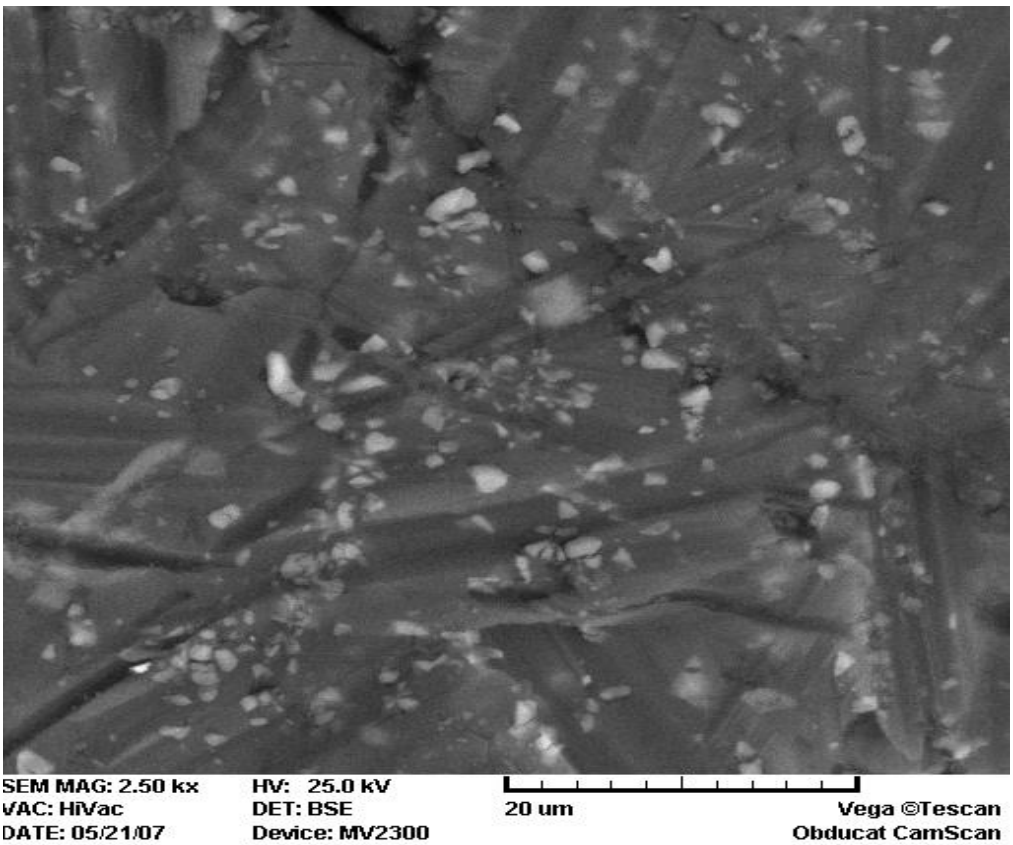

Fig. (3.14) Scanning image of C alloy

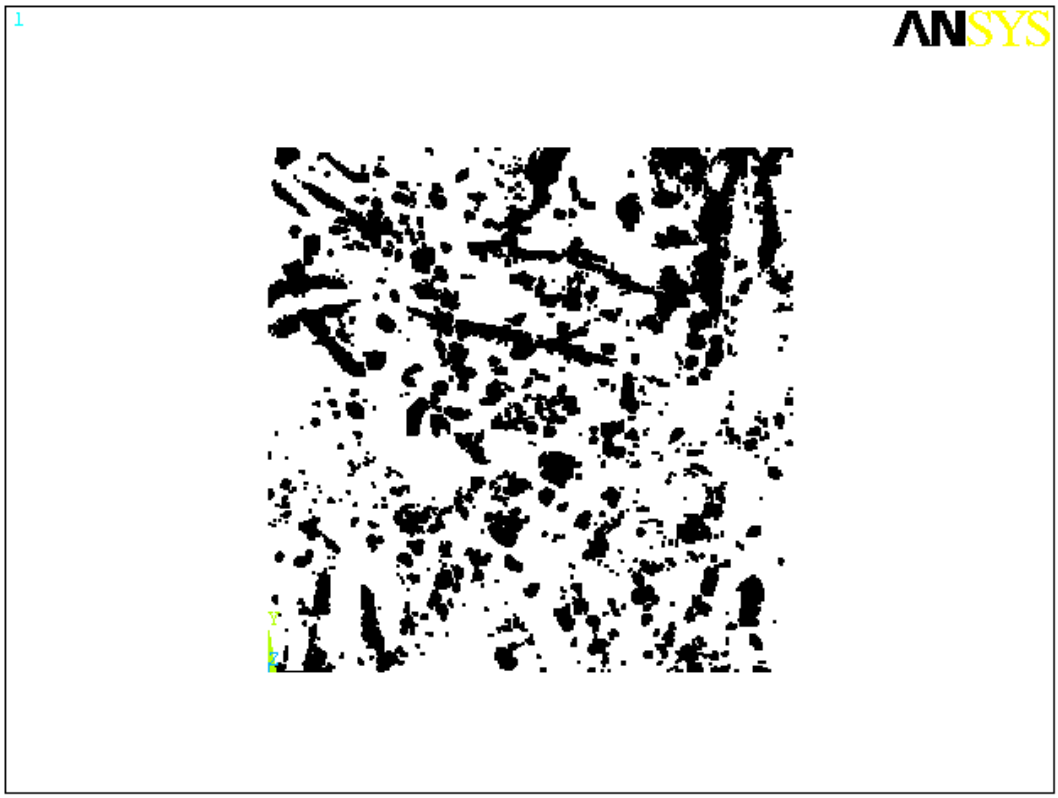

Fig. (3.15) Image processing

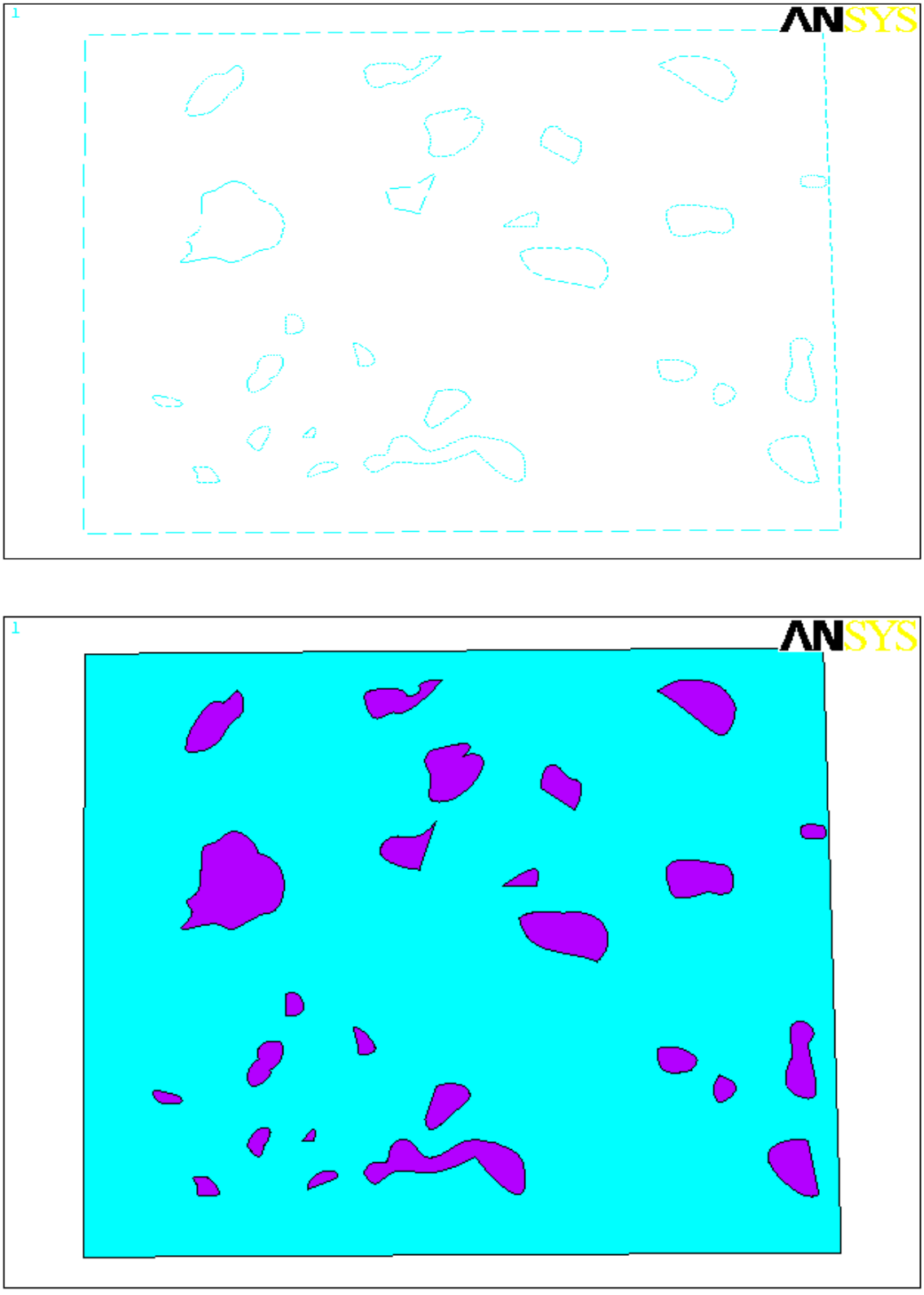

Fig. (3.16) Unit cell micromechanics

The materials which are used in this model are shown the Table (3.4).

Table (3-4): The properties of material in micro model

Material	E(GPa)	UTS(MPa)	T(°C)
AL	65	300	35
AL_2CuMg	160	370	35
SiC	200	600	35

3.5.3.1. Element generation:

The unit is meshed in size as shown in Fig. (3.17)

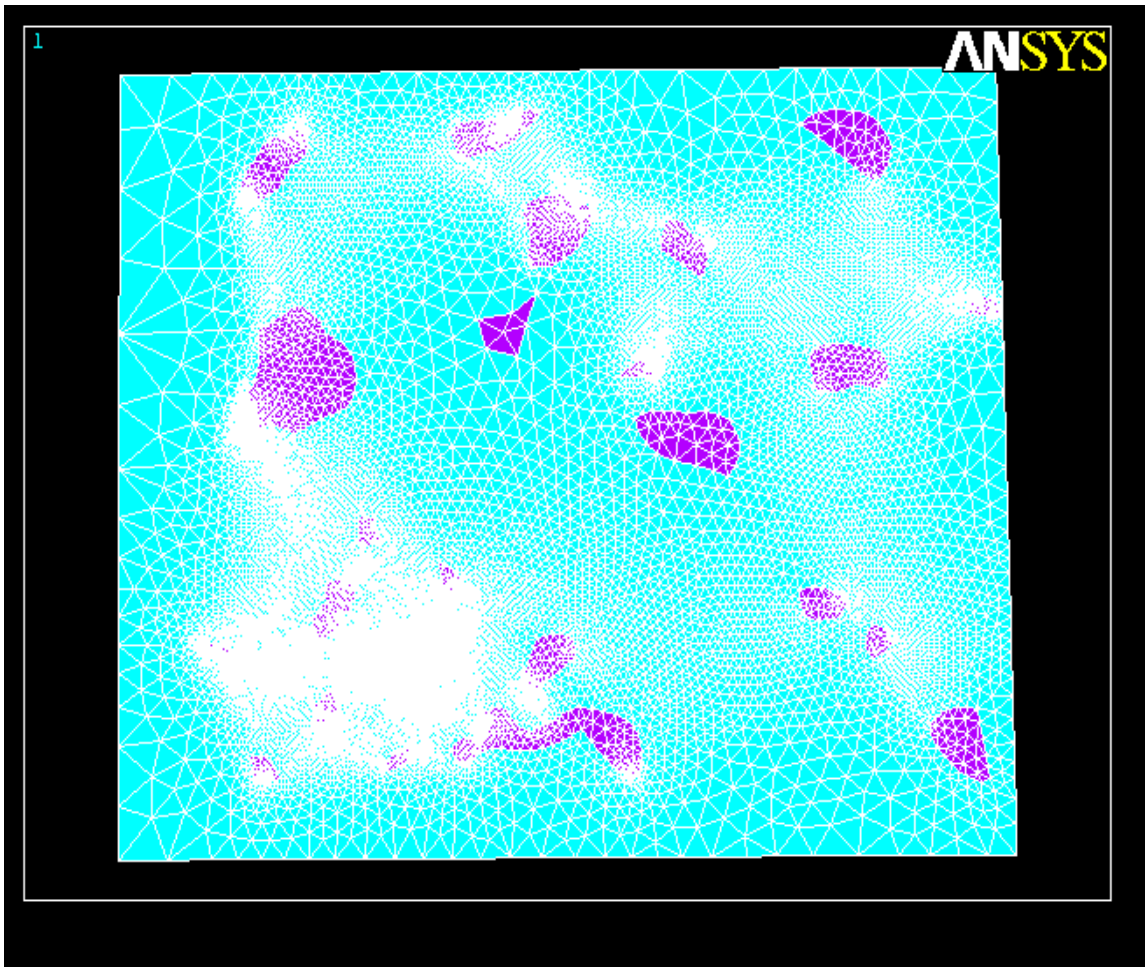

Fig. (3.17) FE micro model

The plane (42) element type is used to describe the aluminum behavior in elastic range and the type plane 42 for the particle strengthening phase as shown in Fig. (3.18)

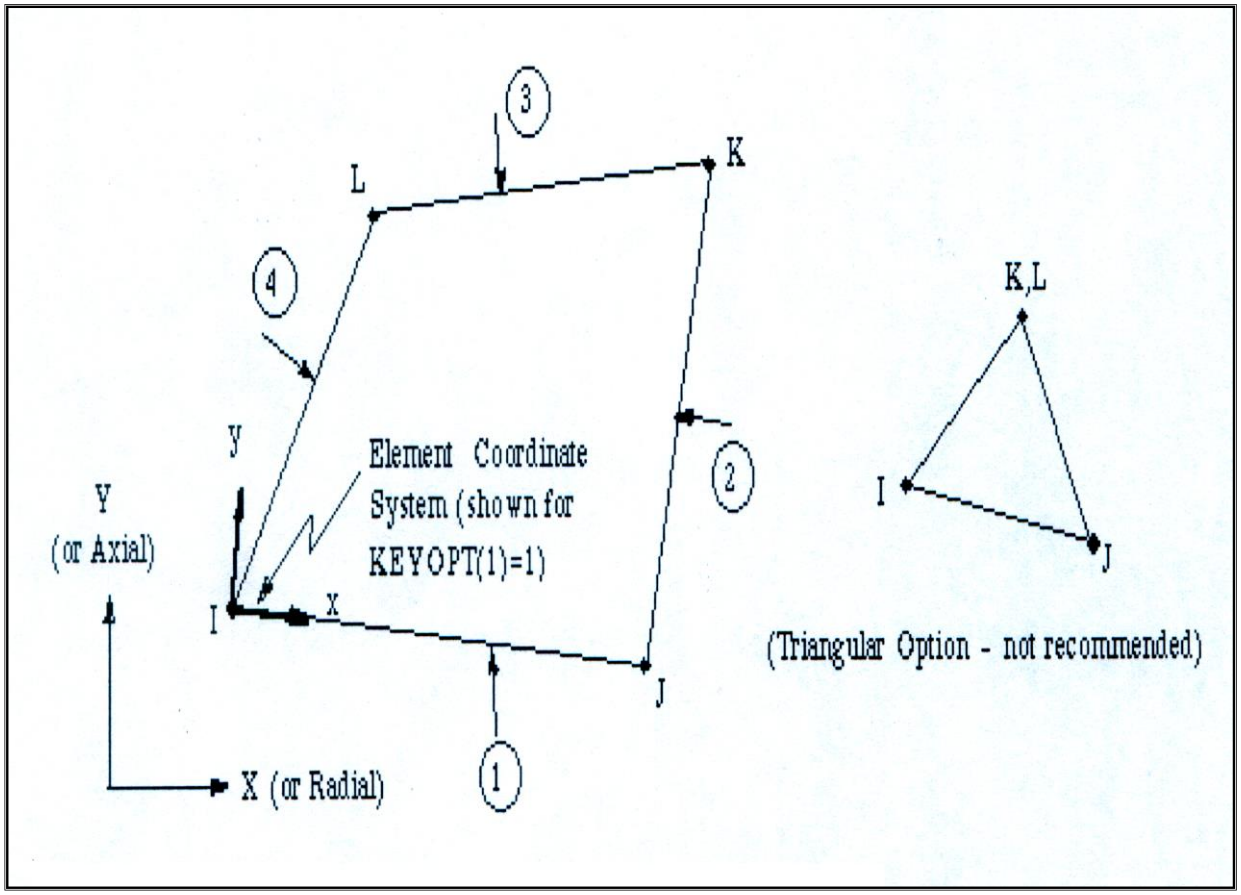

Fig. (3.18): The element type and characteristic

A

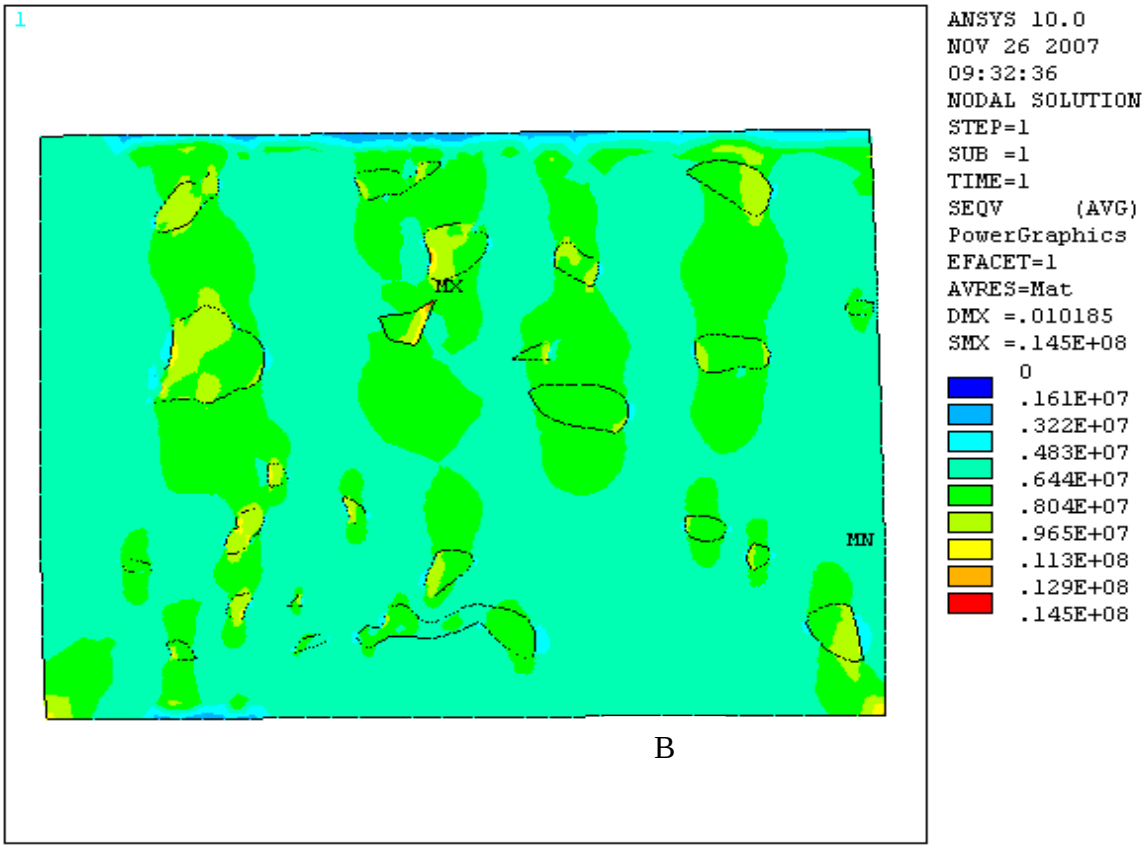

B

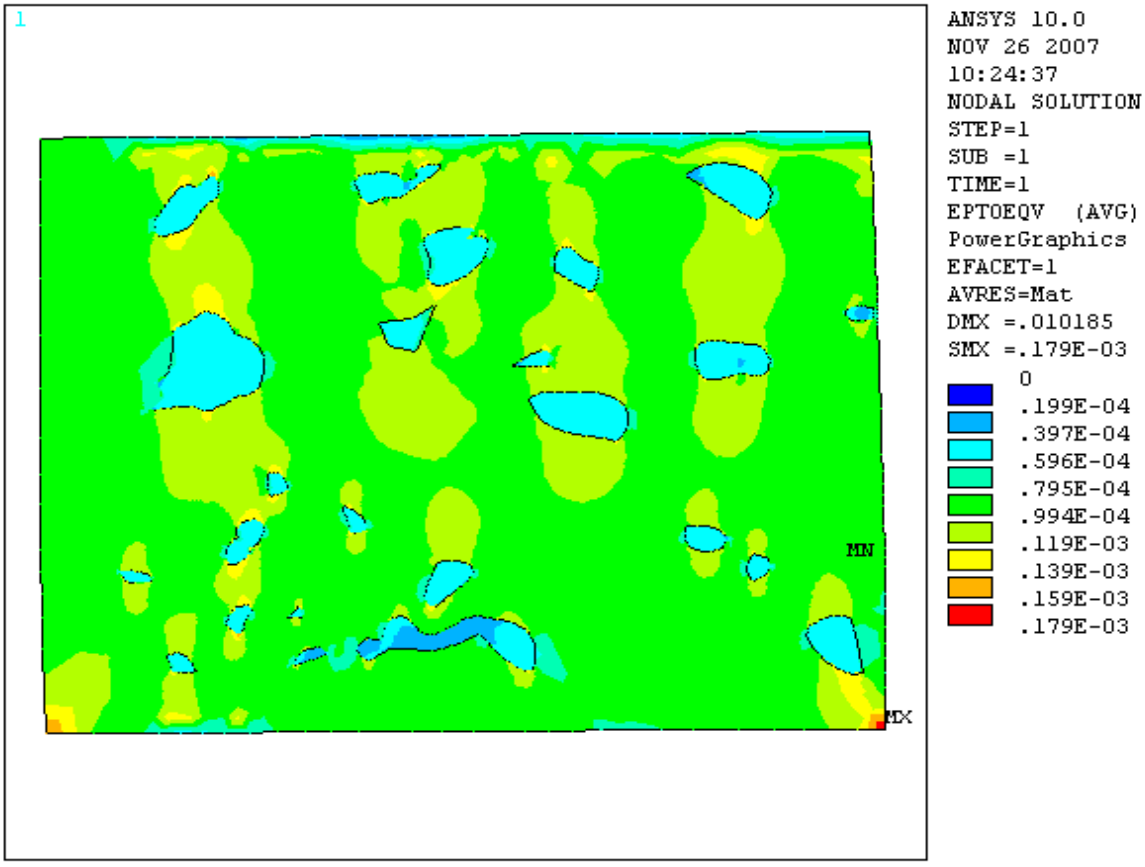

Fig . (3.19) FE micro model results

A-stress B-strain

3.5.4. The Marco mechanic approach (Creep Test):

Two dimensional macro mechanic mode is built to describe the creep test with different aluminum alloy (master alloy & alloying elements), the geometry sub- model of this test is shown in Fig. (3.20).

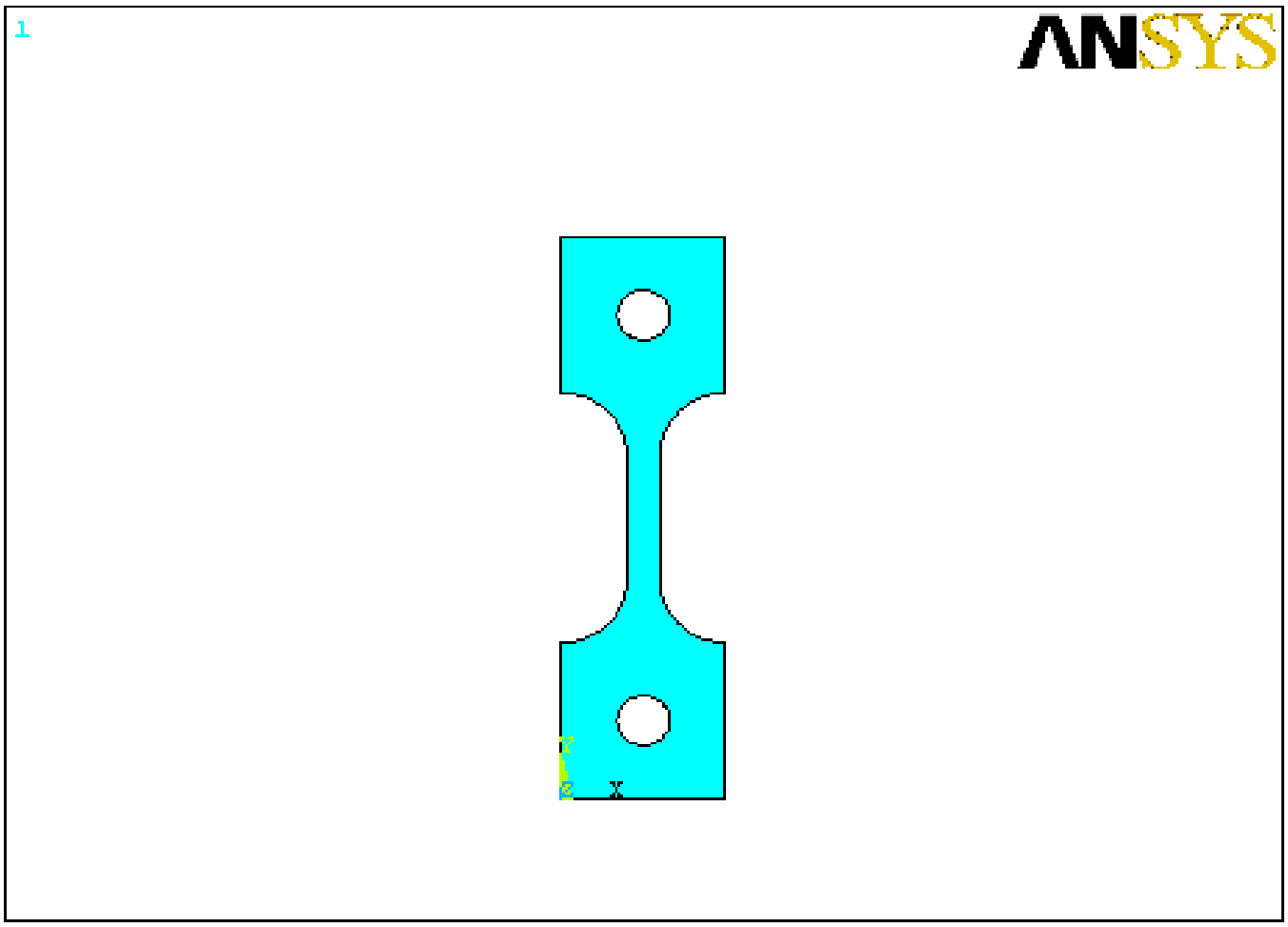

Fig.(3.20):The geometry sub model of creep test with dimension in mm

The material properties for the alloy which are used in this model are taken from the micro mechanic results of alloying element effect also these properties are compared with the experimental properties for the same test in the compression test. These properties are shown in the Table (3.2).

Table (3-2)

Material	E(GPa)	UTS(MPa)	T(°C)
AL	65	300	25
AL-Cu-Mg-	68	360	25
AL-Cu-Mg- SiC	92	400	25
AL-Cu-Mg- Li	75	370	25
AL-Cu-Mg- Li-Zr	80	465	25

The mesh generation is achieved by using the element plane 42 element type as shown in Fig. (3.18) which is containing the creep behavior function, the mesh size with dimensional are generated as shown in Fig.(3.21) .

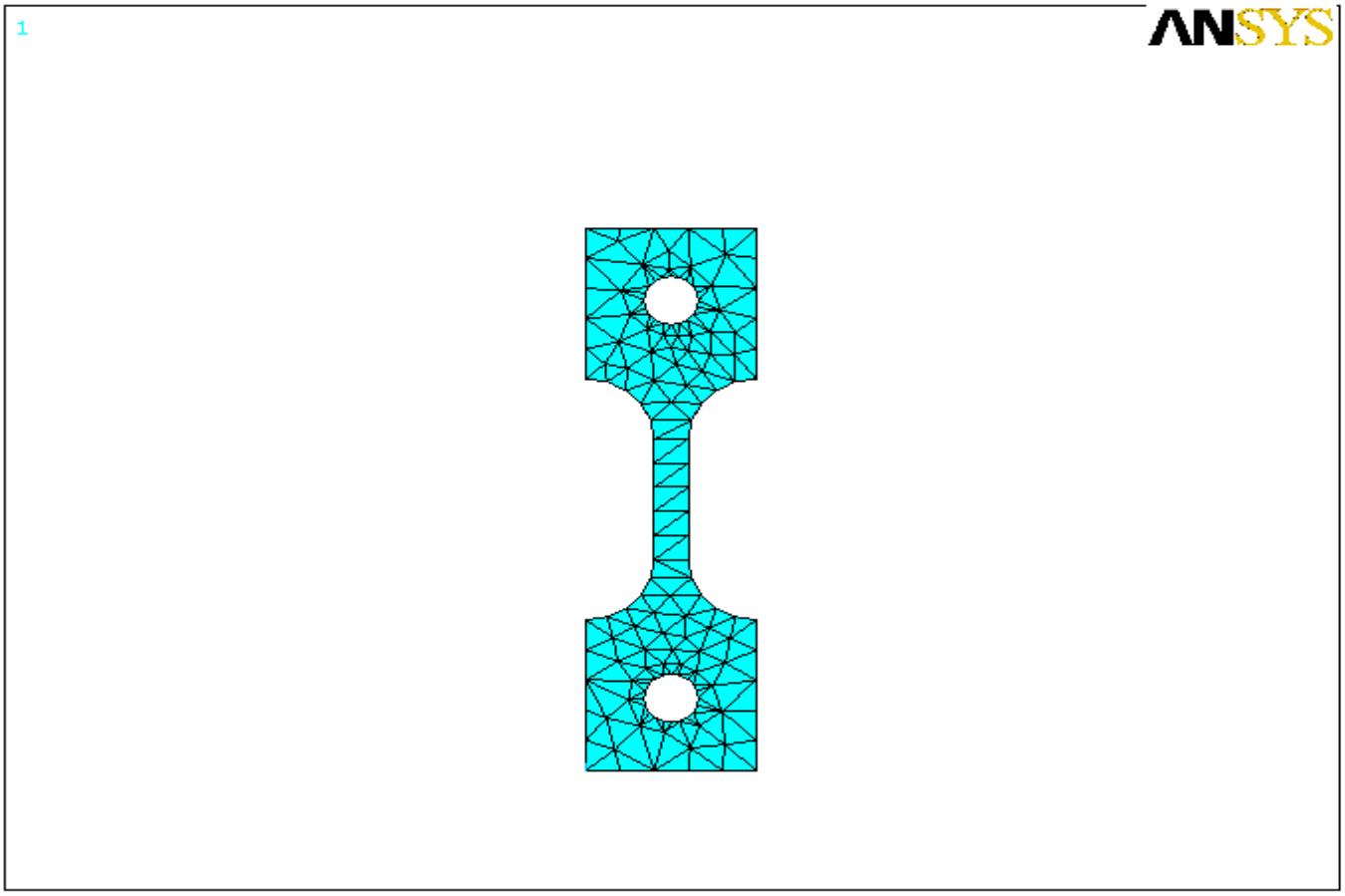

Fig. (3.21) FE of macro model

3.5.5. Parametric Study:

The numerical modeling is conducted to study the effect of different parameters that affected on the creep analysis in the Al-alloys. The parameters which are studying in this model are:

1. Alloying element: the alloying elements are **Li, Zr** with percentage **2%** and **0.12%** respectively.
2. Creep test temperature is from **(175 to 260)°C**, these values are calculate according to alloy temp. **(T > 0.3 T_m)**
3. Applied Stress: the values of applied stresses which are used in the simulation are varying from **(100–180) MPa** .
4. Time: The steady state case is used in the model which are represented the secondary stage of creep time which are used in this function is from **(1 to 25) hrs**.

3.5.6. Boundary condition:

To obtain the stable model for creep test in the modeling process, multi nods on the fixed region is constricted in X and Y dimensions (Ux and Uy = O) as shown in Fig (3.22).

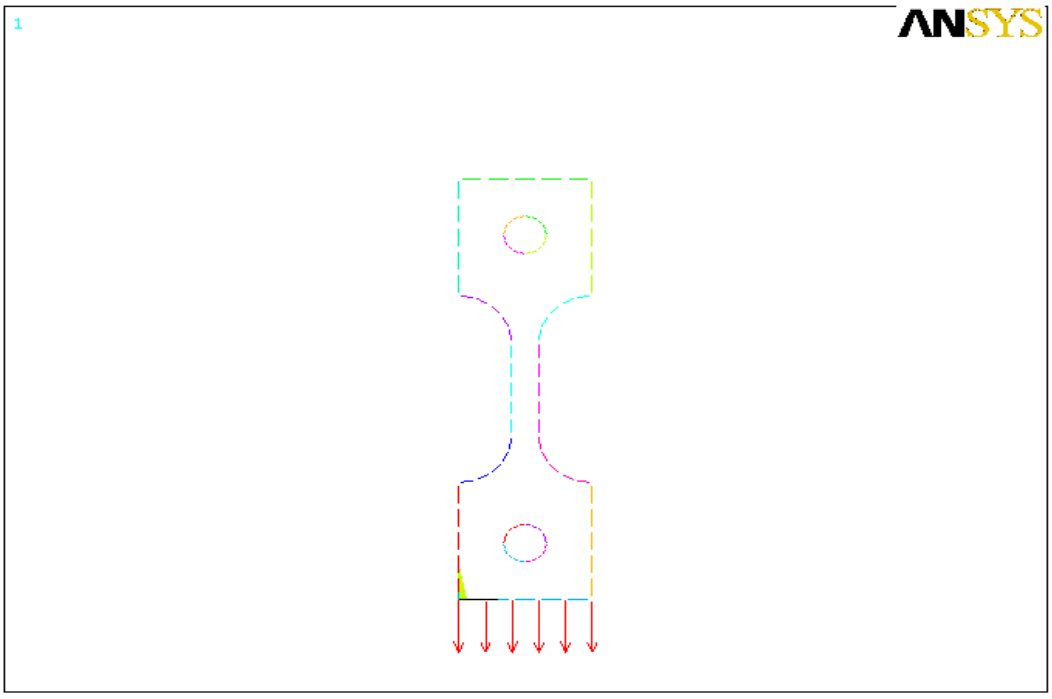

Fig. (3.22) boundary condition

1. Temperature is applied on the creep affected area according to its value.
2. the applied force is fixed on nodes in the

3.5.7. The Output Results:

The numerical results was recorded at every sub-step with time step (1h) for Ux, Uy and U some for the every node on the models as a counter results and curve results as shown in Fig. (3.23) From the first step and last step for every parametric study at under any condition which are studied. The discussion and conclusion which compared with experimented results in the chapter **4.**

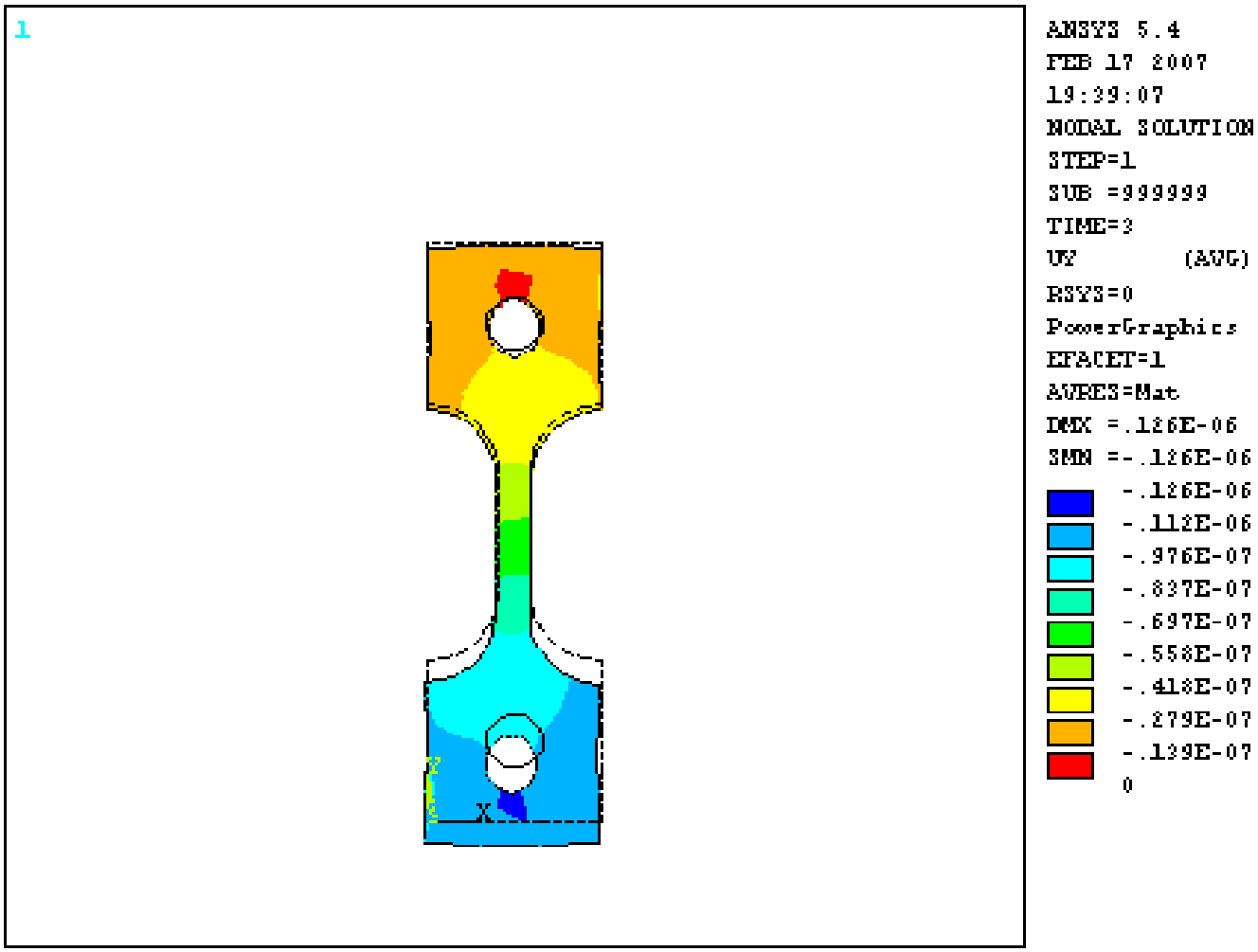

Fig. (3.23) FE micromechanics contour results.

Chapter Four
Results and Discussions

4.1. Introduction

It is well established that operations of engineering component at elevated temperature is associated with decrease in strength and an increase in hostile environment.

Deformation occurred such high temperature, however, happened by creep, (time dependent strain) which operated by certain mechanisms depends on the working conditions.

This chapter deals with the possible improvement introduced by alloying elements, and heat treatment on high temperature behavior of the examined alloys.

A Theoretical analysis was also adopted.

4.2. Effects of Temperature on Modulus of Elasticity (E_m) for Alloy (A) :-

Fig (4.1) represents the relationship between Modulus of Elasticity and temperature. Each point is an average of two readings of tensile test at various temperatures.

It seems that the modulus of elasticity (E_m) varied almost inversely with testing temperature. It is a famous fact that **(E_m)** is a material property. It can be concluded that, it is the change in the microstructure which caused the variation of the **(E_m),** since, it can be expected that the microstructure is changed in such away that it causes variations in **(E_m).**

The possible rotation within crystallography of the building cells is unlikely. Such behavior is also observed in **(Ni/Ti) shape memory** alloys when the **(E_m)** and the yield strength change with temperature which controls the microstructure [Abdul-Raheem, 2007].

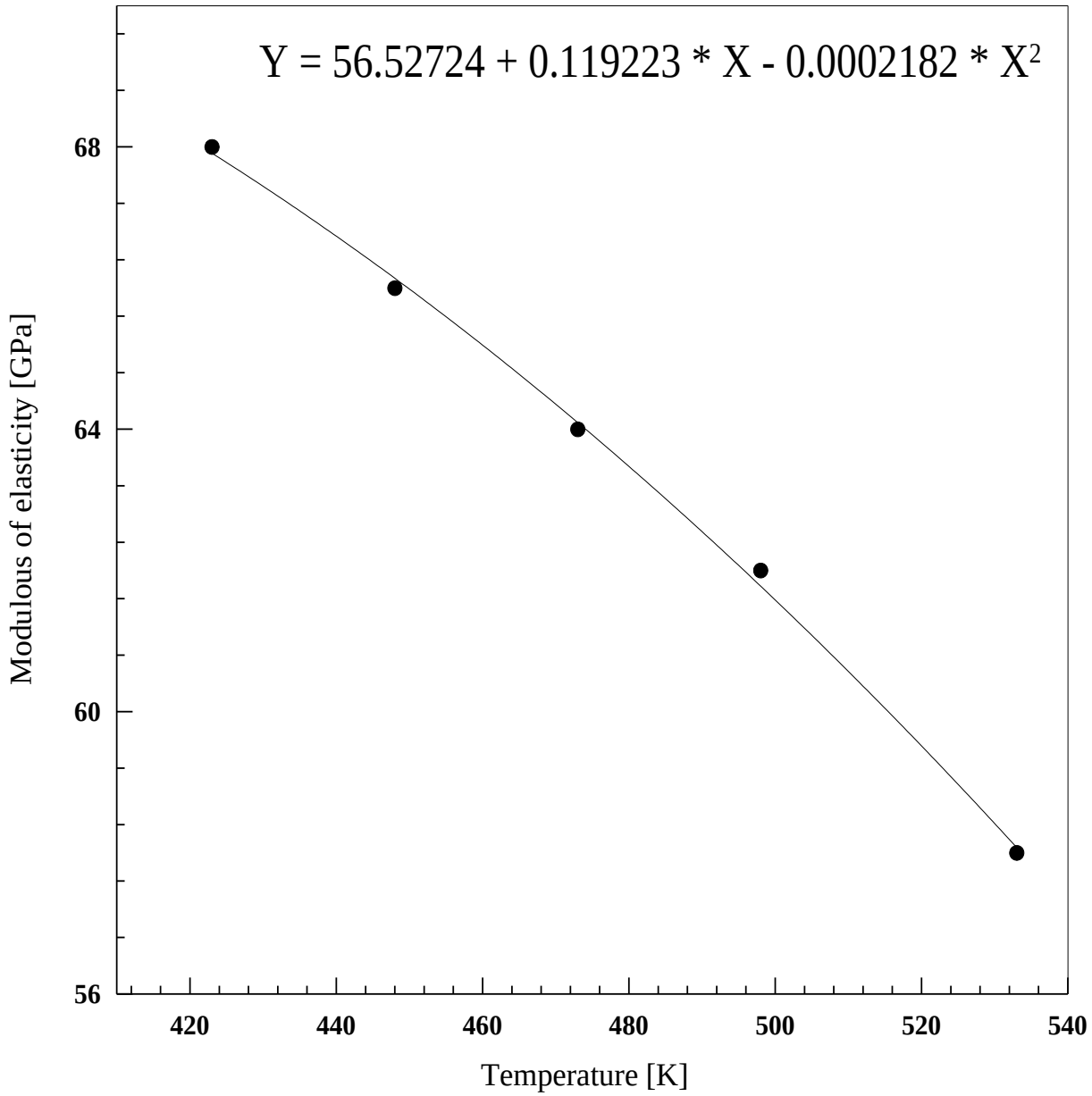

Fig. (4.1) : The effect of temperature on Modulus of Elasticity (E_m) for alloy (A).

Fig. (4.2) shows the effect of testing temperature on ultimate tensile strength **(UTS)** for alloy **(A).**

A similar behavior is observed once again…..

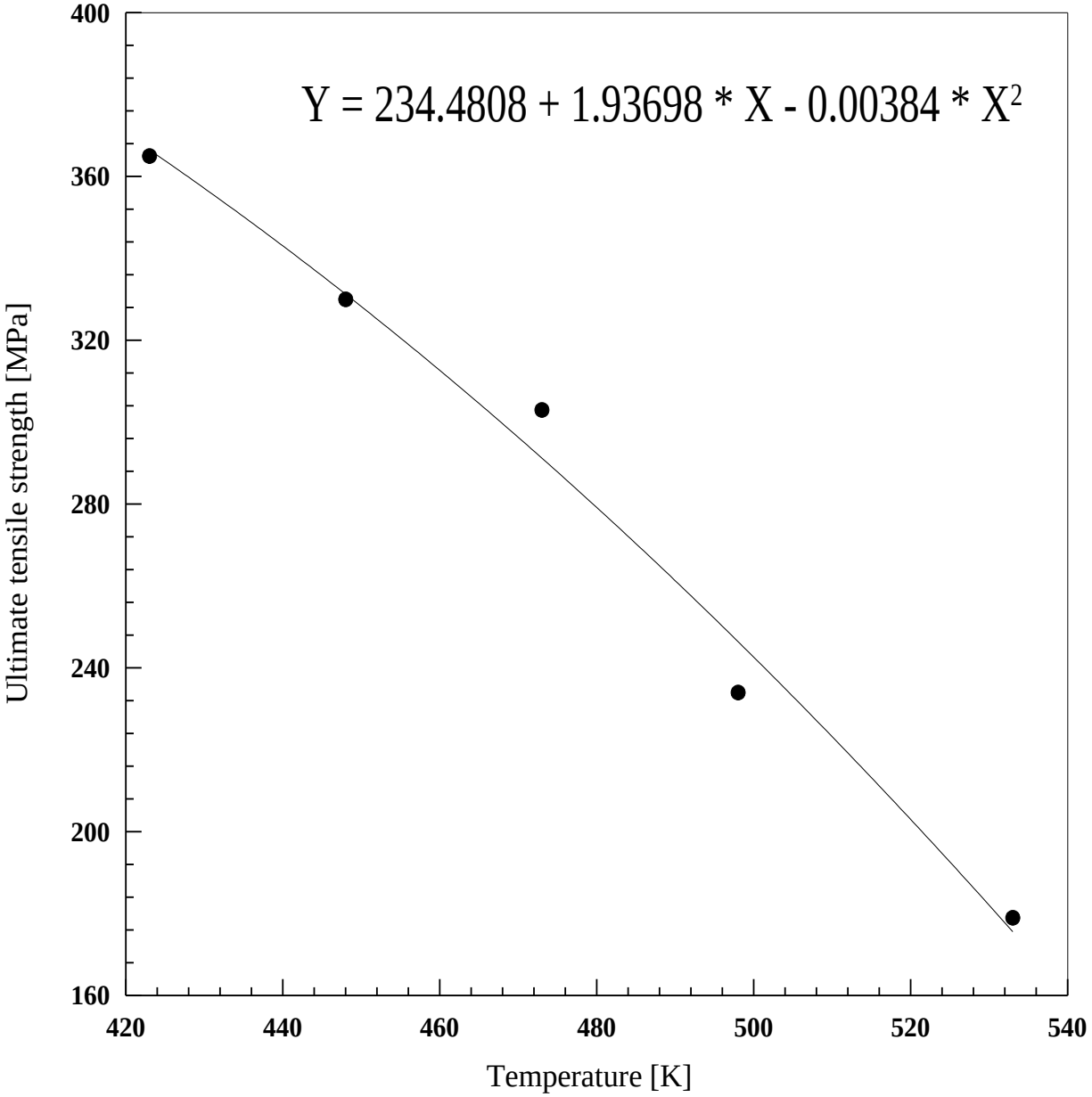

Fig. (4.2): The effect of temperature on Ultimate Tensile Strength (UTS) for alloy (A) :-

4.3. Influence of Testing Temperature on Elastic ….. Modulus (E_m) for Alloy (A_c) :-

Fig.(4.3) describes the behavior of **(E_m)** of alloy **(A_c)** with temperature.

As it is obvious it is similar to Fig. (4.1), of alloy **(A)** in shape but different in values that higher **(E_m)** in all temperature is observed, and an improvement of **(32.35%)** occurred.

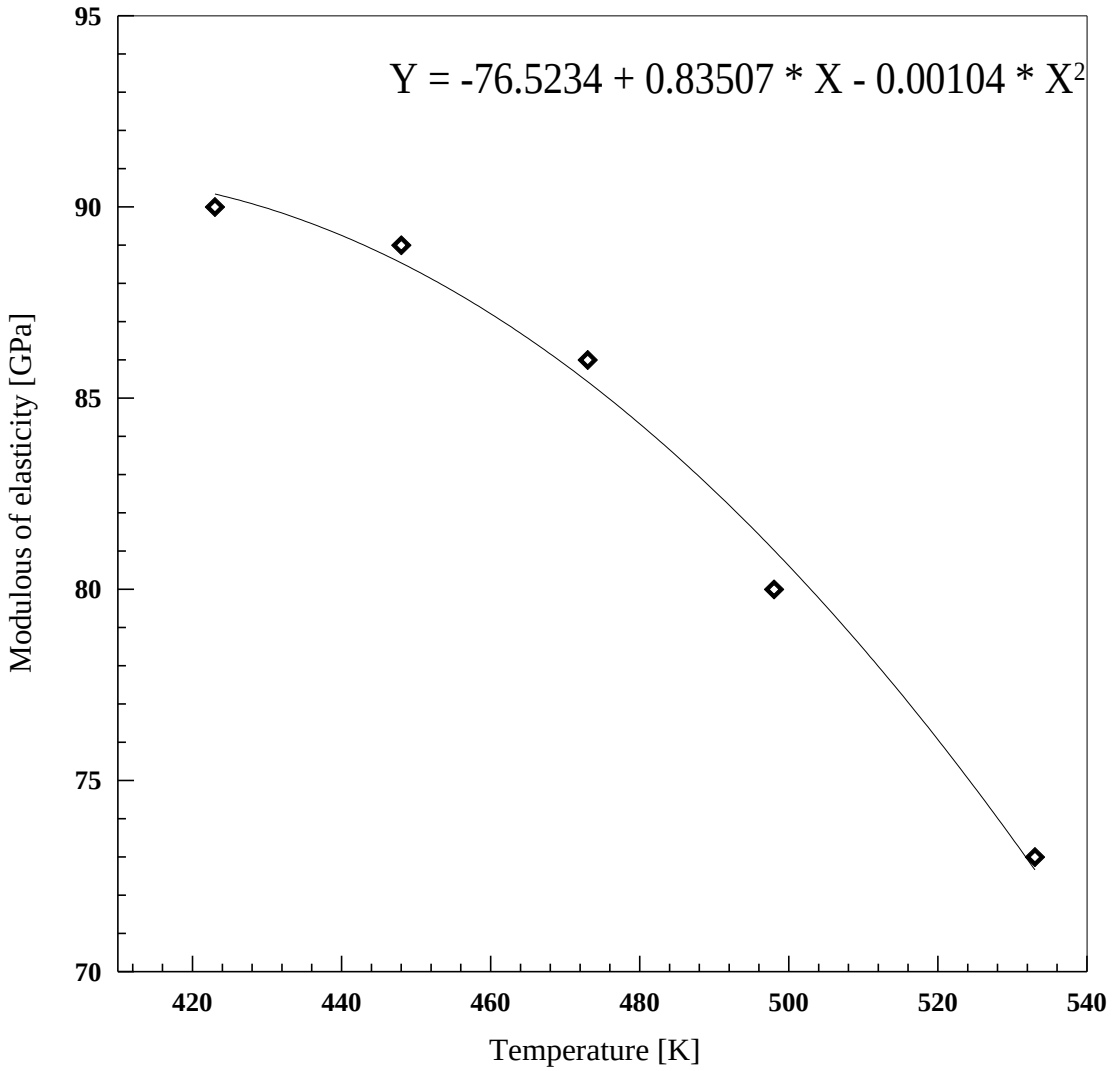

Fig. (4. 3): The effect of temperature on Modulus of elasticity (E_m) for alloy (A_c).

4.4. Effects of Testing Temperature on Ultimate ……Tensile Strength (UTS) of Alloy (A_c) :-

Fig. (4.4) shows the variation of **(UTS)** with testing temperature of alloys **(A_c).** An improvement of approximately **(30%)** is observed compared to Fig. (4.2).

The rate of decreasing in this case is slower than that shown in Fig. (4.2).

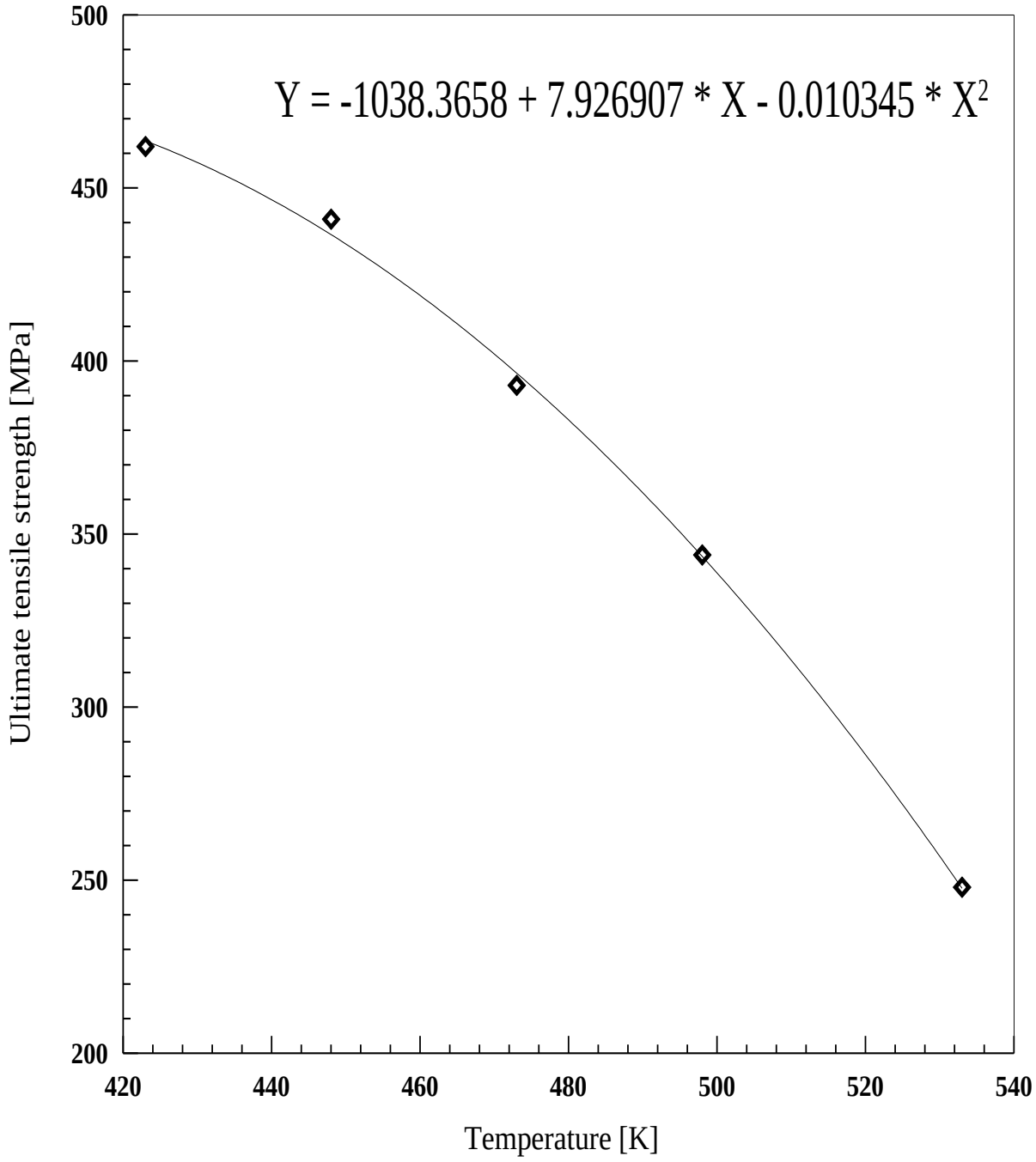

Fig. (4.4): The effect of temperature on Ultimate Tensile Strength (UTS) for alloy (A_c).

4.5. Effects of Heat Treatment on the Examined Alloys :-

Several samples were examined without heat treatment and premature failure occurred, due to several reasons. Therefore it was planned to heat treat all samples; more details are in chapter (3).

4.6. Creep Test :-

Creep is a time dependent strain. It is a tedious, costly, and time consuming test. Therefore fine complete creep rigs were designed and constructed.

4.6.1. Effect of Exposure Time on Strain :-

….. Figs. [(4.5), (4.6), (4.7) and (4.8)], show the Influence of time on strain at testing temperature of **175 °C** and applied load of **(150MPa).**

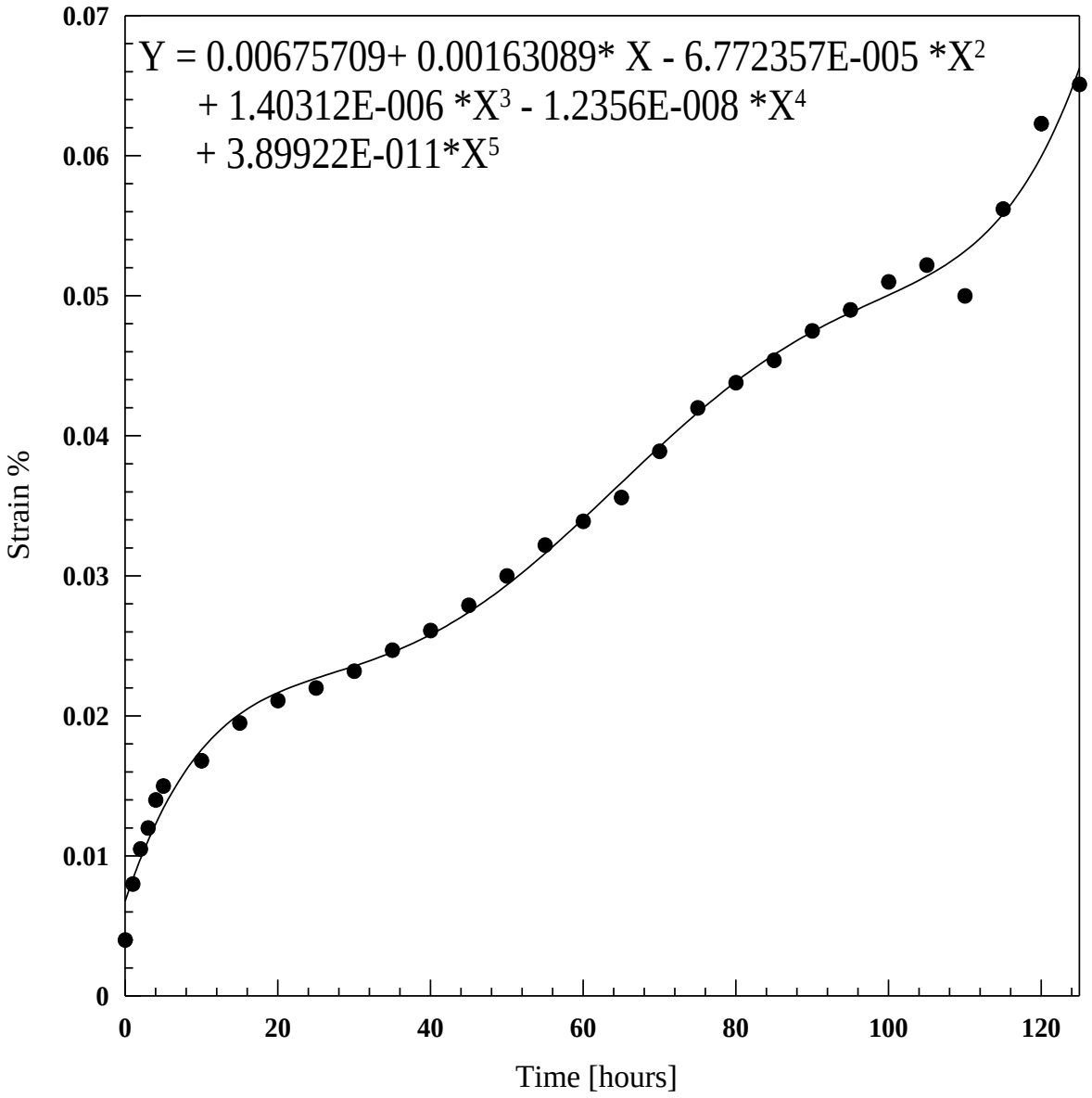

Fig. (4.5): Creep curve for alloy (A) at test temperature of 175°C and the applied stress of 150 MPa.

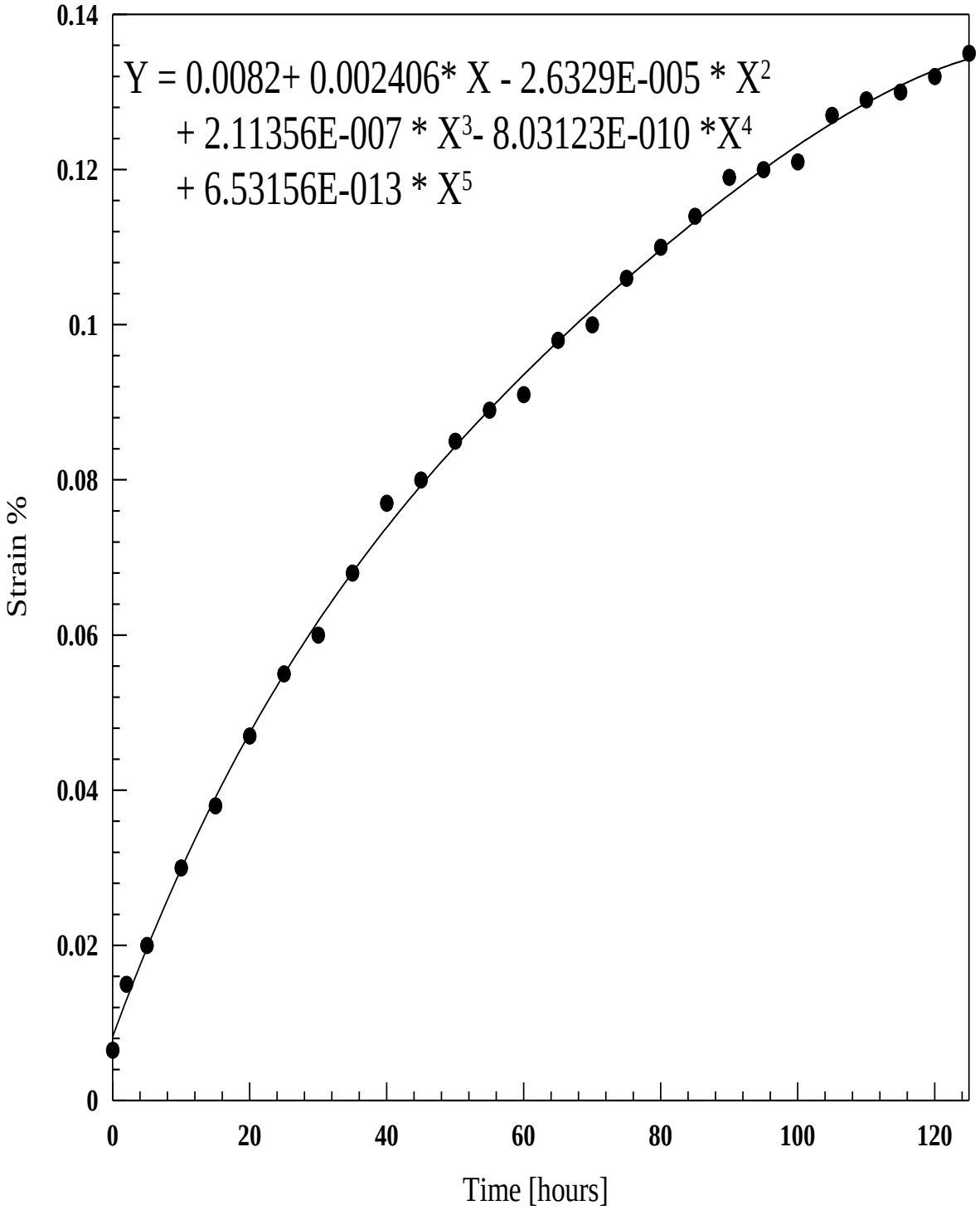

Fig. (4.6): Creep curve for alloy (A_c) at test temperature of 175°C and the applied stress of 150MPa.

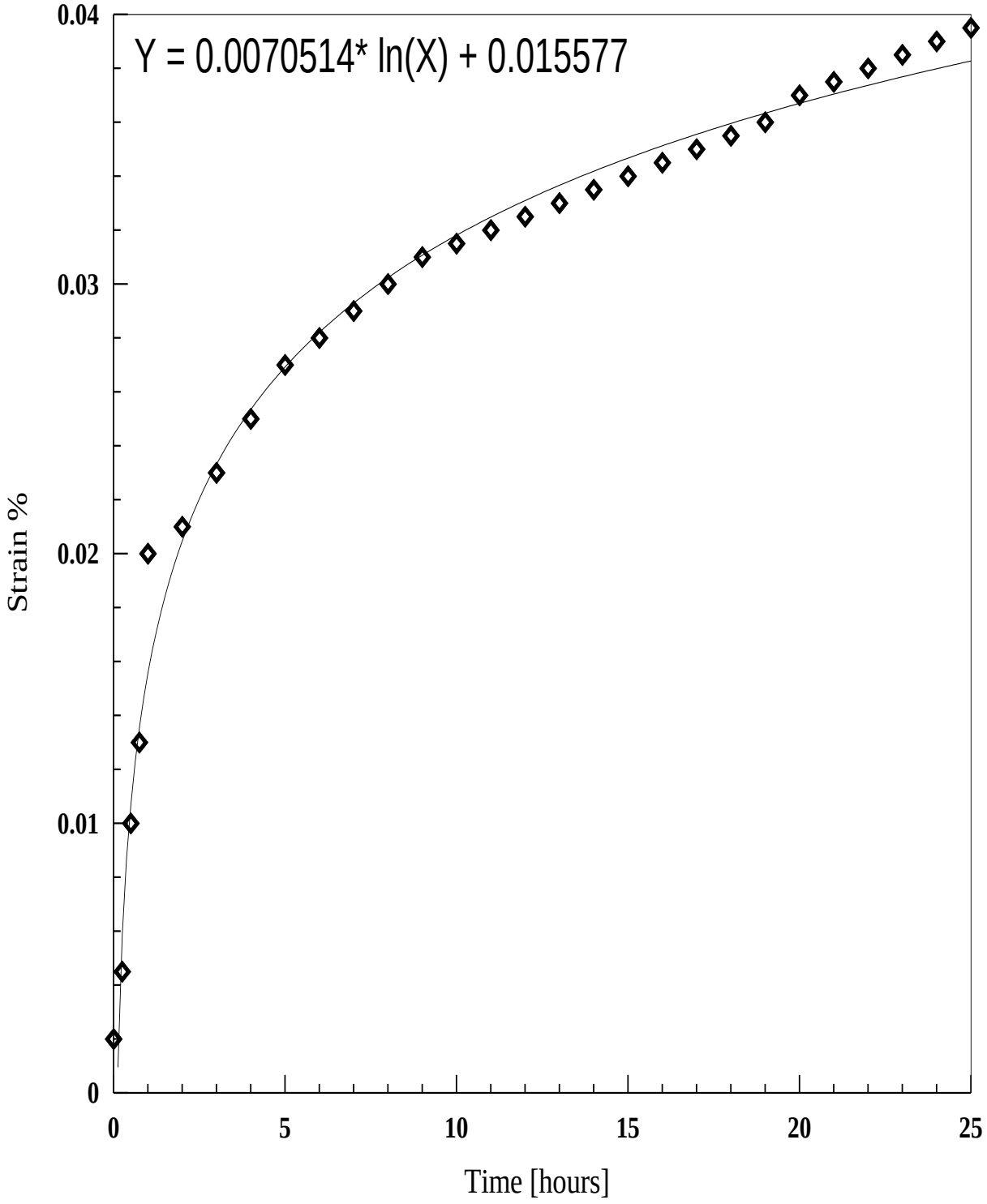

Fig. (4.7): Creep curve for alloy (B) at test temperature of 175°C and the applied stress of 150 MPa.

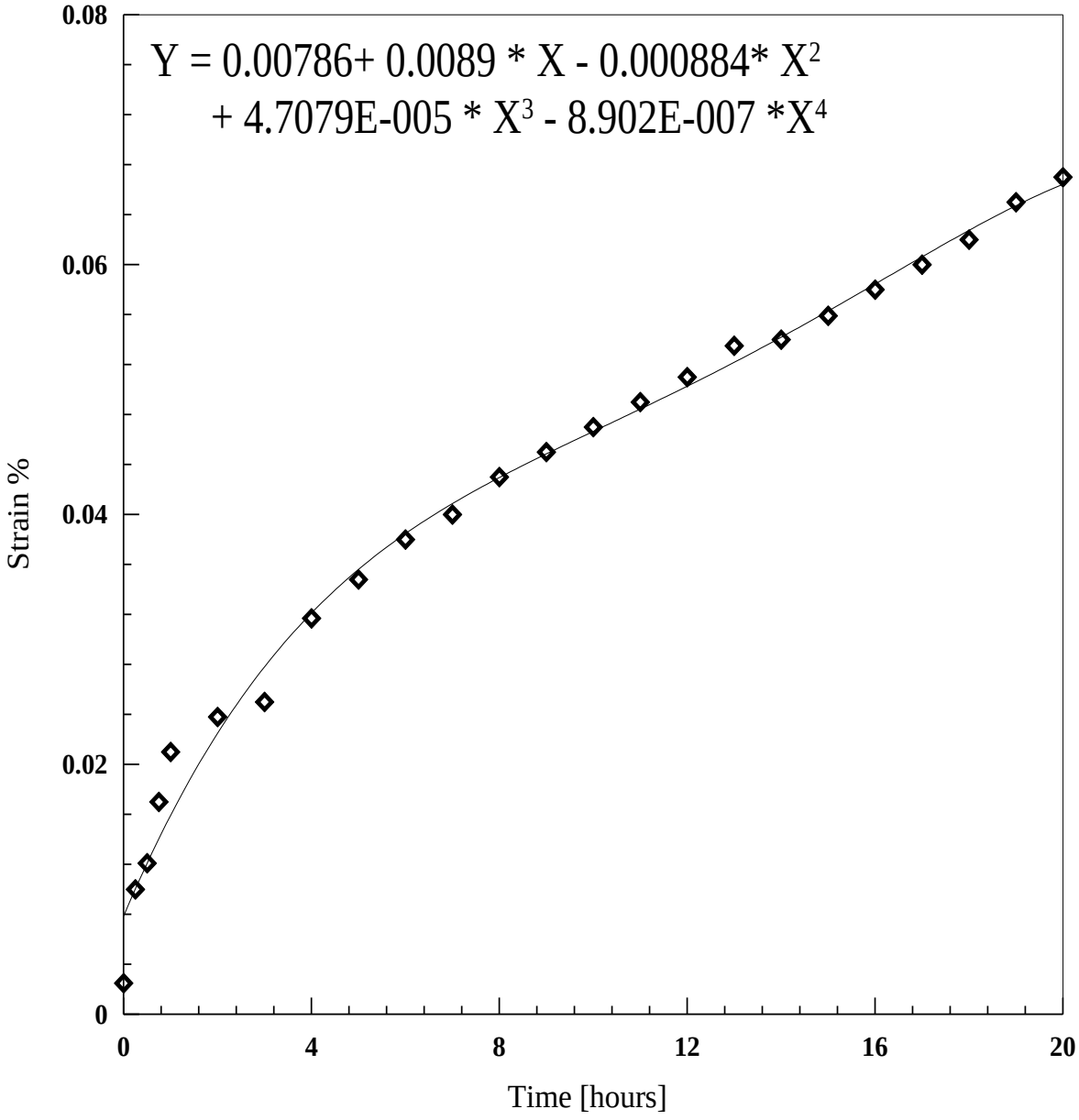

Fig. (4.8): Creep curve for alloy (C) at test temperature of 175°C and the applied stress of 150 MPa..

The creep curve of the base alloy is obvious in Fig (4.5) which describes the behavior of alloy **(A)** (Al- 4%Cu- 1.5%Mg). The creep is almost reaches the fracture point, during the **125 hours**.

According to the phase diagram, Fig. (1.4) the matrix of the alloy is a solid solution **(α)** and precipitation of **(S) phase** (Al_2CuMg), of orthorhombic structural. Its crystallography is available elsewhere [Wang & Starink, 2007] as shown for alloy (A), in Fig.(4-9).

Sample A: Al-Cu-Mg

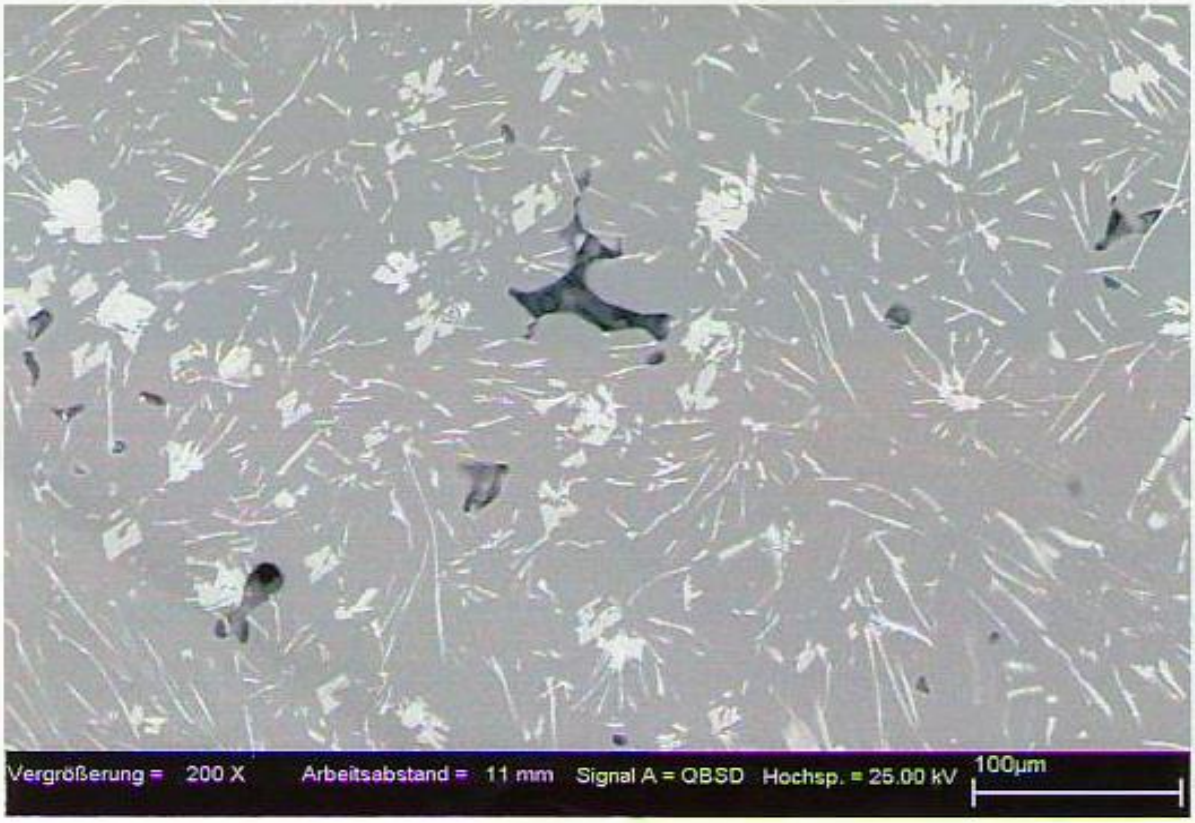

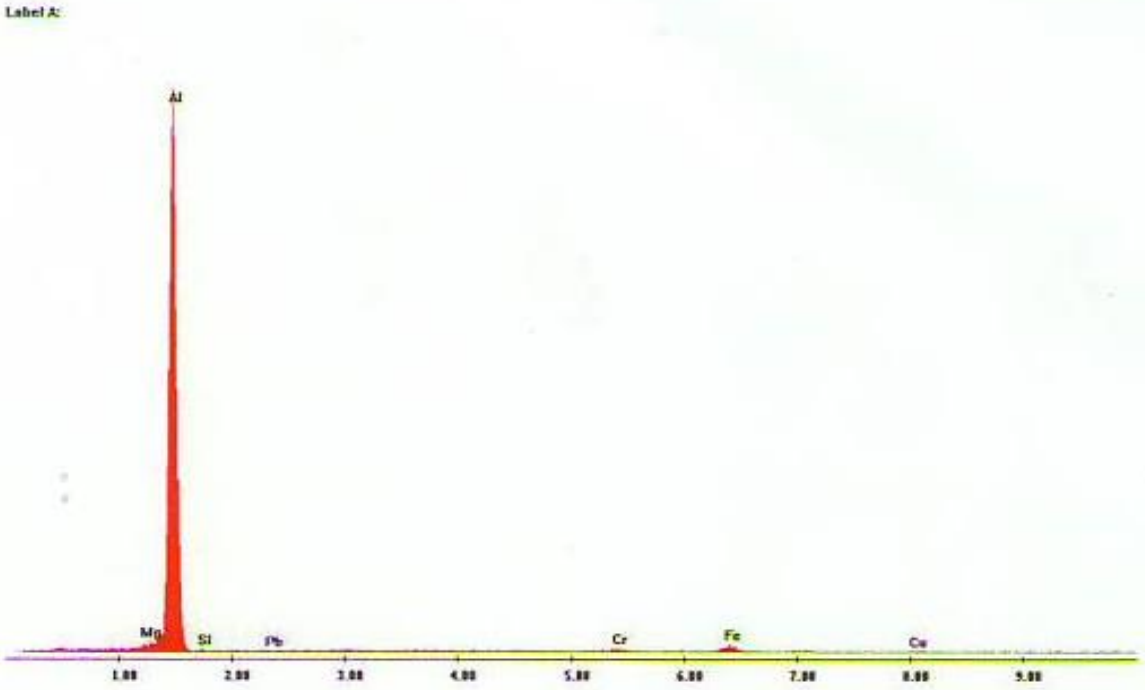

Fig.(4-9): Show the microstructure of the base alloy (A) and its components.

This **phase (S)** is incoherent one, and hence, its role in strengthening is limited, since there is no strain field around such precipitate. Therefore, such particles act as an obstacle for the moving dislocations only when they have to pass through it.

It was believed that the first stage hardening (rapid hardening) was attributed to **(GPB)** zones, while the second stage hardening is due to **(S) phase** (Al_2CuMg). This theory was later on discarded by (Ringer et al., 1997) by using an (Atomic probe field Ion Microscopy) who suggested that the first stage was due to clustering of few atoms of (Cu and Mg), while the second stage hardening is due to **(GPB)** zones. Other workers, however, proposed that it is the formation of **(S) phase** on dislocations which (pins) the dislocations and prevent their movement.

It appears more acceptable that the pinning of active dislocations than the formation of **(GPB)** zones, since some other researcher agreed with this, as thermal analysis did not detect any **(GPB)** zones.

(Al-Cu-Mg) alloys (2xxx) series are however, widely used in structural aerospace applications.

Fig. (4.5) creep curve of alloy **(A)** is almost a typical one with a clear stages. The mechanisms of such stages are discussed in so many references.

The deformation mechanism itself is, however depends on the constituents of the alloy and the operating conditions.

It is essential in all cases of designing a component used at high temperatures to take into account the maximum allowable strains and the effective life of the component.

4-6-2 Effect of Applied Stress and Temperature :-

When the applied stress on alloy **(A)** is decrease to **(115 MPa)** Fig. (4-10). Creep curve almost remains similar to fig.(4.5) except it less tendency towards fraction point. The strain value are lower, as expected.

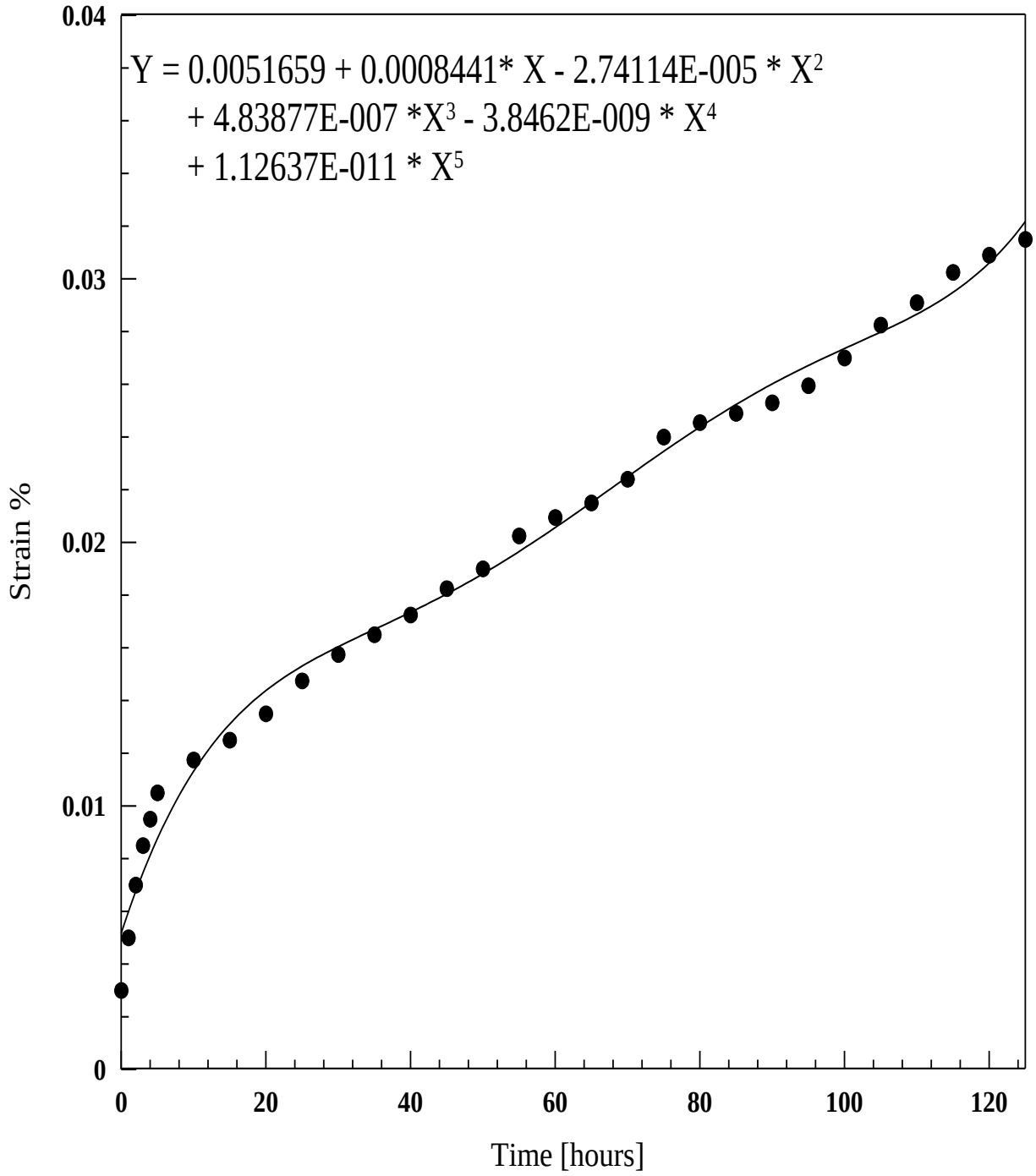

Fig. (4.10): Creep curve for alloy (A) at test temperature of 175°C and the applied stress of 115 MPa.

Fig. (4.11) describes the effect the decreasing the applied load on creep carve of alloy **(A_c)** .It is obvious that this test is in the early stage of the secondary region compared to that of alloy **(A)** . This improvement is attributed to the effect of **(SiC)** partial in reducing creep rate.

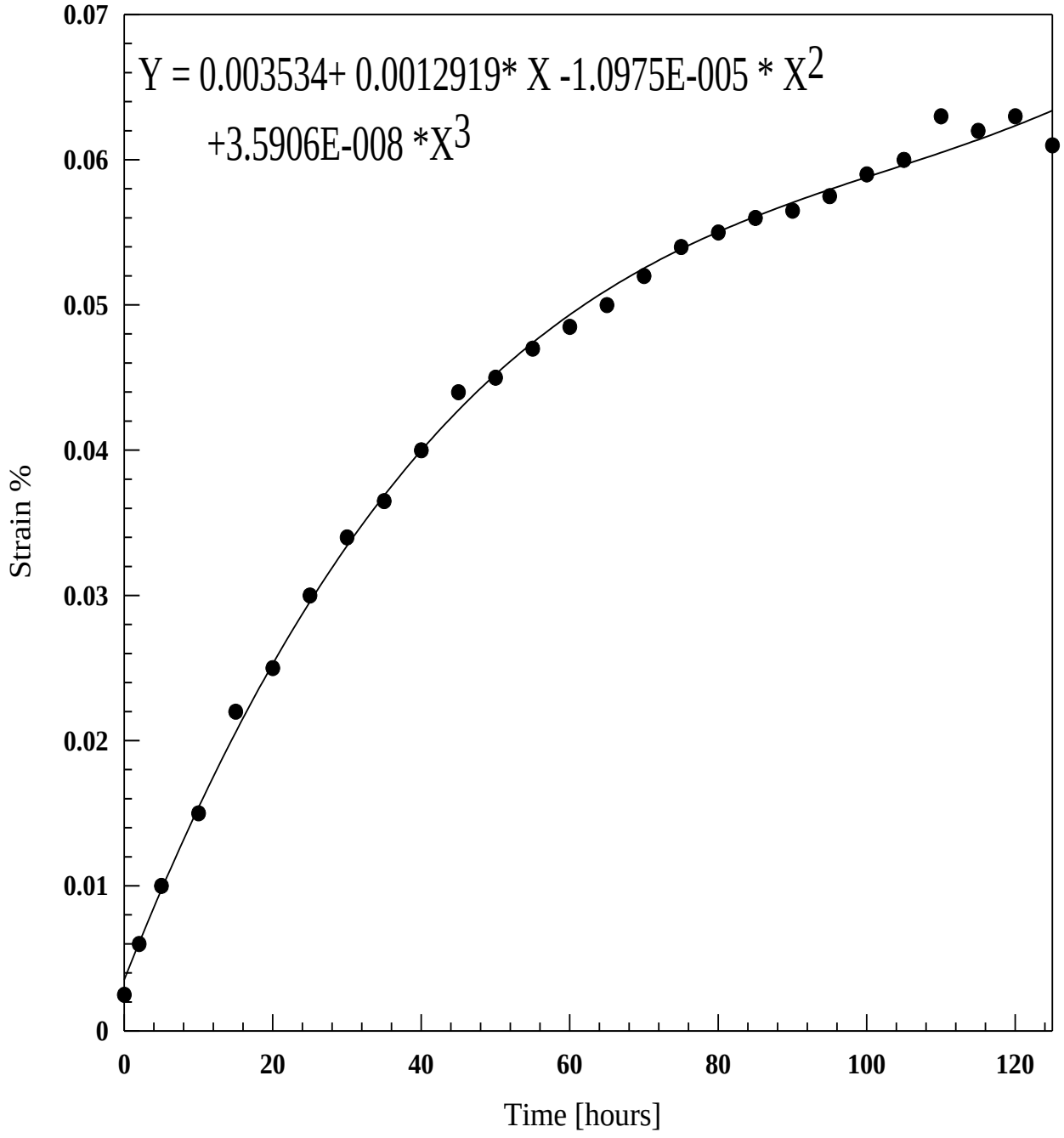

Fig. (4. 11): Creep curve for alloy (A_c) at test temperature of 175°C and the applied stress of 115 MPa.

When temperature was increased to **(200 ºC)** and the applied stress remains constant **(115MPa)** .Fig.(4.12) ,the creep curve of the base alloy **(A)** is behaves in a different way. More strain is observed and the secondary region is extended

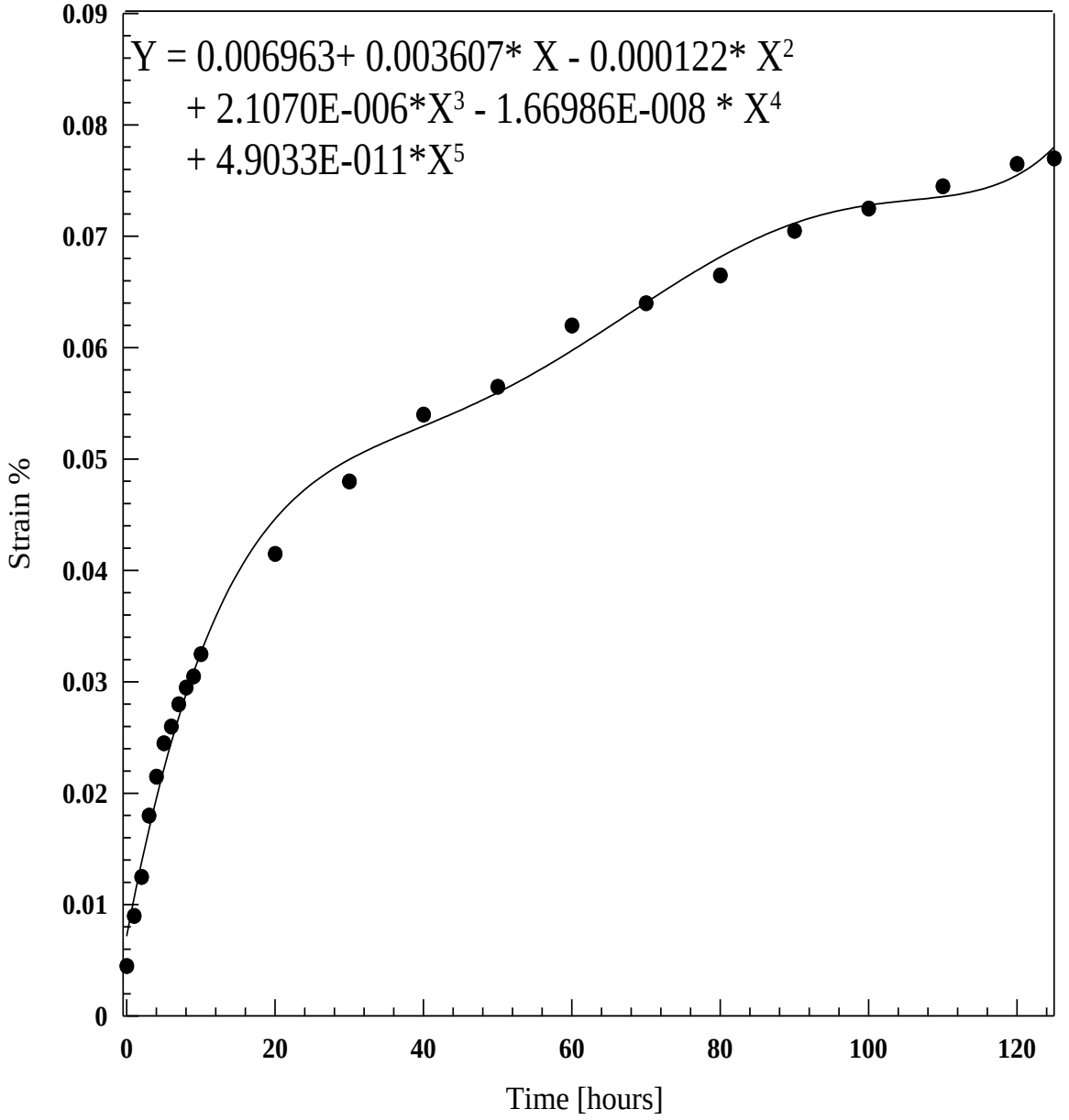

Fig. (4.12): Creep curve for alloy (A) at test temperature of 200°C and the applied stress of 115 MPa.

This is due to the fact that creep is possible **(enhanced)** only because obstacles to deformation can be over come by the companied action of

thermal fluctuation and stress. Since, stress is kept constant in this case, therefore, diffusion control processes are enhanced chiefly at this temperature which is higher that about one-half the melting point of pure aluminum which is expected to higher than that of they alloy.

New slip systems may become operatives when metal are deformed at high temperatures.

In (Al) itself, slip occurs on the {111}, {100} or {211} planes above **(260ºC)** [Dieter, 1986].

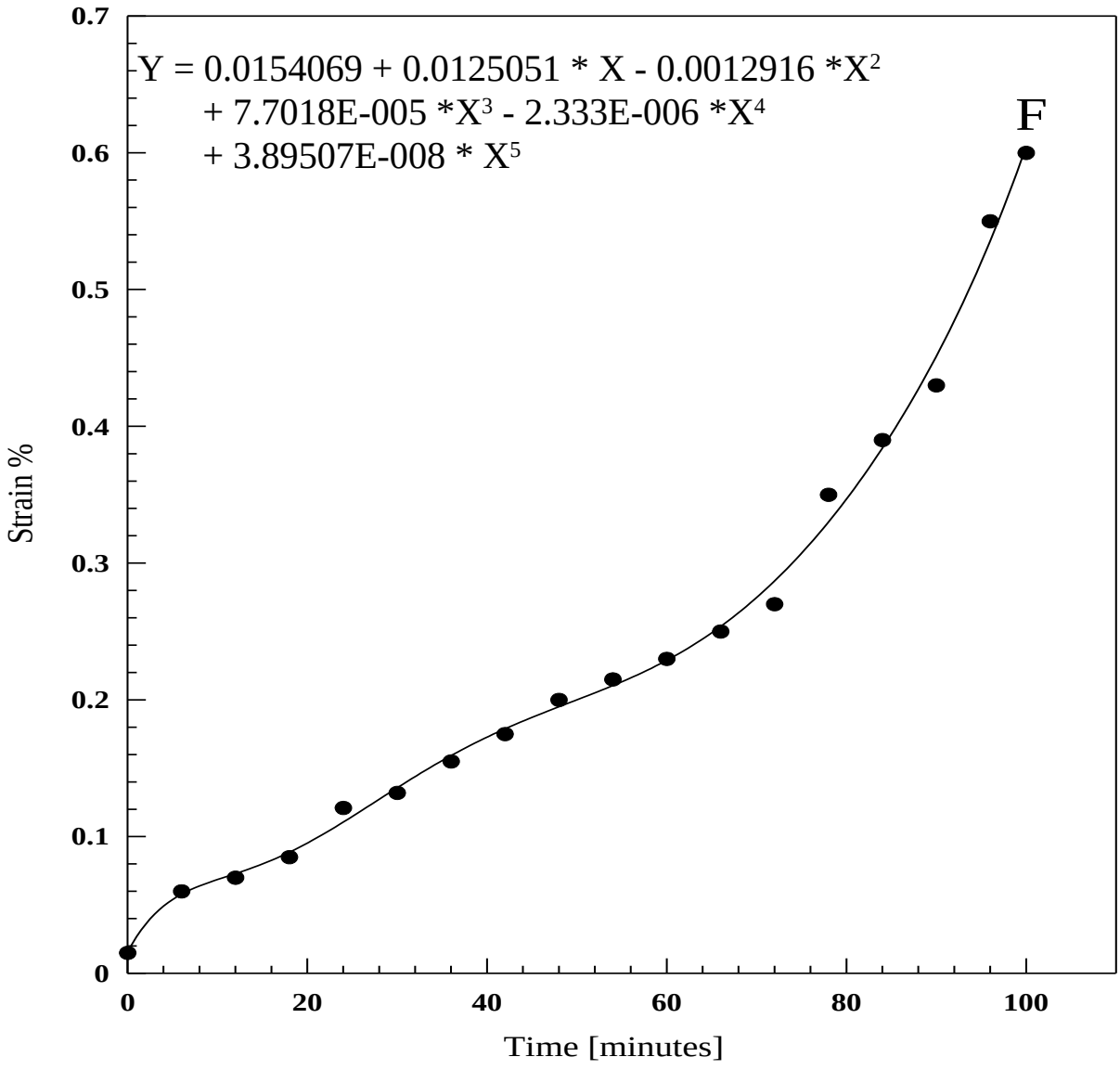

Fig. (4.13): Creep curve for alloy (A) at test temperature of 260°C and the applied stress of 115 MPa.

Fig. (4.13) describes the effect of increasing the test temperature up to **(260ºC)** which high enough to produce failure within shorter time .

This behavior can be attributed to several facts, including the decrease of creep strength as temperature increases, due to unbalance relation between recovery and work Harding since high temperature facilitate the deformation by dislocation climb which became a controlling factor and the available activation energy for movement resulting in decreasing cross-section of the sample and the accelerating of creep rate.

It is also expected a transition form **transgranualar** fracture **to intergranular** one. This is especially occur when temperature is higher than the equicohesive temperature **(ECT),** [Reedhill,1975 Physical Metallurgy principle]

Figure (4.14) shows the effect of increasing the applied stress on alloy **(A)** and keeping temperature constant, i.e. **(200ºC)** in comparison with Fig. (4.12) .

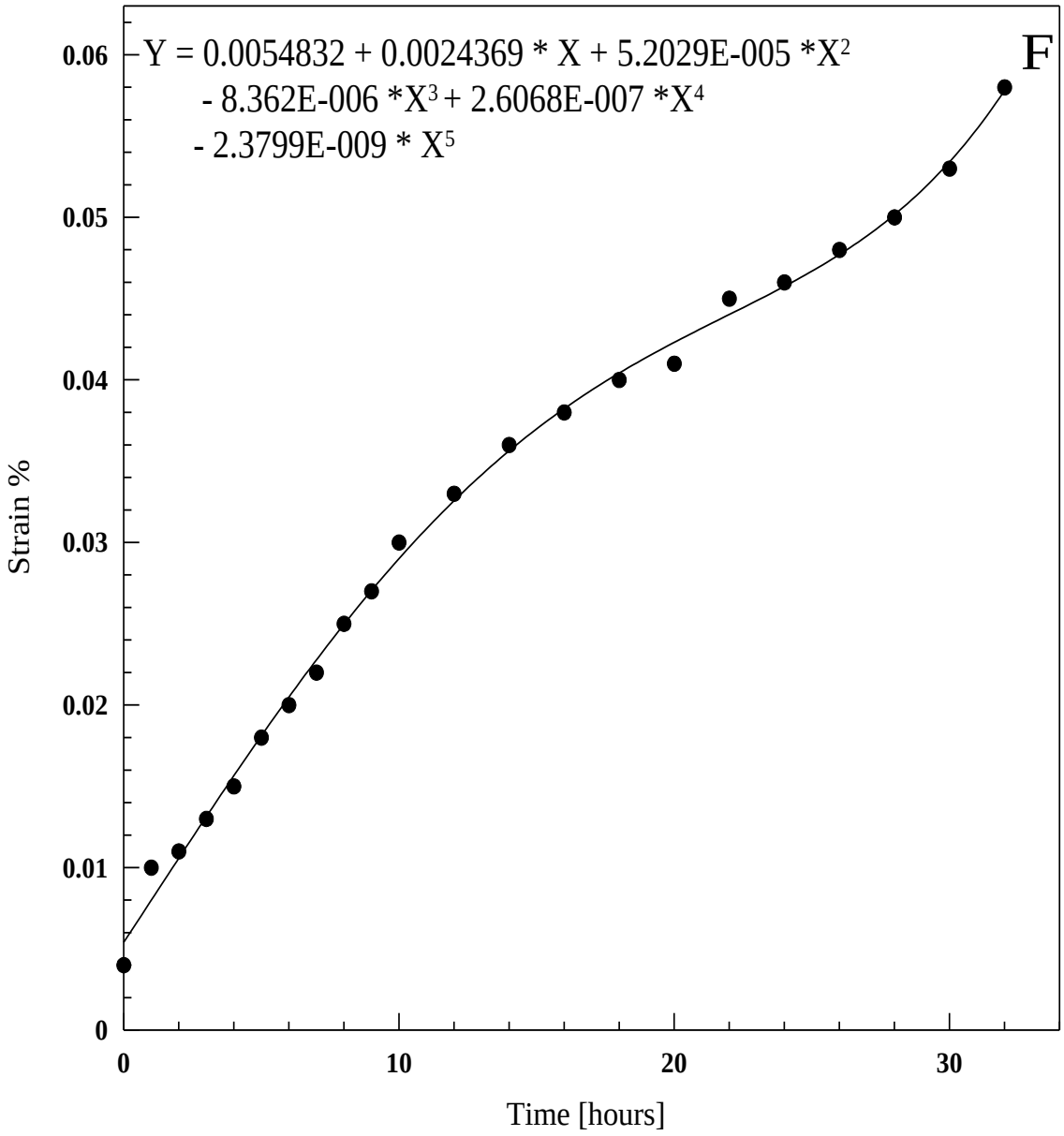

Fig. (4.14): Creep curve for alloy(A) at test temperature of 200°C and the applied stress of 135 MPa.

It is clear that fracture occurs in these case within about **(40) hours**, while an alloy (A) remains almost in the steady state region as in Fig (4.12).

In comparing Fig. (4.14) with Fig. (4.13) in which temperature was raised to **(260ºC)** instead of **(200ºC)**, fracture occurred during very few hours.

This indicates two facts. First, these temperature and applied stresses should be avoided when using such alloy, i.e. alloy **(A).**

Secondly, the effect of temperature is more destructive than increasing stress within these values when, the applied stress was increased to **(150 MPa)** and the temperature was kept constant **(200ºC)** fracture occurs after few hours as expected.

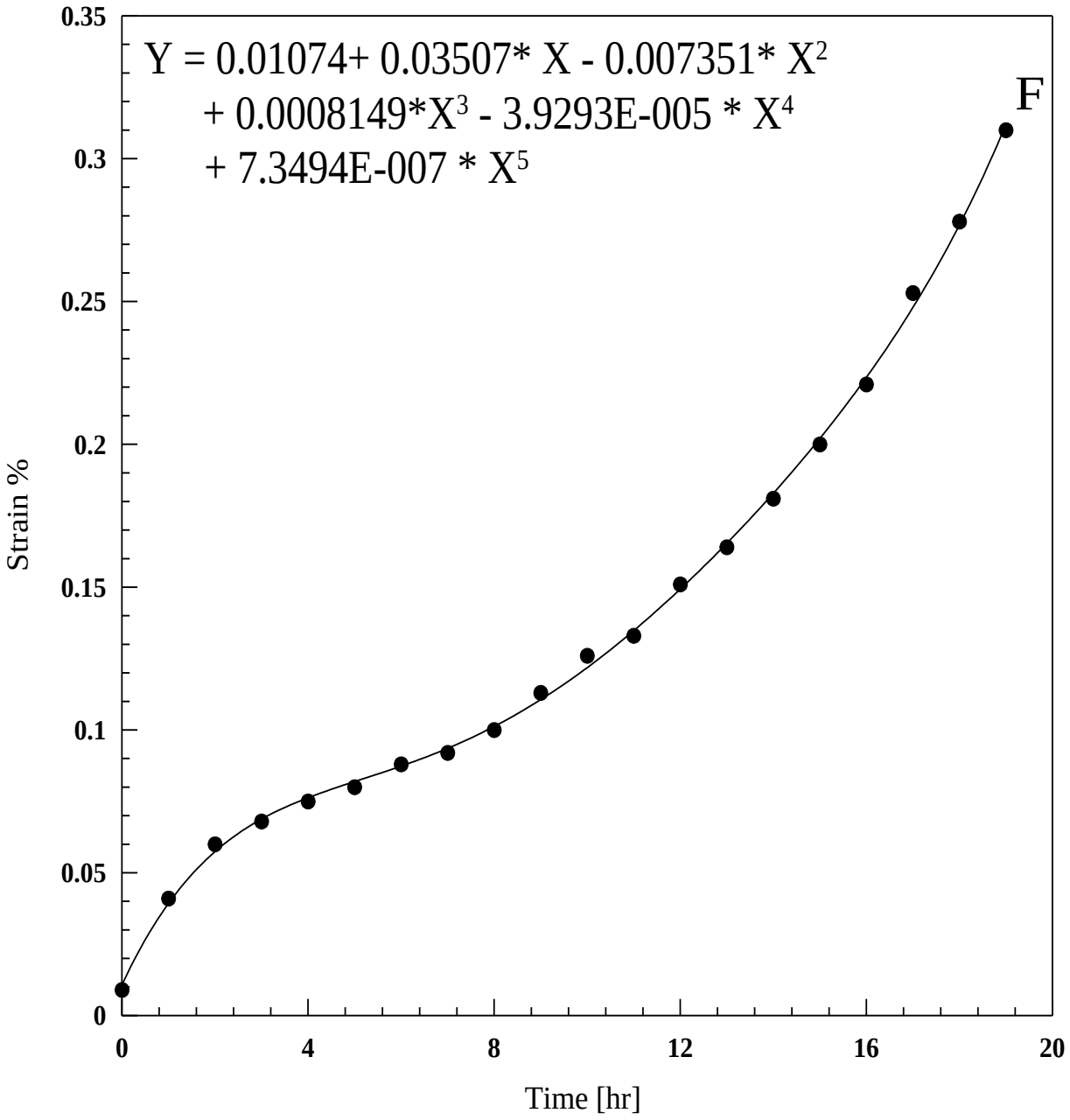

Fig. (4.15): Creep curve for alloy (A) at test temperature of 200°C and the applied stress of 150 MPa.

It appears that, although the Temperature was **(225ºC)** in Fig.(4.16) failure did not occur when the applied load was **(70 MPa).**

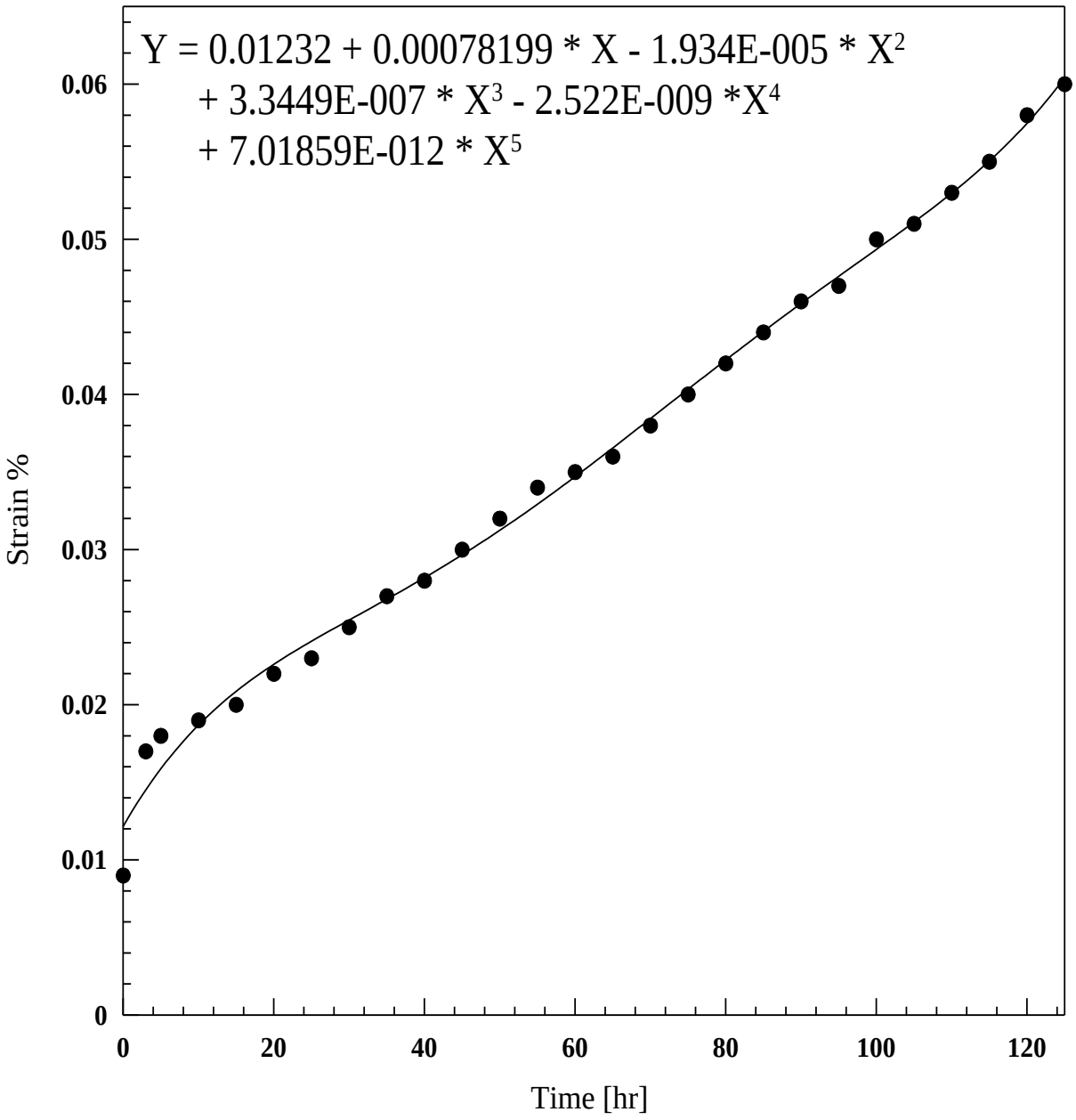

Fig. (4.16): Creep curve for alloy (A) at test temperature of 225°C and the applied stress of 70 MPa.

This may be due to the fact that, in **(FCC)** metals, the thermally activated component of the flow stress **(σ)** is small and only slightly temperature dependent. In addition it is also good evidence that the

precipitin particles and the microstructure are stable within the period of the test.

These alloys exhibits **secondary hardening** within the test periods (Ringer) Recent works proposed a different interpretation of the origin of hardening in this alloy **(A),** a fine uniform precipitation of **(GPB)** zones occurs [Ringer, 1997].

The secondary hardening is due to onset of dispersed precipitation of **(GPB)** zones.

In Fig.(4.17) the increasing in temperature to **(260ºC)** and keeping the applied load **(70 MPa),** caused an increasing in strains, as expected.

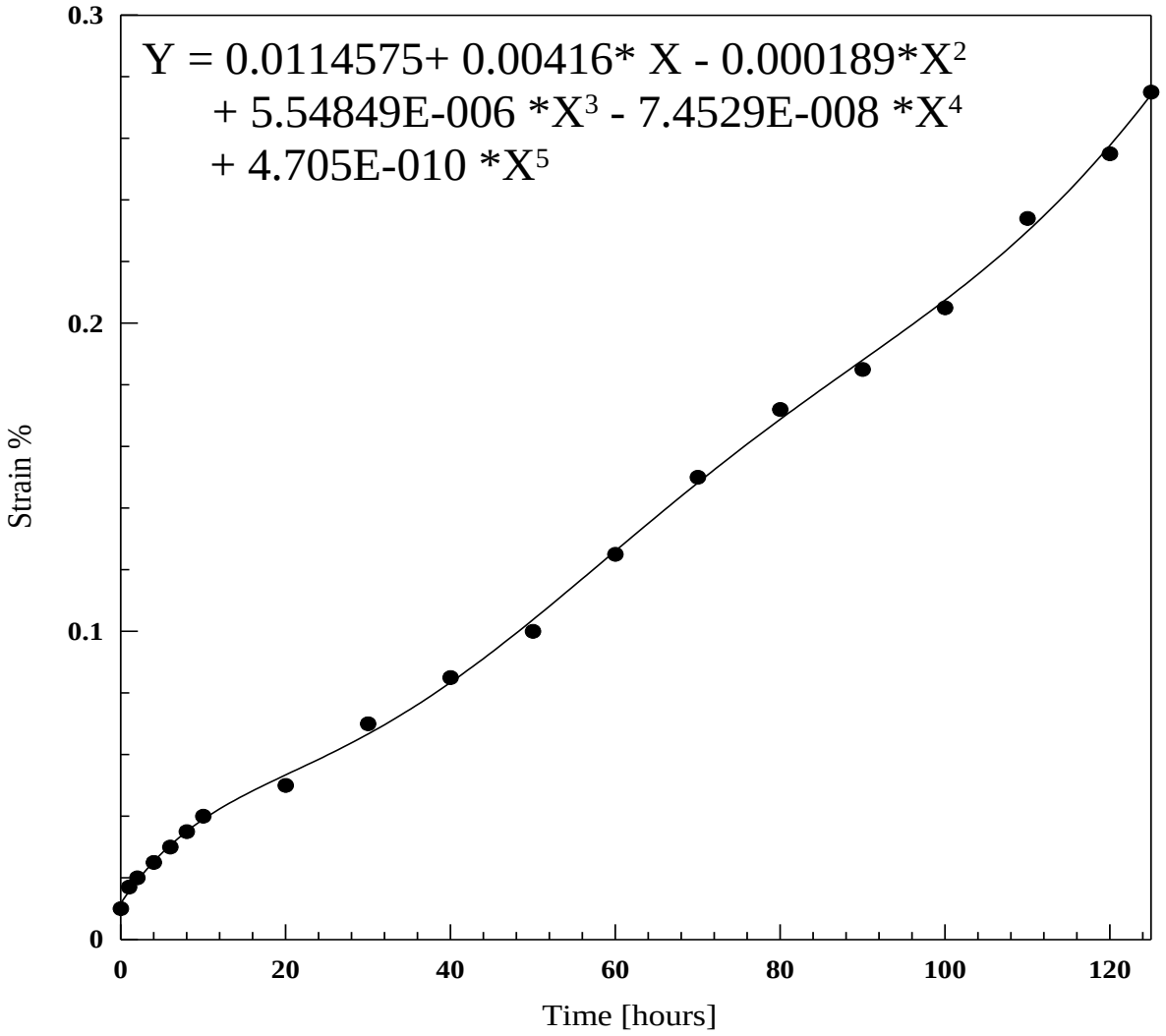

Fig. (4.17): Creep curve for alloy (A) at test temperature of 260°C and the applied stress of 70 MPa.

Fig. (4.18) represent the effect of **(SiC)** particles on creep behavior at **(200ºC)** and **(115 MPa)** applied stress. In comparison with Fig. (4.12) of alloy **(A),** i.e., **SiC** free, it appears clearly that early primary creep region it extended. This is due to strengthening effect of **SiC**.

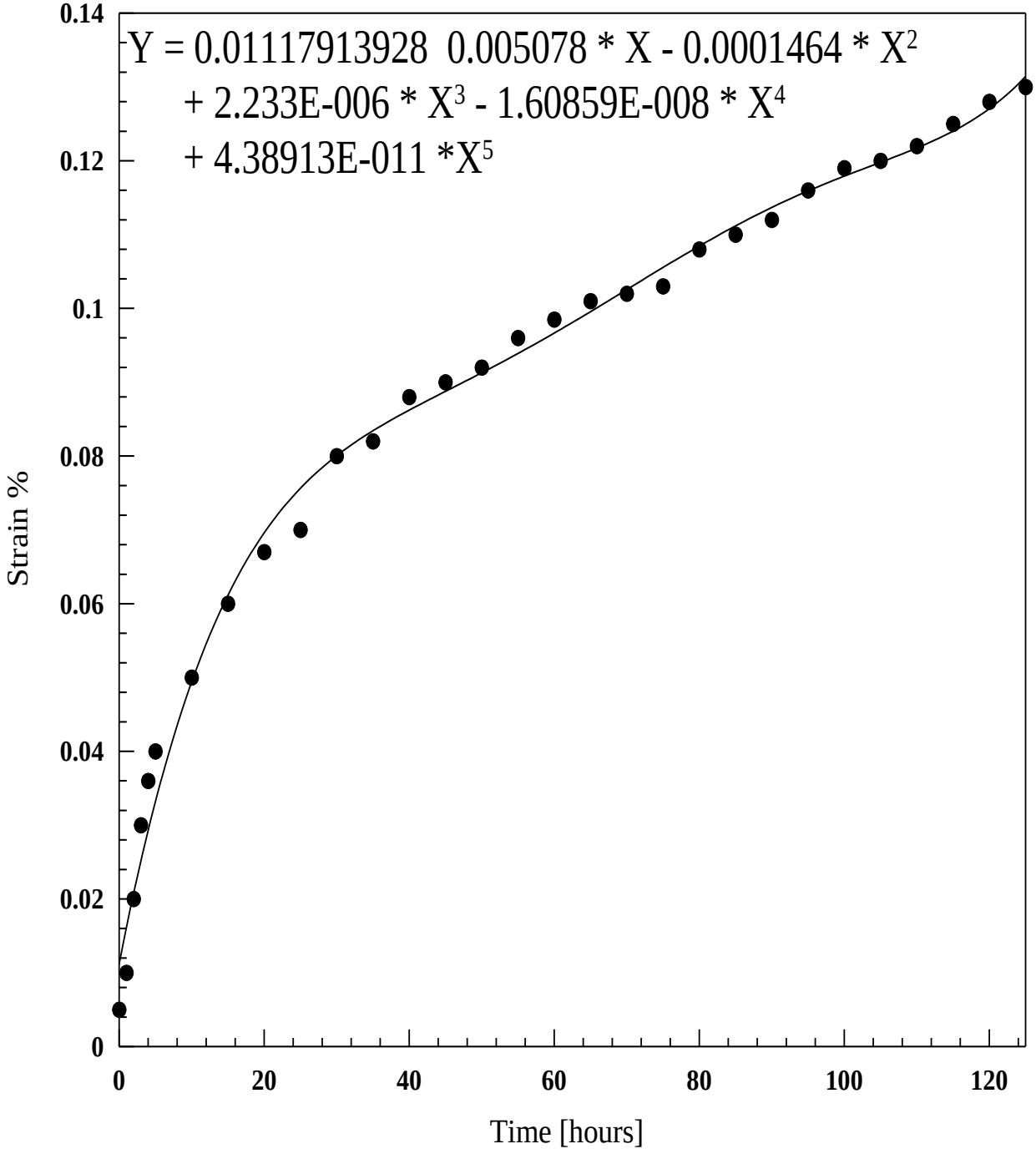

Fig. (4.18): Creep curve for alloy (A_c) at test temperature of 200°C . and the applied stress of 115MPa.

When the applied stress was increased to **(115 MPa),** Fig. (4.19) creep curve tends to move towards tertiary stage. In comparison with Fig.(4.15) of **(SiC)** free alloy it fractures after about **(18) hours**.

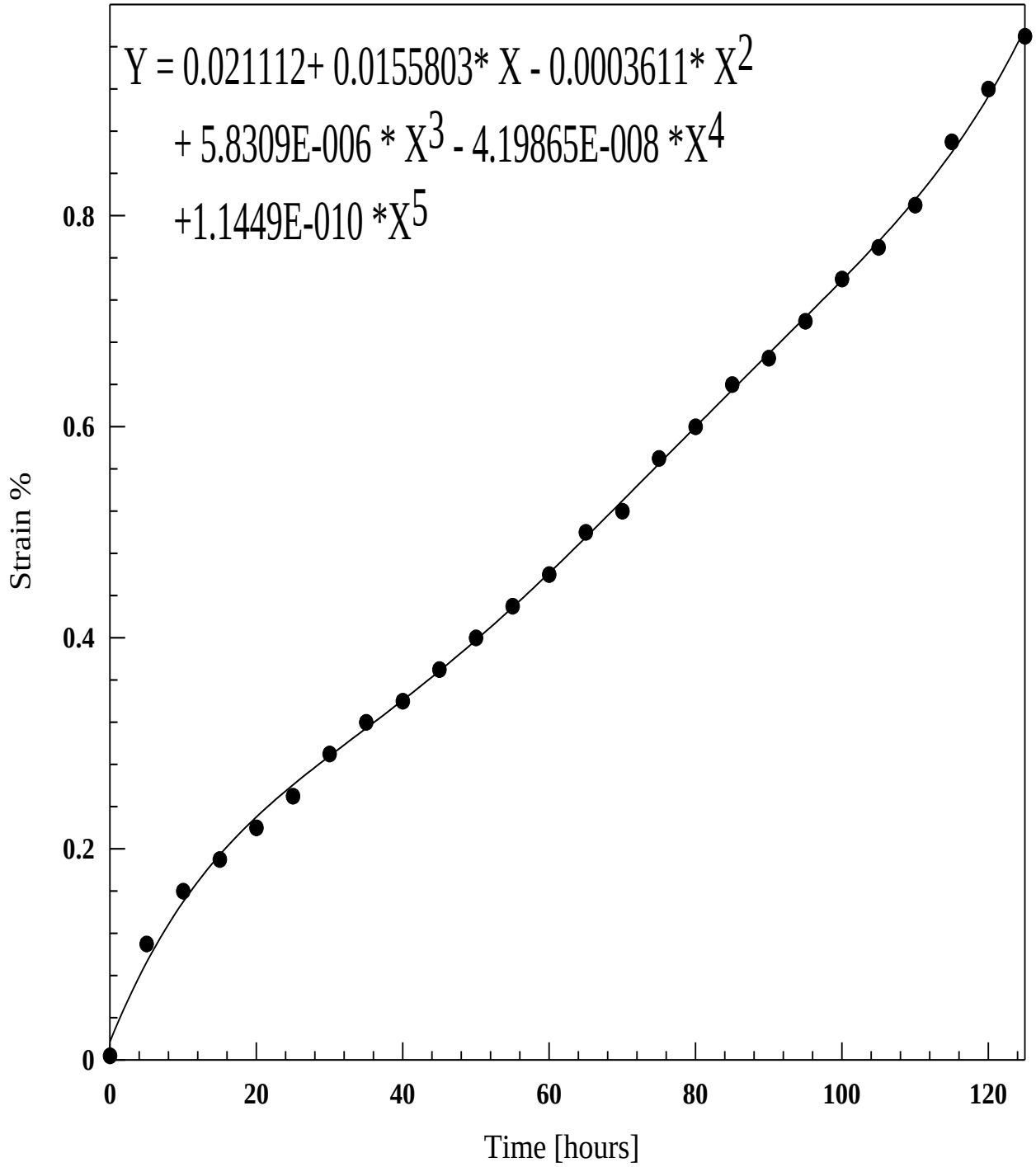

Fig. (4.19): Creep curve for alloy (A_c) at test temperature of 200°C and the applied stress of 150MPa.

When the temperature was increased to **(225ºC)** and the applied stress was **(70 MPa)** the creep rate in the secondary stage decreased, andthe strain increased. In the case of **(SiC)** free alloy Fig. (4.16) the creep rate was significantly higher.

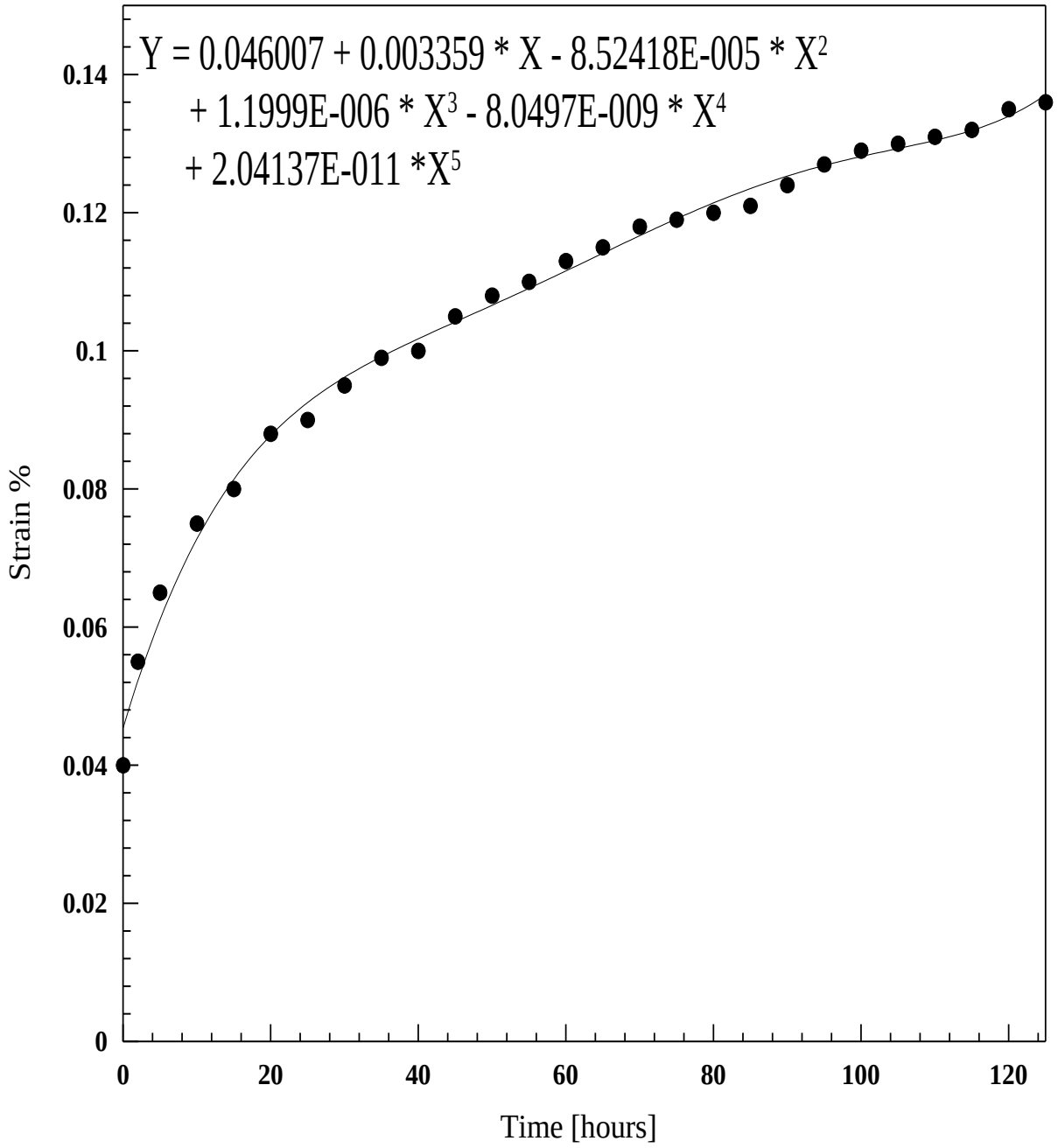

Fig. (4.20): Creep curve for alloy (A_c) at test temperature of 225°C . and the applied stress of 70MPa.

In fact, and strictly speaking it appears controversial result, since **(SiC)** is expected to enhance strength as it is a strengthening agents but it

seems more ductile than **(SiC)** free **(A)** alloy as it gives more strain under some conditions .

This unexpected behavior a can be attributed to the low wet ability of **(SiC)** the matrix (Ref. Basim) low wet ability may means partial low of adhesion with **(SiC)** particle, i.e. forming (cavity like) sites. These sites act as an active vacancy snick .And since deformation by dislocation climb is predominate in this case, therefore the available dislocation interaction restricted ,hence ,the work harding rate is limited ,so ,the observed strain is expected.

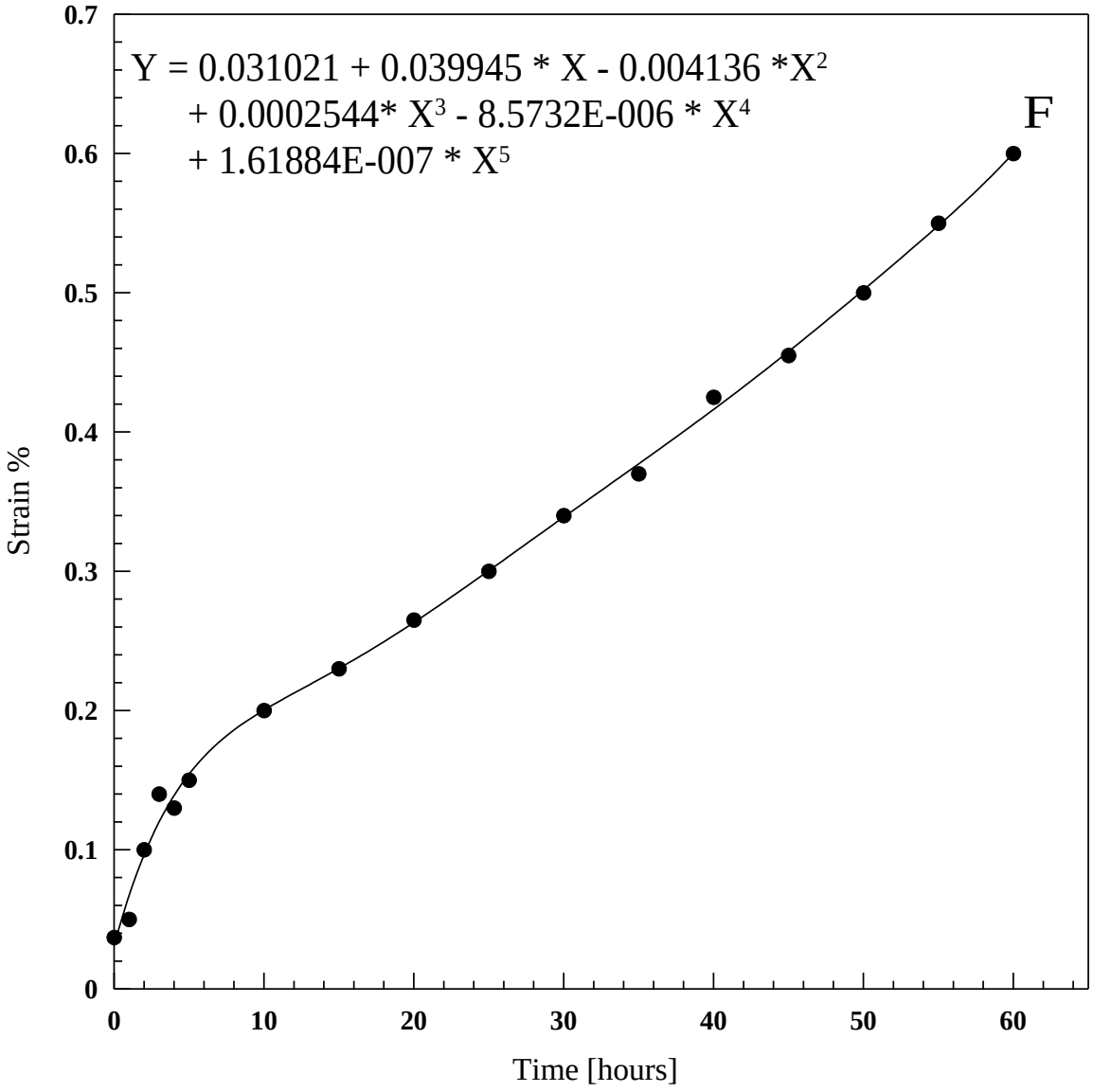

Fig. (4.21): Creep curve for alloy (A_c) at test temperature of 225°C and the applied stress of 115 MPa.

Fig.(4.21) shows that the increase of the applied load to **(115 MPa)** at the same temperature in Fig. (4.20) cause fracture of the sample.

In comparison with Fig.(4.1b) of **(SiC)** free alloy where fracture occurred after about **(1.30) hr.** one a half hours, the creep curve of alloy **(A_c)** with - stand the same conditions for **(=140) hrs.**, the test period without with fracture, Fig (4.28).

4-6-3. Effects of Alloying Elements:-

Fig. (4.6) represent the effect of **(SiC)** particle of size **(1 µm)** dispersed in **(A**) alloy matrix.

It is obvious that this creep curve is still in the early stages comparing with creep curve of **(SiC)** free alloy **(A).** as shown in fig (4-5).

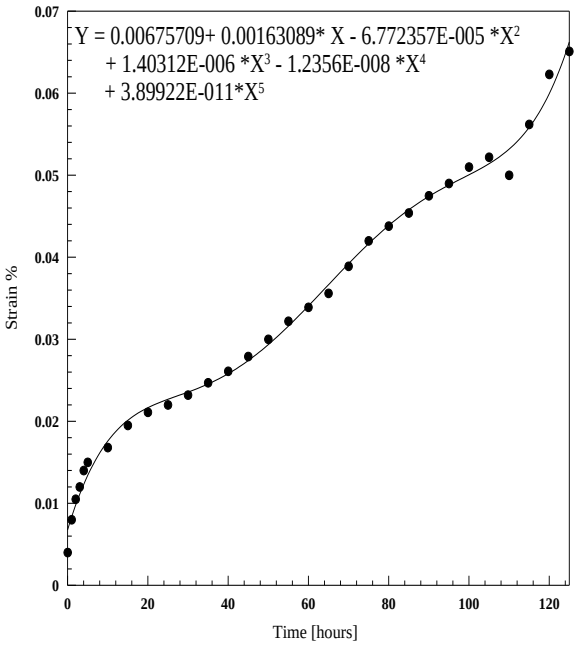

Fig. (4.5): Creep curve for alloy A at test temperature of 175°C and the applied stress of 150 MPa

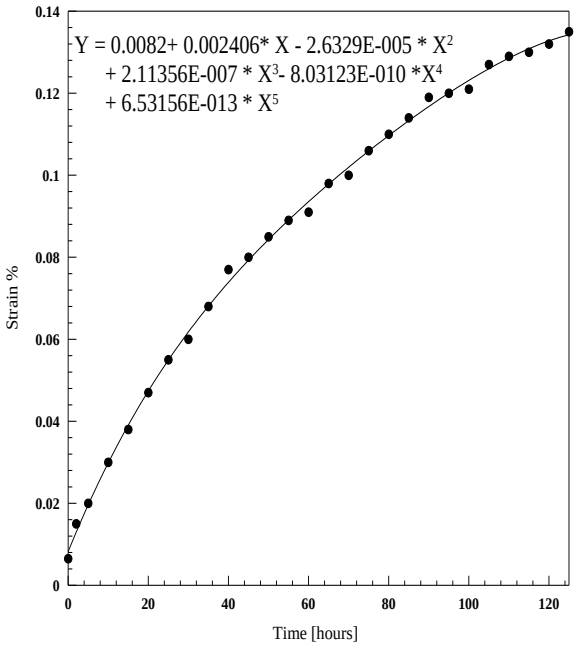

Fig. (4.6): Creep curve for alloy A_c at test temperature . of 175°C and the applied stress of 150MPa.

The wet ability of **(SiC)** in **(A)** alloy is in general **(low).** Therefore, some other workers used powder metallurgy technique to alloy the constitutes [Basem,2004]. It is, however, possible to reach almost a high

bonding by tedious and complex technique (high temperature multi-cycle heat treatment) of the powder technique.

In this work it was intended to enhance wet ability and maintain bonding (chemically) by diffusion during continuous electrical **(mixing)** for about one hour above the melting about **(850°C)** temperature and protecting the melt by argon gas.

The effect of the addition of **(Li)** and **(Li & Zr)** on creep life are shown in Fig (4-7) & (4-8) respectively. The value of copper in these alloys was reduced to **(2%),** in order to decrease the weight.

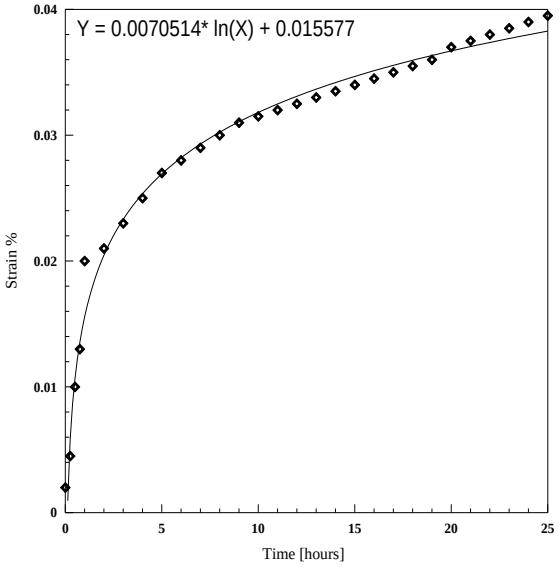

Fig. (4.7: Creep curve for alloy B at test temperature of 175°C and the applied stress of 150 MPa.

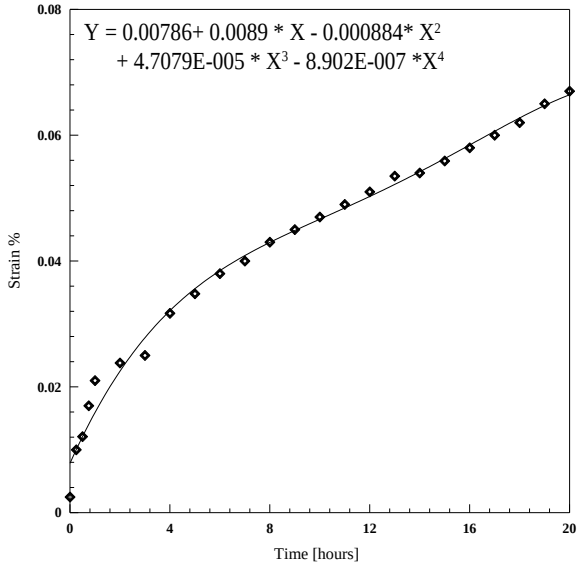

Fig. (4.8): Creep curve for alloy C at test temperature of 175°C and the applied stress of 150 MPa..

Copper addition, however, caused strengthening Figs (4-7) & (4-8) within the test periods, more strain is observed which is expected to be due to grain refining and retarding of recrystallizition and the possible improved strength and fracture toughness modification in creep mechanism due to change in precipitation and restriction of dislocation movement. Unfortunately, for technical and critical time the test was stopped after twenty five hours.

4.6.4. Discussion of Theoretical Model Results:-

From observation of numerical result of micro mechanic model for stress and strain values, Fig.(4.24a, b) for this model under the compression stress, can be evaluate of the modulus of elasticity with different proposal phases with different alloying elements addition in elastic range .

The modulus of elasticity calculated by the ratio between stress and strain in max. and min .values as shown in Fig.(4-22).

From these results can be concluded that the modulus of elasticity increases with increasing of phase strength for the same volume fraction and that belongs to influence of the addition elements, and these results compared with the experimental result which are obtained from the experimental test (tensile test) as shown in Fig. (4-22).

From note the Fig. (4-24) can be observed the effect of strengthening on the strain values specially in the zones around the strengthen phase.

The strain field increases in the interface between two phases (particle phase, matrix), because of strain hardening which are resulted from the restricted of the deformation (dislocation movement).that effect is very clear in the stress field around particle as shown in Fig. (4-24).

From observation of numerical results of macro mechanic model (creep model) with different alloys **(A, A_c, B, C)** as shown in Fig.(4-23) can be concluded that the creep resistance improve with increase of alloy strength due to form of hard phase. as shown in Fig (4-22) .

From comparison between the model results and the experimental result for creep test for these alloy can be conclude that the model is satisfied and the numerical result are agreed with the experimental results in behavior but are different in the values .it give lower values with compared with experimental values and that belongs to accumulative of some error in different sources (production parameters of alloys machining, measurement…etc.).

These rustles which are shown in Fig. (4-23) are taken from contour results for different alloys **(A, A_c, B, C)** which are tested in the theoretical analysis (macro-mechanic model) as shown in Figs.(4.25, 4.28) from beginning of test Fig. (4.25, 4.28a) to the end of test as shown in the Fig. (4.25, 4.28b).

The contour results are very clear and their values are different with alloys difference and that because of increasing of overall strengthen of alloys.

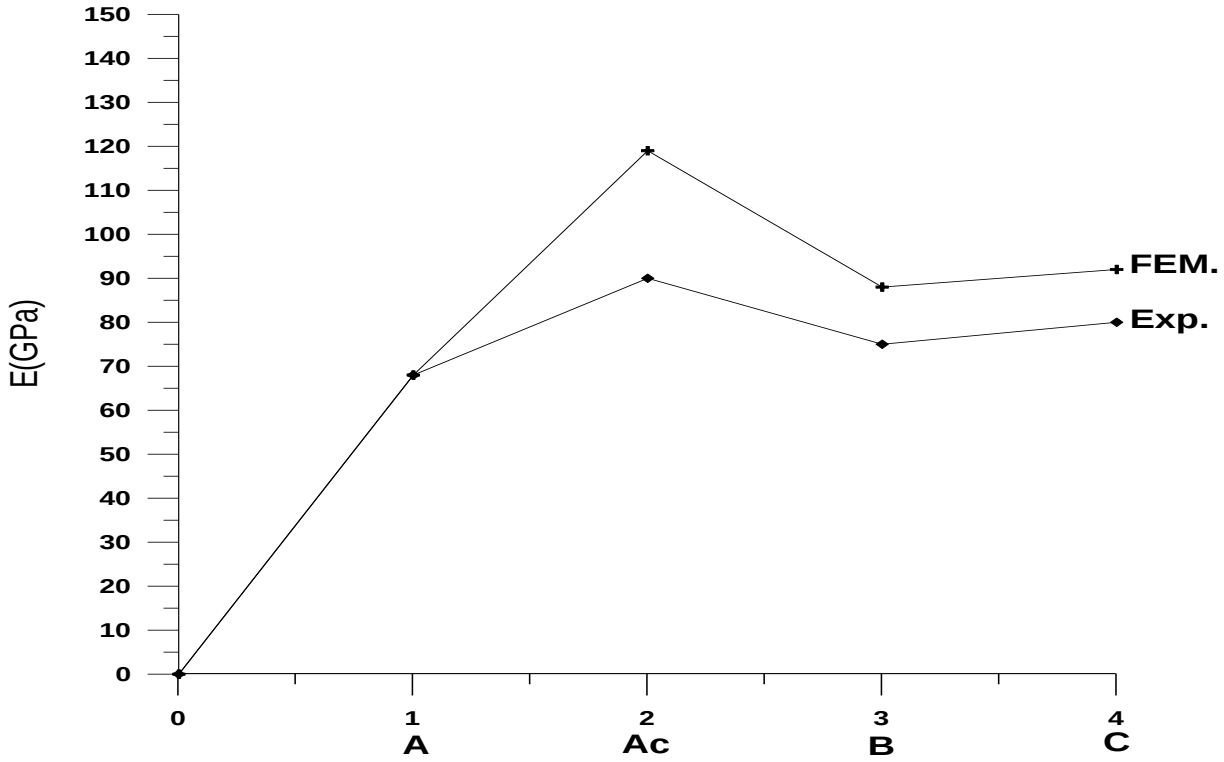

Fig.(4.22): Comparison between modulus of elasticity for FEM and EXP.

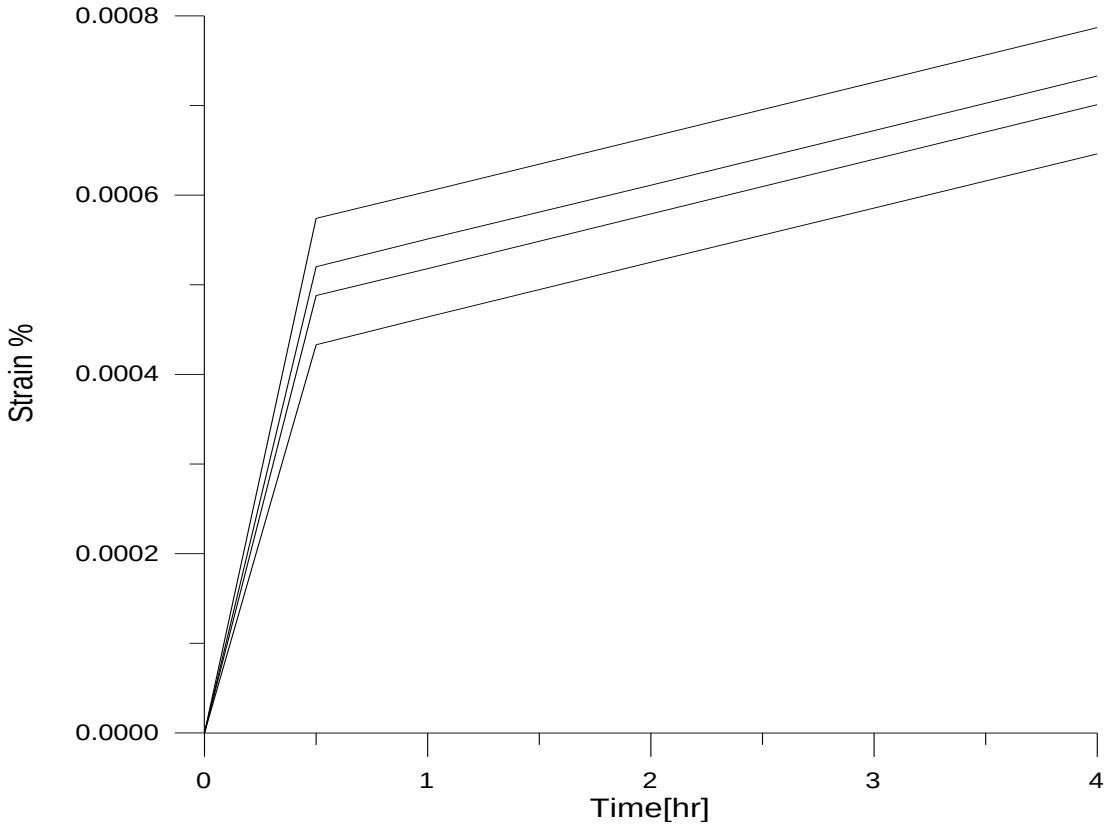

Fig.(4.23): Comparison between creep rate of FEM for different alloys A, A_C, B, and C.

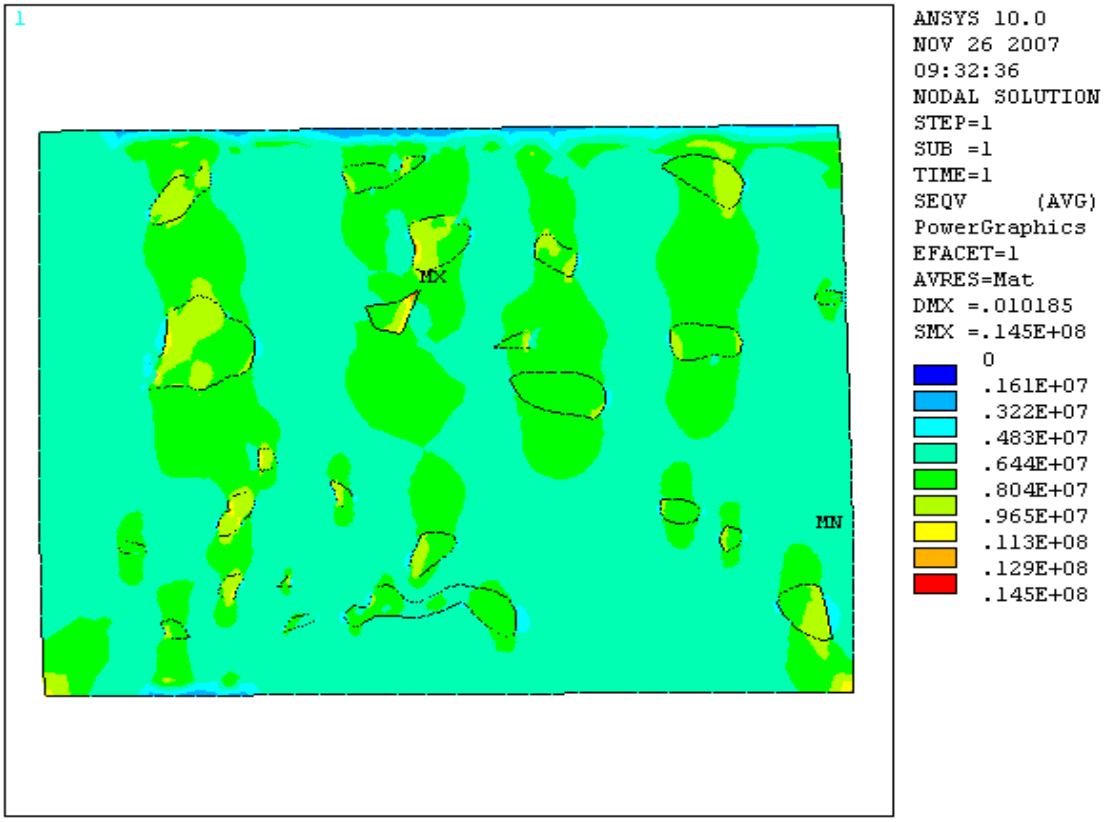

a

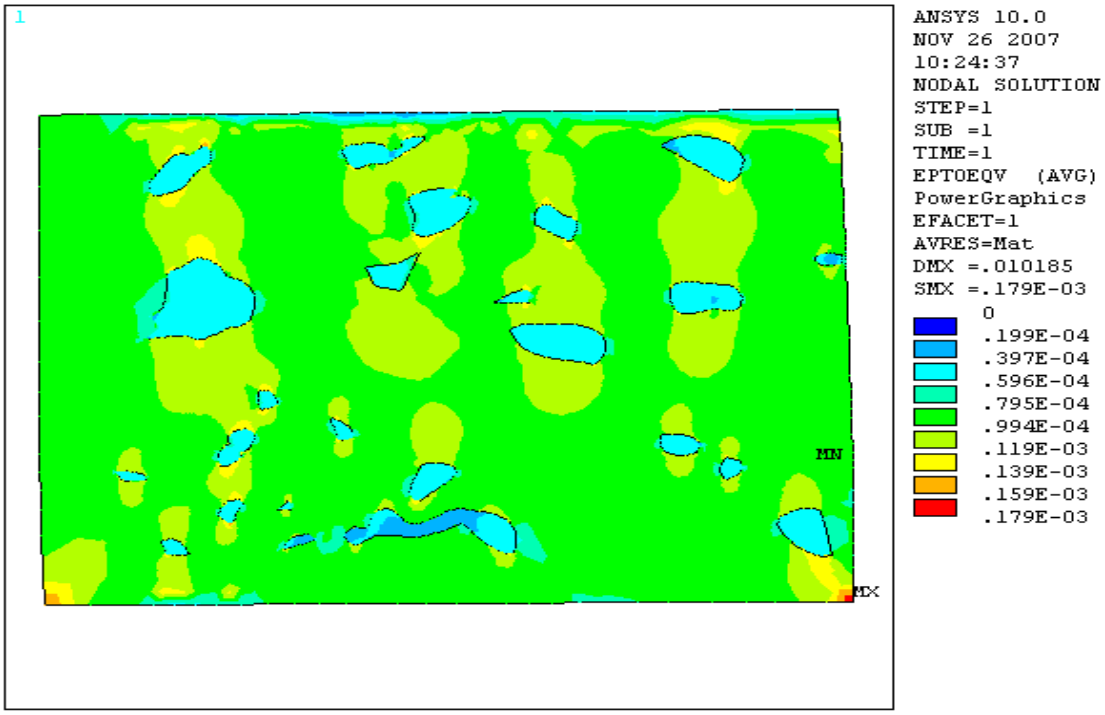

b

Fig. (4-24)FE micro model results

a-stress b-strain

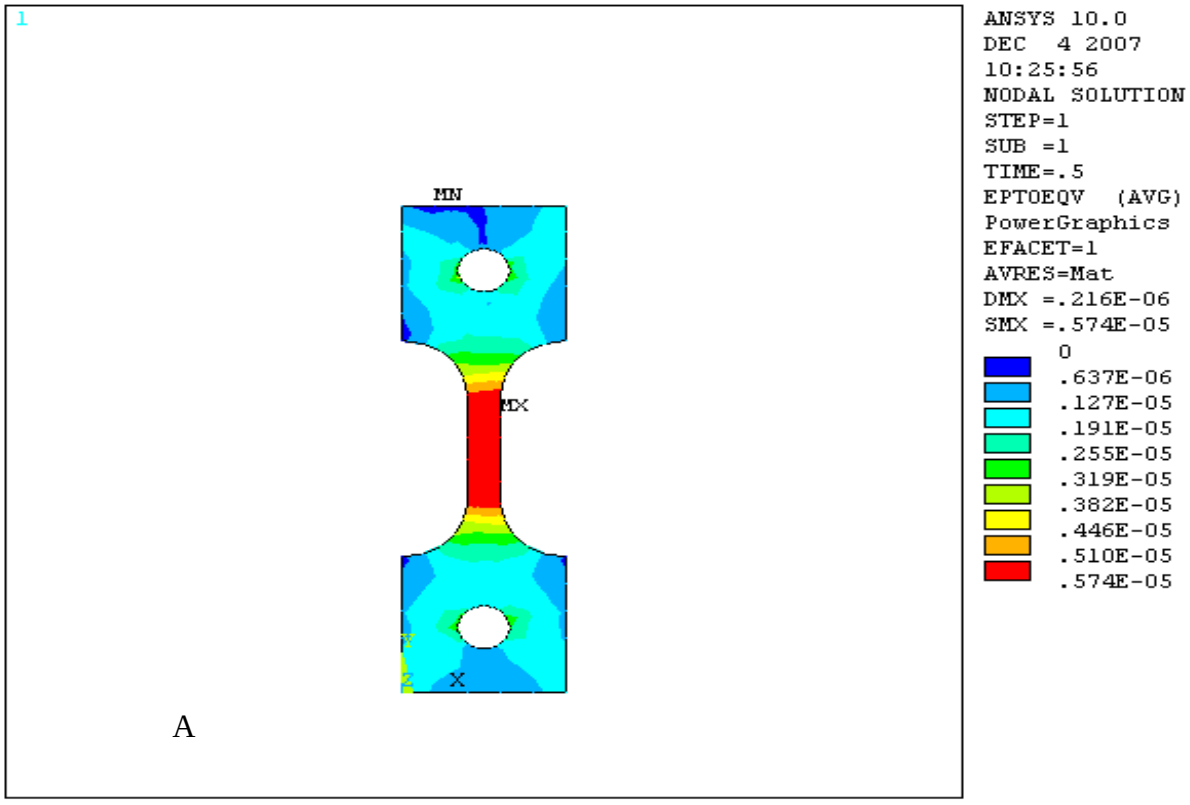

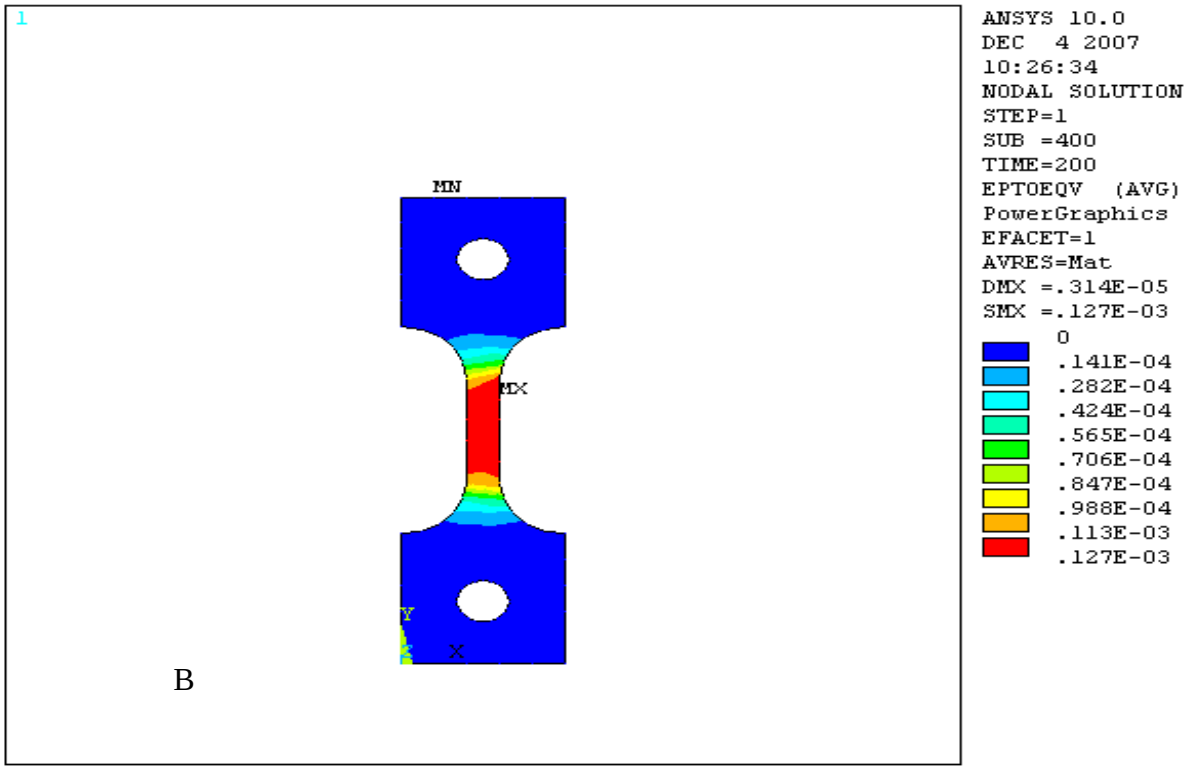

Fig. (4.25) macro mechanic results for alloy A

A-creep (0.5h), b- creep (200h)

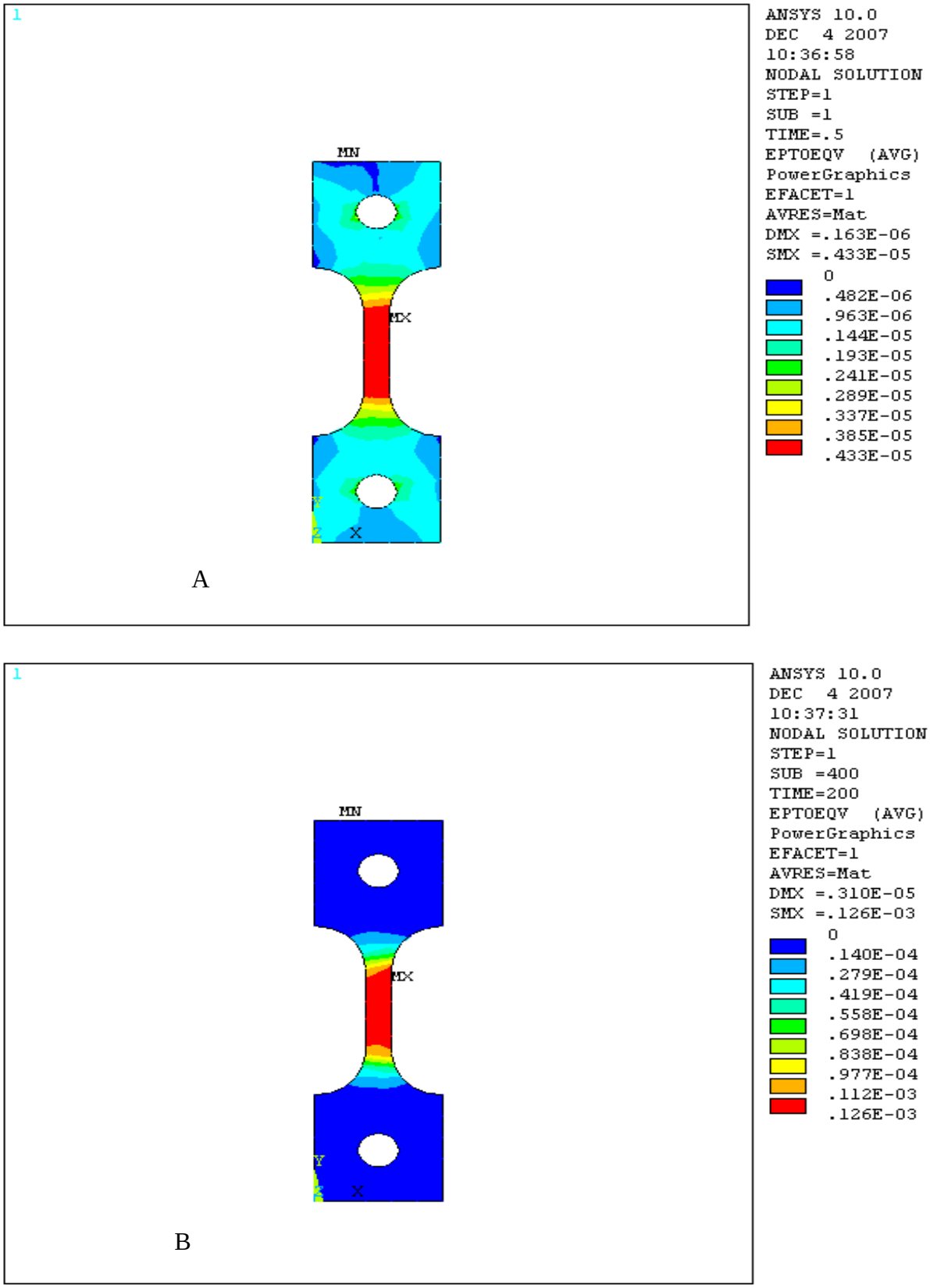

Fig. (4.26)micro mechanic results for alloy Ac

a-creep (0.5h), b- creep (200h)

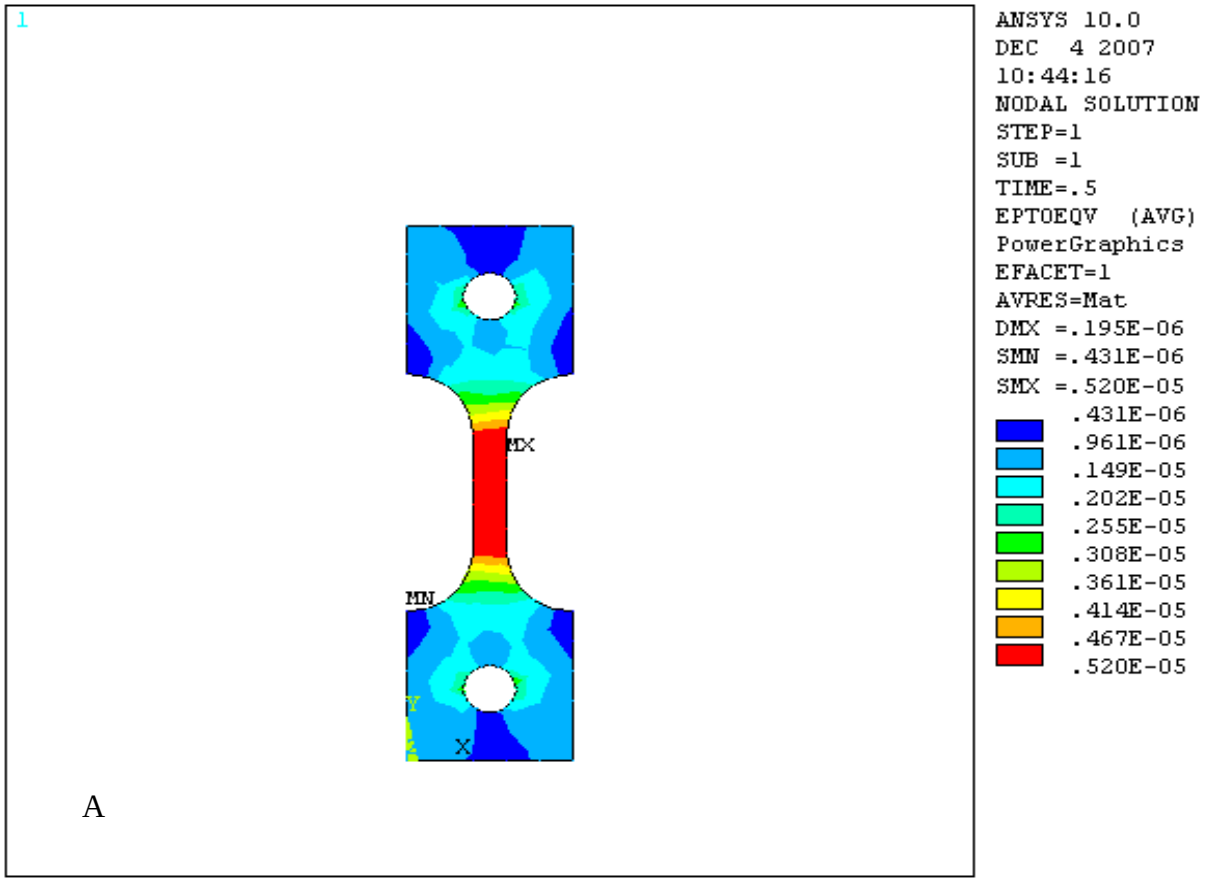

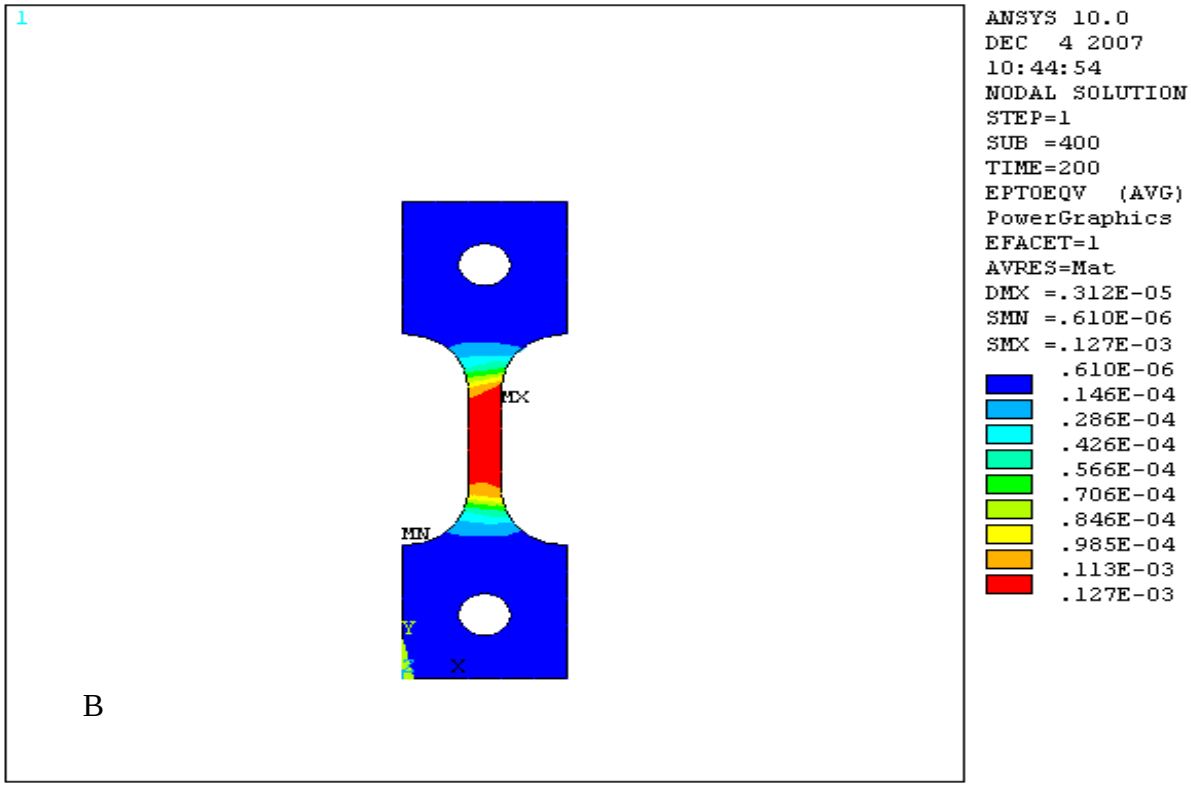

Fig. (4.27)micro mechanic results for alloy B

A-creep (0.5h),B- creep (200h

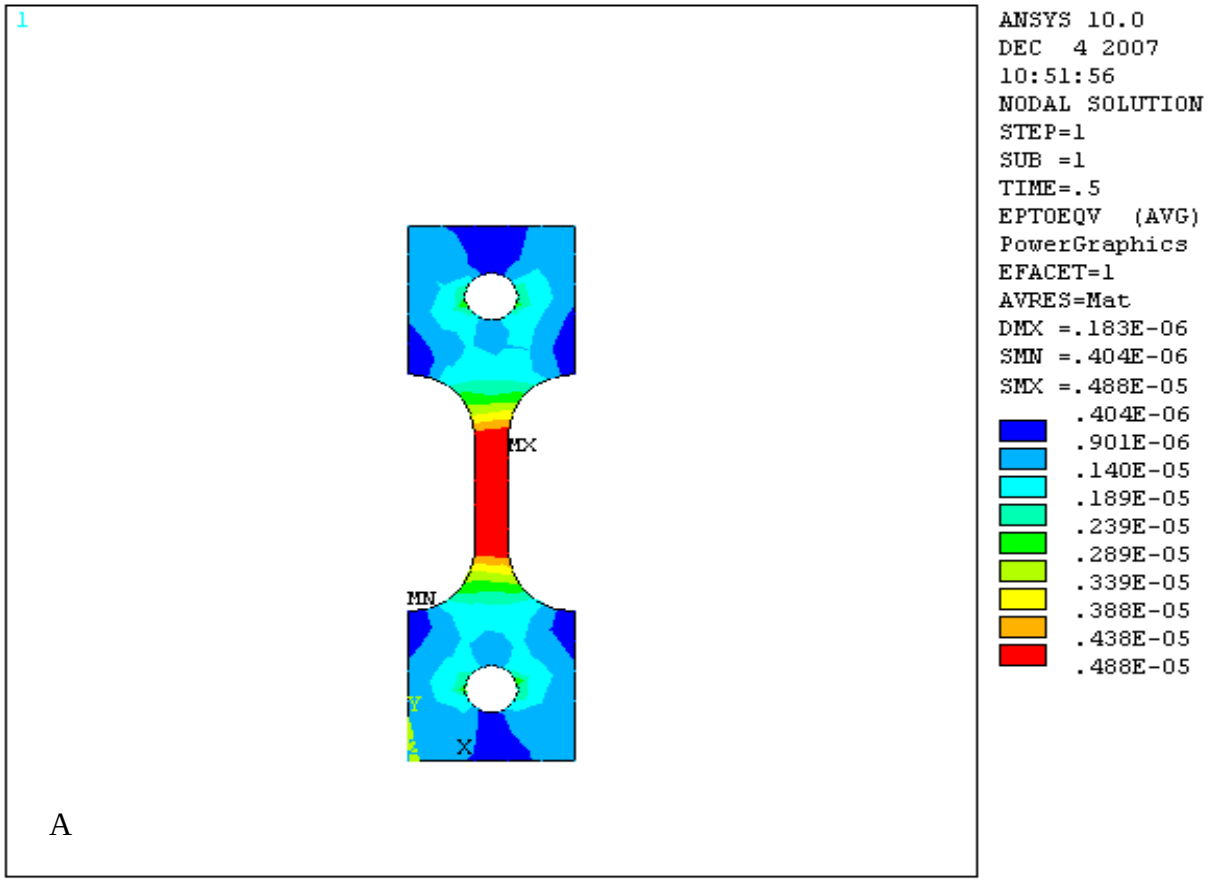

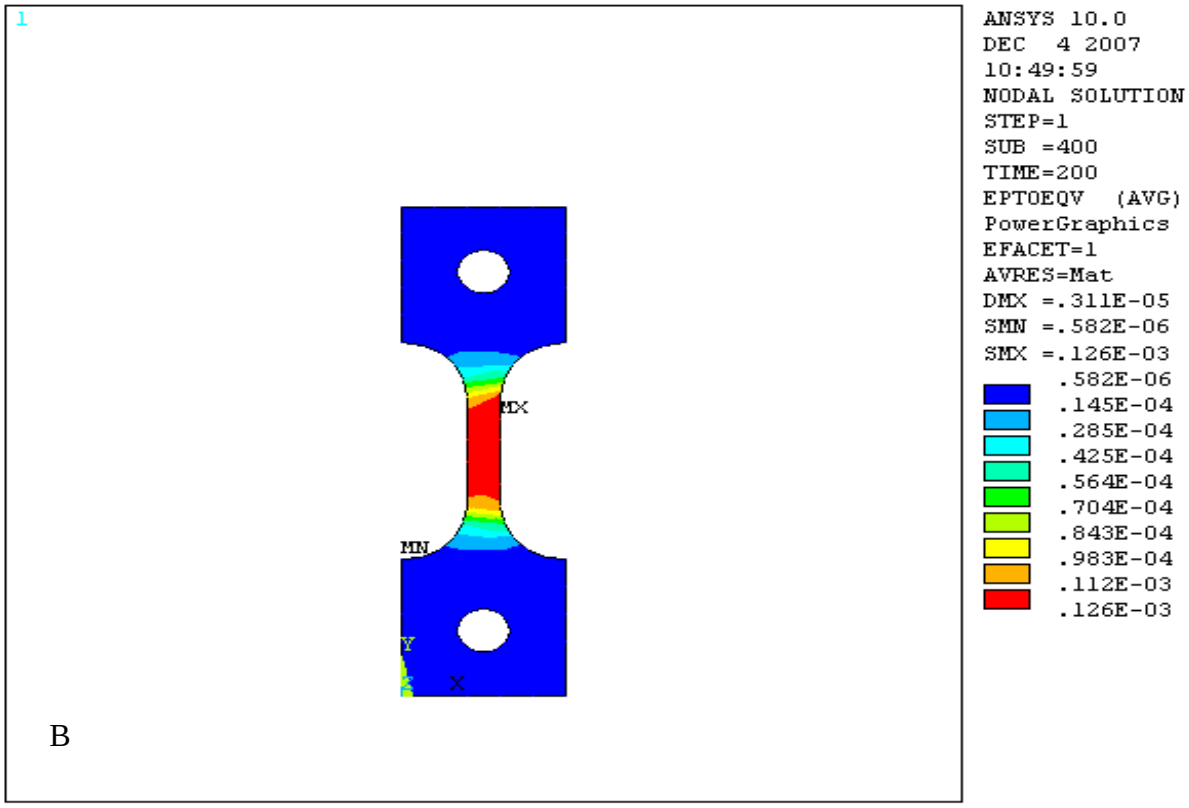

Fig. (4.28)micro mechanic results for alloy C

A-creep (0.5h); B- creep (200h)

Chapter Five

5.1. Conclusions

The following conclusions are drawn from this work:

1. The addition of **(SiC)** to alloy **(A)** caused an increase in strength and strain**.**
2. An increase of **(32.25%)** and **(30%)** in Elastic Modulus **(E_m)** and Ultimate Tensile Strength **(UTS)** was observed in **(SiC)** containing alloys compared to those **(SiC)** free.
3. Variation rate of **(E_m)** and **(UT5)** of **(SiC)** containing samples with temperature was slower than that of **(SiC)** free ones**.**
4. Strain values obtained from the theoretical analysis almost agreed with the experimental results**.**
5. The addition of **(Li)** and **(Li+Zr)** improves creep behavior.
6. Creep curves of the designed and constructed rigs were similar to standard ones**.**
7. Scanning Electron Microscope showed the precipitation of **(s)** phase in a matrix of **(α).**
8. Elastic Modulus **(E_m)** and **(UTS)** remain almost constant up to **~150°C.**

5.2. Recommendations:-

1. Microstructure changes during creep test of these samples required further investigations.
2. Scanning electron microscope is necessary for detailed analysis.
3. The effects of other alloying elements needed to be examined.
4. Some other type of correlation between a certain theoretical analysis and experimental work.
5. Controlled atmosphere durance need to be used.
6. It is essential to conduct creep tests at longer times.
7. Investigation of fiber reinforcement on creep life.
8. Investigation of equi-cohesive temperature effect on creep behavior in different conditions.
9. The work can be conducted in application conditions.
10. The theoretical analysis can be doing by using anther …….numerical packages such as ALGOR, ABAQUS and …….NASTRAN.

Table (1-1) : Composition of typical commercial Al-Li alloys.

No.	Composition w% balance Al / Alloys code	Cu	Li	Mg	Zr	Si	Fe	Others	Company/ country of origin	Ref.
1	1420	-	2.0	5.0	0.1	0-0.15	0-0.15	-	Russia	Fridly ander (1994)
2	1421	-	2.1	5.2	-	0-0.1	0-0.15	0.15 (Sc)	Russia	Fridly ander (1994)
3	1441	1.5-1.8	1.8-2.1	0.7-1.1	0.04-0.16	0-0.1	0-0.1	-	Russia	Bird et al (2000)
4	1460	3.0	2.0	-	-	0-0.1	0-0.1	0.1 (Sc)	Russia	Fridly ander (1994)
5	2090	2.4-3.0	1.9-2.6	0-0.25	0.08-0.15	0-0.1	0-0.12	-	Alcoa	Starke & Csontos (1998)
6	2091	1.8-2.5	1.7-2.3	1.1-1.9	0.04-0.16	0-0.2	0-0.3	-	Pechiney	Starke & Csontos (1998)
7	2095	3.9-4.6	0.7-1.5	0.25-0.8	0.04-0.18	0-0.12	0-0.15	0.25-0.6 (Ag)	Martin Marietta	Starke & Csontos (1998)
8	2195	4.0	1.41	0.35	0.13	0-0.12	0-0.15	0.4 (Ag)	Martin Marietta	Starke & Csontos (1998)
9	8090	1.0-1.6	2.2-2.7	0.6-1.3	0.04-0.16	0-0.2	0-0.3	-	Alcan & Pechiney	Starke & Csontos (1998)
10	8091	1.8-2.2	2.4-2.8	0.5-0.12	0-0.1	0-0.2	0-0.3	-	Alcan & Pechiney	Starke & Csontos (1998)

Table (1-2): Phase encountered in Al-Li-Cu-Mg-Zr alloy system [Lavernia et al., 1990**].**

Phase	Composition	Crystal Structure
δ`	Al_3Li	LI_2
δ	Al Li	B_{32} (cubic)
θ`	Al_2Cu	Tetragonal
T_1	Al_2CuLi	Hexagonal
T_2	Al_6CuLi_3	Icosahedra
T_8	$Al_{15}Cu_8Li_2$	Cubic
β`	Al_3Zr	LI_2
S^1	Al_2CuMg	Orthorhombic

The addition of zirconium results in the formation of a fine dispersion of fully coherent and ordered cubic β` ($Al_3Zr$) particles. The formation of β` starts during the ingot solidification stage and the subsequent homogenization treatment. It is present as very fine and homogeneously distributed particles which are very effective in retarding grain boundary migration during annealing [Palmer, 1984].There-fore, the presence of β` in this alloy suppress static recrystallization and also the grain growth subsequent to dynamic recrystallization. The β` dispersoids are unaffected by the solution-heat treatment which is usually carried out at 530 ^oC [Quist & Narayahan, 1989].

The metastable ordered δ` ($Al_3Li$) phase is the basic strengthening precipitate phase in this alloy. It nucleates homogeneously throughout the matrix [William, 1980; Sanders & Starke, 1980]. Because β` is isostruct-ural with δ`, the former also acts as preferential site for the nucleation of the latter during artificial aging.

The addition of copper decreases the maximum solid solubility of lithium in aluminum at all temperatures [Silcock, 1959-1960]. Three copper containing phase, viz. θ` (Al_2Cu) with tetragonal crystal structure, T_1 (Al_2CuLi) with hexagonal crystal structure, and T_2(Al_6CuLi_3) with icosahedra symmetry, may precipitate due to the addition of copper in Al-Li alloys. T_1 is the predominant strengthening phase present after artificial aging to the near-peak-strength condition.

T_1 nucleates heterogeneously on dislocations, low- angle grain boundaries and substructure feature. T_2 nucleates predominantly on high-angle grain boundaries. The formation of T_2 leads to the development of δ` precipitate- free zones adjacent to the grain boundaries with concomitant reduction in ductility and fracture- toughness. T_2 phase is stable over temperature range of 170–520^{o}C [Cassada et al., 1986].

The addition of magnesium also decreases the solubility of lithium in aluminum at all temperatures below 425^{o}C [Mondolfo, 1976].

Similarly, the solubility of magnesium in aluminum is drastically reduced by the presence of lithium. When magnesium is added to Al-Li alloys containing copper, precipitation of δ` ($Al_2CuMg$) occurs. δ` phase has an orthorhombic crystal structure and has a tendency to nucleate heterogeneously on matrix dislocations, low angle grain boundaries, and other structural in homogeneities. Unlike the case of T_1 precipitation the heterogeneous precipitation of δ` does not result in the precipitate- free zones along either low- or high- angle grain boundaries.

However the exact nature of the phase equilibrium of quaternary Al-Li-Cu-Mg alloys depends on the relative concentrations of all three alloying elements [Sainfort & Dubost, 1987].

1.6. Al-Li-Cu Alloys:

The precipitation sequences observed in this system are complex and are dependent upon the Li:Cu ratio. For low Li:Cu rations the sequence is dominated by that which occurs in binary alloys, with the co-precipitation of δ'[John, 1988].

Super saturated solid solution $\longrightarrow$ G_p Zones $\longrightarrow$ $\overset{=}{\theta}$ $\longrightarrow$ $\bar{\theta}$ $\longrightarrow$ $\overset{\theta}{\theta}$

Super saturated solid solution $\longrightarrow$ δ' (Al_3Li) $\longrightarrow$ δ(AlLi)

At aging temperature greater than 200°C, T_1(Al_2CuLi) and / or T_n($Al_{15}Cu_8Li_2$) and (T_2(Al_6CuLi) phases also be present. A high Li: Cu ratio leads to δ' precipitation at all aging temperature below 250°C.
The partially coherent T_1 phase precipitation as plates and has a hexagonal structure [Yao et al., 1989].

The major influences of Copper additions to Al-Li are similar to those of Mg during the early stages of aging i.e. copper addition force Lithium out of solution factor upon aging. During later stages of aging, T_1 or Al-Cu type of phases is co -precipitated which increases the alloy strength and density but planar slip is not reduced.

However, the T_1 phase forms on sub-boundaries resulting in Li-depletion at these boundaries.

1.7. Al-Li-Mg Alloys:

The magnesium content in Al-Li alloys has been selected to impart solid solution strengthening, by reduction in Lithium solubility whilst avoiding precipitation of Al_2MgLi along grain boundaries which Sanders[Gregson & Flower,1985] reported to deteriorate the properties [Grimes et al.,1985]. Therefore no precipitation additional to that of δ'

occurs during age hardening. Furthermore there is no significant increase in lattice misfit between δ' particles and the matrix as a result of the Mg being incorporated into precipitates as well as matrix. Mg addition alone therefore cannot alter substantially the deformation characteristic of the alloy.

1.8. Al-Li-Cu-Mg Alloys:

Replacement of part of the Copper additions with Mg is not only advantageous from density consideration, but it also offers the possibility of forming A(Al_2CuMg) phase precipitates in the Al-Cu-Mg system [Ahmad & Ericsson, 1986; Smith et al., 1989].

Since S is heterogeneously nucleated at dislocations, a stretch before aging is applied to refine the distribution of S precipitates and this phase could enhance the strength, as well as help to homogenize the coplanar slip distribution characteristic of the shearing or ordered, coherent phase (such as δ' in Al-Li alloys).

The S phase, face-centered orthorhombic crystal structure precipitates as rods thickening to laths on (210) planes in the [100] growth direction [Ahmad & Ericsson, 1986, Smith et al., 1989].

With regard to the nucleation of S phase, the strong Lithium atom – vacancy binding energy, coupled with the very large atomic concentration of Li, inhibits vacancy condensation and bence the formation of dislocations loops and helices upon quenching. The only available heterogeneous nucleation sites are dislocation, grain boundaries, sub grain boundaries and stray dislocations [ABBAS, 1995].

1.9. Numerical Simulation:

To carry out a numerical simulation process by using the Finite Element Method, we must understand the general guidelines for using that method.

1.9.1. General Guidelines for Using the (FEM) Finite . Element Method:-

Finite element programs should be used as “black boxes” without a firm understanding of the underlying theory and, principles behind the technique .Therefore, before using any one of a commercial FE software packages, one should understand the principle of FEM Technique, and then the stages of modeling in FE software [Beuker, 2004].

1.9.2 . Finite element Method (FEM):

Finite element (FEM) technology has been very well established as the main tool for engineering analysis since the early 1980s, engineering analysis uses FE Method in analysis of many engineering problems including the forming processes [Beuker, 2004].

FEM is one of three main approaches (FEM finite element method, Finite difference (FD) method, and BE Boundary element method. As shown in Fig. (1.8). the main features of FE method are:

The entire solution domain is divided into small finite segments (hence- the name finite-element).

- Over each element, the behavior is described by displacement of elements and the material law.
- All elements are assembled together and the requirements of continuity and equilibrium are satisfied between neighboring elements.

- Provided that the boundary conditions of the actual problem are satisfied a unique solution can be obtained to the overall system of linear algebraic equations.
- The solution matrix is sparsely populated (i.e. with relatively few nonzero coefficients).

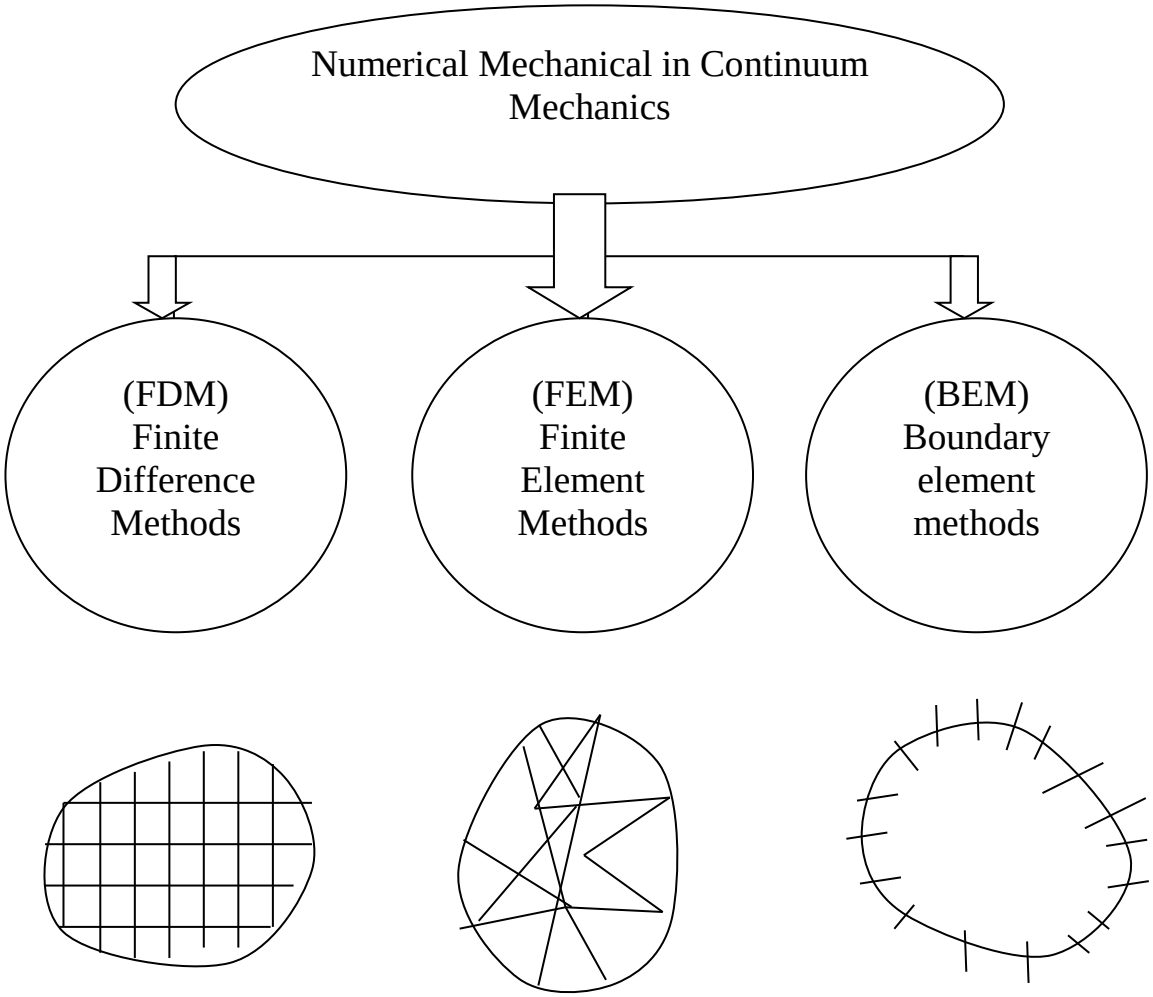

Fig. (1-8) Numerical method [Beuker, 2004]

These features are shown in fig.(1-9) as steps, with the general formulation

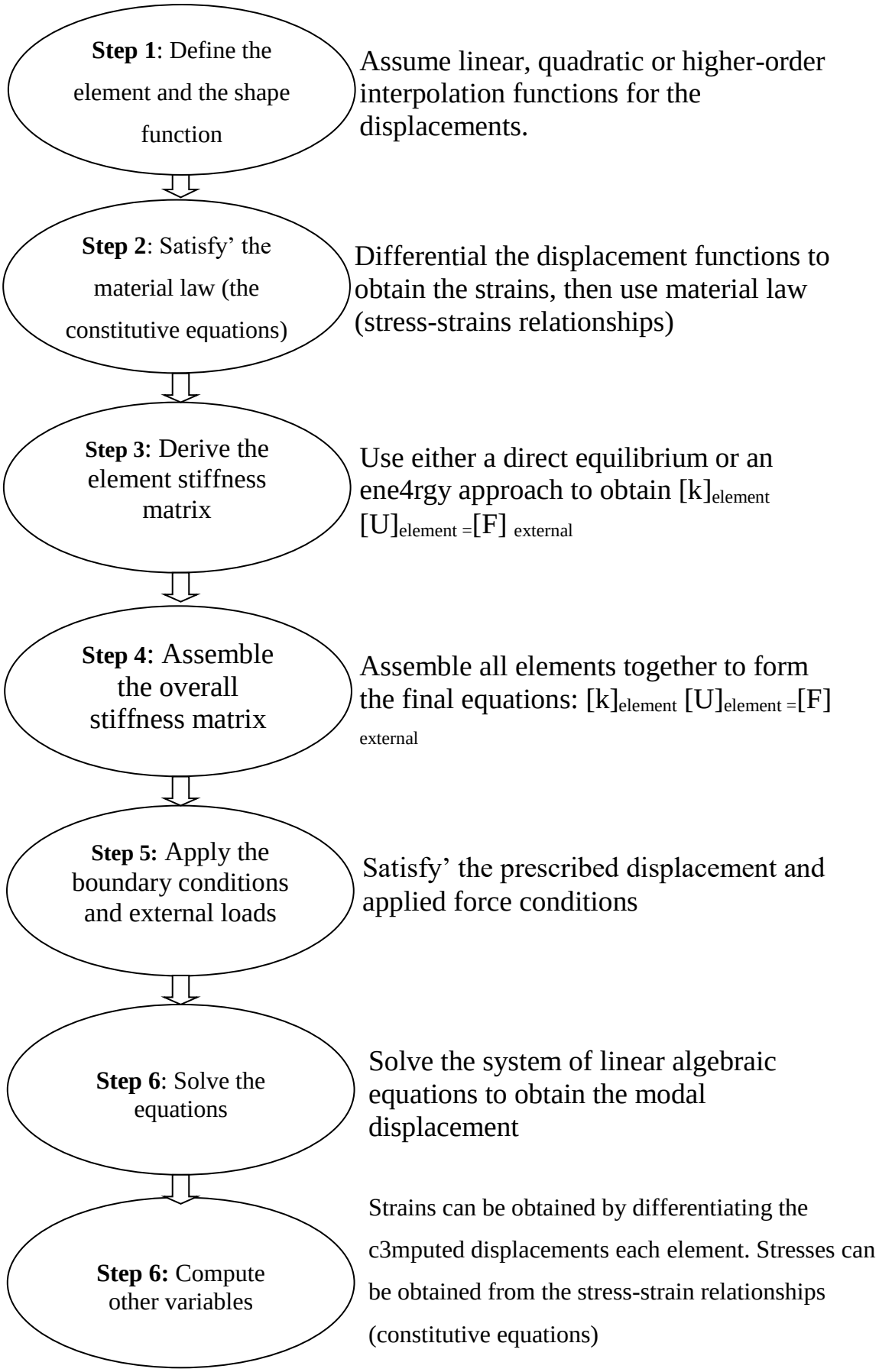

Fig(1-9) features and general formulations

1.9.3 . Modeling by FEM Software:

To model a given problem using FE Method, the user must specific, without ambiguity, all of the data required to define a problem with a unique solution. These include.

• Geometry.

• Material properties.

• Analysis type.

• Displacement boundary condition.

• Applied loads

• Elements type.

• Other information, such as the objectives of the analysis.

Most commercial FEM software packages are available on a wide range of computer hardware systems ranging from personal computers to large mainframe computers. The Finite element analysis by this software can be broken down into three distinct stages as in fig (1.10):

Stage 1: the pre-processor, in which the mesh is generated and the data input file is constructed.

Stage 2: the solver, in which the matrices are assembled, and solved.

Stage 3: the post-processor, which is used to view the results of the

solve.

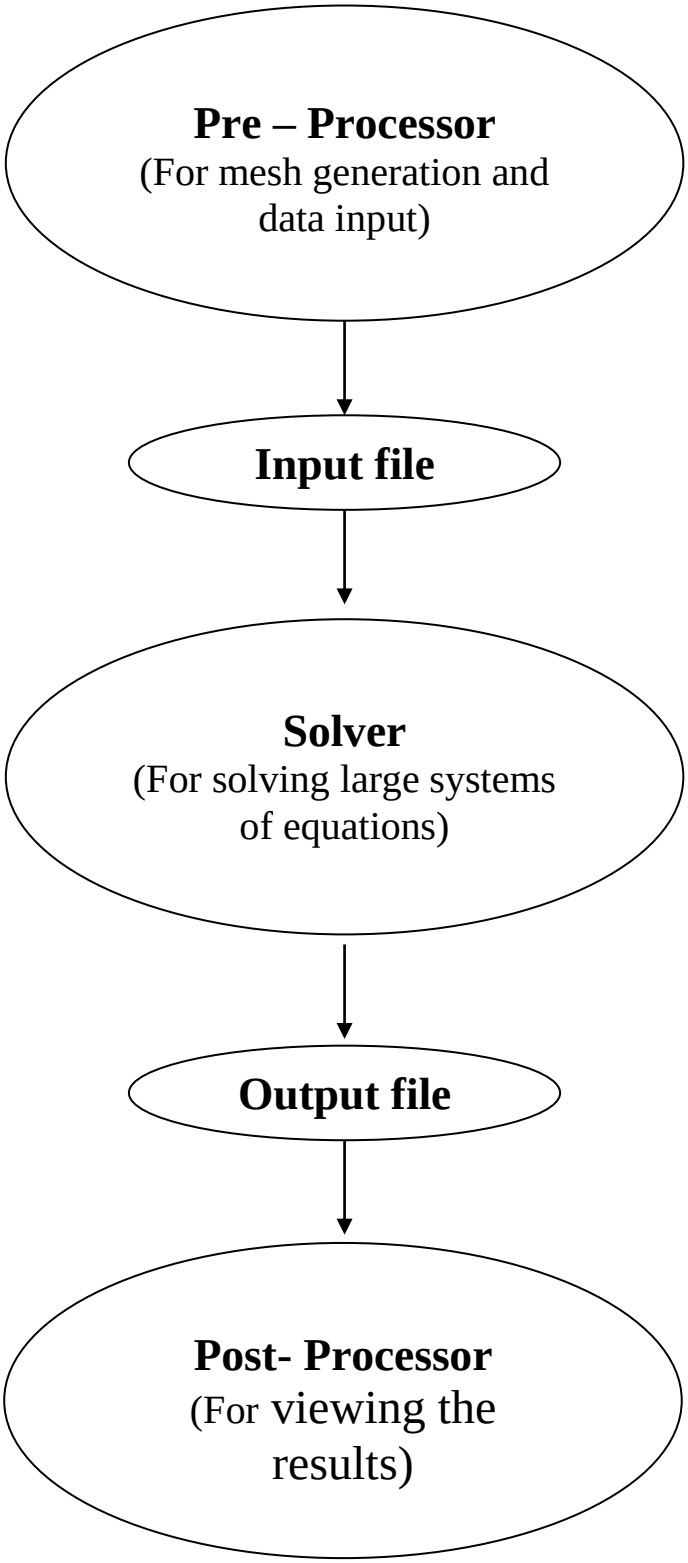

Fig. (1.10) Finite Element analysis [Beuker, 2004]

1.10. Literature Review:

There is a numerous study about Al-alloy creep as follows:

S. C. Wang and M. J. Starink, (2007): They use TEM and DSC to study the formation of two variants of phase precipitation in an Al-4.2Cu-1.5Mg-0.6Mn-0.5Si and an Al- 4.2 Cu - 1.5 Mg. 0.6 Mn - 0.08 Si alloy . In DSC experiments on as solution treated samples two distinct exothermic peaks are observed In the range 250-350°C.

Nong Gao et al., (2006): They study the evaluation of microstructure and precipitation in heat-treatable aluminum alloys during ECA pressing and sequent heat treatment by using TEM and DSC. Micro structural examination showed the grain singe of both alloys where reduced the grain size to the range of 0.3 – 0.5 μm.

M. J. Starink and J. L. Yan, (2006): There study a multi mechanistic model for evaluation of yield strength during heat treatment of Al – Cu – Mg based alloys is derived. The model is computationally very efficient, as all formulations are closed form, and it shows good predictive capabilities for alloy with Cu contents in excess of about 1wt%. the model also explains the local hardness variations in Al – Cu – Mg based welds.

S. C. Wang et al., (2005): They study the Estimation of dislocation densities in clod rolled Al –Mg –Cu –Mn alloys by combination of yield strength data, EBSD and strength models the present a simplified model for the yield strength contributions and apply that to obtain the dislocation densities by determining the orientation factors, which can be batained via the crystal information of electron backscatter diffraction.

Robert A. Edahl et al., (2004): In their study the tensile properties were evaluated for four aluminum alloys that are candidates for airframe structural applications at elevated temperature. Measured properties were compared with the Concorde material and the Russian alloy 1143. All four alloys showed significant tensile property improvement over CMOOL and 1143.

V**. Yamakov et al., (2004):** A multiscal modeling strategy is used to study the effect of grain- boundary sliding on stress localization in a poly crystalline microstructure with an uneven distribution of grain size, the development of the molecular dynamics (MD) analysis used to interrogate idealized grain microstructures with various types of grain boundaries and the multi scale modeling strategies for modeling large systems of grains is discussed. Both molecular-dynamics and finite-element (FE) simulations for idealized poly crystalline models of identical geometry. The models allow for study of the load transfer between adjacent grains of very different size through grain-boundary sliding during deformation.

Cynthia L. Lach and Marcia S. Domack, (2003): Their development of Al-Cu-Mg-Ag alloys for thermal stability also offer attractive ambient temperature strength – toughness combinations, and therefore , can be considered for a bread range of airframe structural applications. The study evaluated Al-Cu-Mg-Ag alloy RY226-T8 in plate gages and compared performance with sheet gage alloys of similar composition.

W. M. Johnston et al., (2002): In their study tensile test were performed to demonstrate the anisotropy of Al – Li alloy 2195-T_8. ciruci form biaxial test were used to determine the effect of biazial loading on yield strength for specimens machined from two thickness of 2195-T_8, 0.45 in and 1.75 in. test were conducted at seven biaxial load ratios for each plate thickness. The 0.2% yield load was determined

from these tests and compared to the base line aluminum alloy 2219.The result of this study indicate the uniaxial tensile strength of 2195-T_8 is anisotropic. The rolling direction has the highest tensile strength and an 18% reductron in strength was found at 55°.

N. GaO et al., (2002): They studied the hardening an micro structural evaluation during ageing of a Al - 1.2Cu – 1.2 Mg alloy. Artificial ageing at 150°C of stretched and naturally aged samples initially (up to about 48hr) leads to very limited further strengthening, but ageing at 190°C results a quick increase in strength.

M. S. Yaghmace and G. Kaptay, (2002): In their study a thermodynamic analysis of S.C/ Al-Si-Mg system has been performed in order to find the conditions to produce SiC/ Al-Si-Mg composite materials with the stable SiC/ alloy interface and with the solidification of primary α-Al solid solution. A certain minimum critical Si-content of the melt is needed to avoid the formation of Al_4C_3 at the SiC/ liquid alloy interface. The critical Si-content has been found to increase both with temperature and Mg-content of the melt.

Stephen J. Hales et al., (2001): An investigation of the structure property relationship in Al – Li alloy extrusions has been conducted. The micro structural characteristics of the 2195, 2099 and 2096 extrusions are similar, comprising a laminar structure of high aspect ratio grains exhibiting location- dependent variation in morphology.

L. P. Troeger et al., (2000): Their research is an investigation of the processing microstructure-property relationship for shear formed cylinders of the Al-Cu-Li-Mg-Ag alloy 2195 for space applications and the Al-Cu-Mg-Ag alloy C_{415} for airframe applications. Cylinders which have undergone various amount of shear-forming strain have been studied to assess the microstructure and mechanical properties developed during and after shear forming. The grain structure of the

2195 cylinders appeared partially recrystallized and become less homogenous as shear – forming strain increased. The grain , structure become finer and more equiaxed toward the inner surface of the cylinders.

W. F. Miao and D. E. Laughlin, (2000): Investigation of effect of Cu content and presaging treatment on precipitation sequence and artificial aging response in aluminum alloy 6022 were investigated using (TEM), (DSC), and hardness tests. It was sound that Cu increase the formation of Q and its precursor metastable phases and has a beneficial effect on the kinetics of artificial aging. For the alloy with 0.07 wt pct Cu, the precipitation sequence is GP zones $\rightarrow$needle like $B'' \rightarrow$ rod like B'+ lath like $Q' \rightarrow \beta$+Si On the other hand, the precipitation sequence in the alloy with 0.91wt pct Cu is:GP zones $\rightarrow$needle like $B'' \rightarrow$ lath like $Q' \rightarrow$Q + Si For the artificial aging condition of 20 minutes at 175°C, which is the typical automotive paint bake condition, suitable presaging treatments, were found to significantly reduce the detrimental effect of the natural aging on artificial aging response.

M. J. Starink et al., (2000): They studied a rolled 8090 sheet in three under aged heat treatment conditions, including T_3, T_{81} and a multi stage temper designated RSW, was exposed for 1000h at 70°C. exposure of T_3, T_{81} and RSW 8090 at 70°C causes an increase in yield strength and a decrease in toughness. Toughness reduction is limited for the RSW condition.

G. Gralss and M. A. Mohammed, (2000). Conducted a creep test under the effect of cyclic stress reduction to Al-16et% Ag and Al-16 wt% Ag-0.1 wt% Zr alloy aged at S48 and 673k. The steady stat creep rate was found to be higher under cyclic stress reduction condition than that under static creep condition for the same maximum stress.

R. K. Bird et al., (2000): Conducted a cooperative investigation to evaluate Al-Cu-Mg-Li alloy 1441 for long service life fuselage applications. Cold-rolled 1441 Al-Li sheet specimens were tested at NASA Langley Research Center (LaRC) and at the All-Russia Institute of Aviation Materials (VIAM) in Russia to evaluate tensile properties. The results of this study have shown that Russian 1441 Al-Li alloy mechanical properties are better than or similar to those for a conventional aluminum fuselage skin alloy 1441 Al-Li sheet specimens exhibited strength toughness, and tensile fatigue life similar to shat for 1163 Al(2524 Al) sheet.

M. J. Starink et al., (1999): Developed a model to measure yield strength of four Al – Li –Cu – Mg type alloys and composite. A detailed model for the strengthening of monolithic alloys and composite. The model incorporates precipitation strengthening, solution strengthening by dissolved atoms, grain and sub grain strengthening, strengthening by dislocation and load transfer to ceramic inclusion, and it includes a new description for the effect of precipitate free zone (PFZ) around the reinforcing phase.

Roberto Cocomazzi, (1999): In his work a tensile tests carried out on two particles reinforced composites (20 vol% Al_2O_{3p} and 10 vol.% Al_2O_{3p}) showed a significant increase of the elastic modulus and tensile strength respect to the corresponding unreinforced alloys, while they exhibited a much lower tensile elongation. The tensile strength decreased in the temperature range investigated, while elongations increased. Particle fracture was the main damage prior to final fracture, mainly at room temperature and with large particles or clusters of particles, while at high temperature void nucleation was found in the matrix.

K. Hono et al., (1998): Discuss 3DAP analysis of the pre-precipitation stage of Al – 1.9 Cu – 0.3 Mg – 0.2 Ag alloy have revealed that Mg – Ag Co- clusters are formed after 5 s aging at 180°C . Cu atoms are not incorporated in the Mg. Ag Co-clusters at the initial stage and the morphology of the Co-clusters is not well defined.

A. B. Pandeyet and R. D. K. Misra, (1989): Described the work deals with the production and chemical segregation of solute elements in ultrasonically gas atomized aluminum lithium alloy powders of nominal composition Al – 1.36Li – 0.92Cu – 0.66 Mg (all in mass%). An attempt has been made to study the extent of micro chemical segregation of the alloying elements. In their work presented demonstrates the significant of micro chemical characterization of rapidly solidified powders which of considerable importance in the subsequent processing of powders.

J. C. Hvang and A. J. Ardel, (1988): In their study. The room temperature yield strength of two alloys, Al – 2.3wt Li 2.88 Cu – 0.12Zr (the 2-3 alloy) and Al – 2.9 Li – 0.99 Cu – 0.12 Zr (the 3-1 alloy), was investigated as a function of aging time at 160 and 190°C. reversion experiments were used to separate the contributions of δ and T_1 precipitates to the overall strength of the aged samples.

Terence G. Langdon and Parviz Yavari, (1982): Proposed a several deformation mechanisms to explain the flow process of Harper-Dorn creep. The implications of these various mechanisms are compared with the available experimental data and it is concluded that flow occurs by the climb of edge dislocations under saturated conditions. Using the theoretical model for this process, it is possible to specify the experimental criteria for observations of Harper-Dorn creep in terms of the upper limiting stress and the lower limiting grain size.

T. Balakrishna et al., (1977): Proposed a model for climb-controlled creep in two – phase materials is proposed which invokes the presence of back-stress for providing the necessary mobile dislocations for creep. It is shown that by incorporating this stress in the creep equation it is possible to reduce both the activation energy for creep and the stress exponents to values normally observed in single – phase materials. Creep data on TD nickel and yttriated super alloy when analyzed on this basis confirm the applicability of this model. High n and Q values observed during creep in two phase material due to the thermal barrier offered by second phase particles to dislocation motion. Until this stress barrier is overcome there can be no free dislocations for climb.

1.11. Aim of the Thesis:

The aim of the present work is to improve the creep resistance for certain Al-alloys which are used in aerospace industries. This object was achieved by using different roles which are:

1. Alloying elements and compound (SiC) technique.
2. Heat treatment.
3. Mechanical deformation.

Also a theoretical analysis was used to predict the effect of these parameters on creep behavior. Then an experimental work was conducted and then the results were compared to verify the accuracy and activity of that model.

Nomenclature and Abbreviations

$\in$	Strain (%)
$\in'$	Strain rate (sec^{-1})
σ	Stress (MPa)
σ_y	Yield stress (MPa)
UTS	Ultimate tensile strength (MPa)
b	Burger vector
d	Grain size
D_0	Diffusion coefficient ($cm^3. sec^{-1}$)
E(E_m)	Young's modulus (Elastic modulus) (GPa)
G	Shear modulus (GPa)
k	Boltzman constant.
K	Material constant when only the strain rate sensitivity is considered.
K'	Material constant when only the strain hardening sensitivity is considered.
K"	Material constant both strain rate sensitivity and strain hardening are considered.
M	Strain rate sensitivity index.
n	Stress exponent.
n_s	Strain hardening exponent.
Q or Q_i	Activation energy (for: a=apparent, t=ture, gb=grain boundary diffusion) (cal. $Mol^{-1}.ok^{-1}$)
R	Gas constant.
T	Temperature (^oC)
T_c	Critical temperature of GP zones formation. (^ok)
T_m	Absolute melting temperature of material. (^ok)
MPa	Mega Pascal.
GPa	Gega Pascal
TEM	Transmission electron microscopy.
3DAP	Three dimensions atom probe
AA	Artificial aging.
APFIM	Atom probe field ion microscopy.
CNC	Computerized numerical control.
GPZ	Guinier Preston Zones.
NA	Natural aging
OA	Over aging.
UA	Under aging.
PA	Pre-aging.
PFZ	Precipitate free zones
SST	Solid solution treatment.
SSSS	Super saturated solid solution.

Temper Designation

Basic temper designations

F – As fabricated. No control over the amount of strain hardening; no mechanical property limits.

O – Annealed and recrystallized. Temper with the lowest strength and highest ductility.

H – Strain–hardened (see below for subdivisions).

T – Heat-treated to produce stable tempers other than F or O (see below for subdivisions).

Strain-hardened subdivisions

H1 – Strain-hardened only. The degree of strain hardening is indicated by the second digit and varies from quarter hard (H12) to full-hard (H18), which is produced with approximately 75 percent reduction in area.

H2 – Strain-hardened and partially annealed. Tempers ranging from quarter hard to full-hard obtained by partial annealing of cold-worked materials with strengths initially greater than desired. Tempers are H22, H24, H26, and H28.

H3-- Strain-hardened and stabilized. Tempers for age softening aluminum-magnesium alloys that are strain-hardened and then heated at a low temperature to increase ductility and stabilize mechanical properties. Tempers are H32, H34, H36, and H38.

Heat-treated subdivisions

T1– Naturally aged. Product is cooled from an elevated-temperature shaping process and naturally aged to a substantially stable condition.

T3 – Solution heat-treated, cold-worked, and naturally aged to a substantially stable condition.

T4 – Solution heat-treated and naturally aged to a substantially stable condition.

T5 – Cooled from an elevated-temperature shaping process and then artificially aged.

T6 – Solution heat – treated and then artificially aged.

T7 – Solution heat – treated and stabilized.

T8 – Solution heat – treated, cold-worked, and then artificially aged.

Abstract

It is well established from thermodynamics that, the higher the operating temperature the higher the efficiency. This is actually the reason behind elevated temperature applications. Unfortunately, the increases in operating temperature intensified the aggressive attack of hostile environments and involve a significant drop in mechanical properties of the components.

The aim of this work is to investigate the effect of alloying elements and certain parameters on high temperature behavior of, **(Al-Cu-Mg)** based alloy.

A theoretical analysis was also adopted to predict creep strain. Time dependent strain is a tedious, costly and time consuming test, therefore, five complete creep test rigs were designed and constructed, which involved the preparation of about **(100)** samples.

Casting process also involved the designed and manufacturing the gas furnace of a capacity of more than **(10kg)** and temperature of about **(1000°C),** and a special steel die to be able to enhance the directional solidification.

An electric furnace of about **(1000°C)** was also designed and built for heat treatment of the examined samples.

Samples were then computerized numerical control **(CNC)** machined for the standard profile. Scanning electron microscope was also used for metallography.

A certain modifications were introduced to carry out tensile tests at different temperatures to measure modulus of elasticity **(E_m)** and ultimate tensile strength **(UTS)** by elevated temperatures**.**

Results showed that the elastic modulus **(E_m)** of examined alloys is depending on the testing temperatures i.e. microstructure and crystallography.

Similar behavior was observed in the ultimate tensile strength **(UTS)** values.

An increase in **(E_m)** and **(UTS)** of silicon carbide **(SiC)** containing alloy was about **(32%)** and **(30%)** respectively compared to **(A)** alloy.

The effects of **(SiC)** addition on creep curve also clear, since when creep curve of **(SiC)** free **(A)** alloys reaches fracture point, the corresponding curve of **(SiC)** containing **(A_c)** alloy still in the beginning.

It appear that the addition of **(Li)** alone or **(Li & Zr)** to alloy **(A)** improves creep behavior by modification and precipitation, grain size and the deformation rate, especially in earlier stages.

Fast fracture of samples due to high temperatures or applied load or both are also indicated in this work.

Strain values obtained from the theoretical analysis gave lower values than that obtained by experimental work.

References

A. B.Pandey, R. D. K. Misra & Mahendra Kuamr**:** Production and Microchemical Characterization Ultrasonically Gas Atomized Aluminum-Lithium Alloy Powders, Poser metallurgy international , vol.21, no.4, (1989).

ABBAS M. K.**:** Effect of trace additions of alloying elements on oxidation and some properties of Al-Li alloys. A thesis submitted to the department of production engineering and metallurgy in the University of Technology in partial fulfillment of the requirement for the degree of PhD in Metallurgical engineering, (1995).

Abdul-Raheem K. A.**:** Investigation of Certain Shape Memory Alloys In Space Systems. Athesis submitted to the department of Engineering materials /College of Engineering/University of Babylon in partial fulfillment of the requirement for the degree of PhD in Materials Engineering, (2007).

Abe T., Miyazaki K. and Hirano K.**:** Imaging of pure Al and aged Al-4wt. % Cu alloys by field ion microscopy. Acta Metall. 30: 357-366 (1982).

Ahmad A. & Ericsson T. E.**:** Coarsening of δ', T_1, S^- Phase and Mechanical Properties of Two Al-Li-Cu-Mg Alloys, 3rd Int. Al-Li conf., London, (1986), P.509.

Aluminum Federation**:** The properties of Aluminum and it's alloys, Published by the aluminum Federation, Broad way house, Birmingham, third edition, (1998), PP. 244-251.

Anderade E.N.da L.**:** Flow of metals under large constant stress, Proc. Roy. Soc. A 90: 329-342. (1914). : The viscous flow in metals and allied phenomenon, Proc. R. Soc. London A 84: 1-12. (1910).

Ashby Michael F. & Joues David R. H.: Engineering Materials1**:** An Introduction to their Properties and Applications. Pergramon Press. ISBN 8-08-026138-8. (1980).

Avner H. Sidney.**:** Introduction physical metallurgy, second edition,, pp. 481-499 (1987).

Basem M. M. **:** Increasing hgigh temperature aerospace aluminum alloy resistance. Thesis submited to materials engine. Dep. College of eng. Babylon Univ.,(2004)

Bagaryatsky A. Yu,**:** Doklady Aknd. Nauk SSSR 87**:** 559-562 (1952).

Beton R. H. & Rollason E. C.**:** Hardness reversion of dilute aluminum copper and aluminum copper magnesium alloys. J. Inst. Met. 86: 77 (1957-58).

Beuker A. A.**:** An Introductory Guide to Finite Element Analysis, Professional Engineering Publishing Limited London, U.k, (2004).

Bigot A.**:** PhD thesis, The University of Rouen, France (1998).

Bradley A. J. and Jones P.**:** An X-ray investigation of the Cu-Al alloys. J. Inst. Met. 51: 131-162 (1933).

Brook G. B.**:** Precipitation in Metals, Spec. Rep. No.3, Fulmer Res. Inst, UK (1963).

Brown ,A.M and M.F.Ashby ,scripta ,Metall,14,1297,(1980).

Cahn J. W. and Kalonji G.**:** Symmetry in solid state transformations morphologies. In Proc. Intl. Conf. on Solid-Solid Phase Transformations, Camegie-Mellon University, Pittsburgh, PA, Aug. 10-14, 1981, H. I. Aaronsson, A. E. Laughlin, R. F. Sekerka, and C. M. Wayman, eds., The Metall. Soc. of the AIME, Pittsburgh, PA, PP.3-14 (1981).

Cahn Robert W. & Haasen Peter **:** Physica Metallurgy. 4th. Edn. (1999)-Elsevier Science B. V. ISBN: 0 444 89875 1.
Cambridge, UK, Trans Tech Puplications, 2002, Mater. Sci. Forum Vols. 396-402, 2002.

Cassada W. A, Sheflet G. J. and Starker Jr. E. A.**:** Aluminum Alloys-their Physical and Mechanical Properties, edited Starke, E. A. Jr. Sanders, T. H. Jr. (EAMS, Warly West Midlands, UK), (1986) ,695.

Chang Y. C. **:**Ph.D.thesis,Crystal and nucleation behaviour of {111} pre-Capitates in an Al-3.9Cu-o.5Mg-0.5Ag (wt.%) alloy. Carnegie Mellon University (1992).

Chen R. T. and Strake E.A. Jr.**:** Microstructure and mechanical properties of mechanically alloyed, Ingot Metallurgy and Powder

Metallurgy Al-Li-Cu-Mg alloys, Mat. Sci. & Rng., Vol.67, (1984), P.229.

Collins J. A**:** Failure of Material in Mechanical Design (pp.31-32,435 - 478).New York: John Wiley and sons, Inc. .(1981)..

Cynthia L. Lach & Marcia S. Domack**:** Characterization of Al-Cu-Mg-Ag alloy RX226- T8 Plate, NASA/TM, (2003), 212639.

DeSorbo W., Treaftis H. N., and Rumbull D.**:** Rate of Clustering in Al-Cu alloys at low temperatures, Acta Metall 6: 401-413 (1958).

Dieter G. E. **:** Mechanical Metallurgy (3rded. pp. 275-334, 432-470). New York: McGraw-Hill Book Co. (1986).

Dmstry G. Eskin Marina L. Kllara Kteroja.**:** The effect of silicon and copper an precipitation hardening of sheet of 6xxx series alloy, material in technology ije, 35 (2001), PP.5-8.

Ekvall JC, Rhodes JE & Wald GG**:** Methodology for evaluating weight saving form basic material properties ASTMSTP761 (Philadelphia, PA: Am. Soc. Testing Mater), pp. 328-441, (1982).

Enare Romhanji, Drugomir Glisic & Vojin Milenkovin**:** Foming Aspects of high strength Al-Mg alloy sheet, material in technology, ije (2001), PP.21-26.

Enrique, J. Lavernia & Nicholas J. Grant**:** Review Aluminum-Lithium alloys. J. Mat. Sci. Vol 22, P.1521. (1987).

Evans H. **:** Mechanisms of creep rupture, Elsevier, London.

Evans R. W. & Wilishire B.**:** Introduction to Creep. The Institute of Materials. London. (1993). 1-75.

Federighi T.**:** Quenched-in vacancies and rate of formation in aluminum alloys, Acta Metall. 6: 379-389 (1958).

Gargali M. B. Aksakal**:** Effect of various homogenization treatment on the hot workability of ingot Aluminum alloy A2014, Materials Science and Engineering, A254 (1998), pp.189-199.

Gorafalo F.**:** Fundamentals of creep and creep-Rupture in metal, New York: the Macmillan Company. (1965).

Graiss G. & Mahmoud M. A.**:** Effect of cyclic stress reduction on the creep behavior of Al-Ag and Al-Ag-Zr alloys containing and γ' and γ precipitates, Cryst. Res. Technol. 35, (2000).

Gregson P. J. & Flower H. M.**:** Micro structural control of toughness in Al-Li alloys, Acta Metall., Vol.33, no.3, (1985), P.527.

Gregson P. J. & Harris S. J., Proc. 8th Inter. Conf. on Aluminum Alloy,

Gregson P. J. and Flower H. M., Acta Metall., 33, 527. (1983).

Grimes R., Cornish A. J., Miller W. S. & Reynolds M. A .**:** Al-Li based alloys for aerospace applications, Metals Materials, Vol. , No.1, (1985), P.357.

Grims R., Miller W. S., Reynolds M. A. & Gry A. **:** Aluminum-Lithium Development , Applications and Super plastic forming, edited by Agrawal, S. P. and Kar, J. R. (ASM, Metals Park, Ohio), 38. (1986).

Guinier**:** Structure of age hardenable Al-Cu alloys, Nature 142: 569 (1938).

Gupta A. K. , Gaunt P. and Chaturvedi M. C. **:** The crystallography and Morphology of the S' –phase in an Al(CuMg) alloy. Philos. Mag. A55: 375-387, (1987).

Hardy H. K.**:** Ageing curves at 110°C on binary and ternary Al-Cu alloys. J. lint. Met. 8: 236-238, (1953-54).

Haupt.P**:** Continum Mechanics and theory of material ,springer-Verlag ,Berlin/Heidelberg /Newyork.

Hertzberg R. W.**:** Deformation and Fracture Mechanics of Engineering Materials John Wile ,Sons, Inc. (1989).third edition. pp. 145-192.

Huang J. C. & Ardell A. J.**:** Addition rules and the contribution of δ' precipitates to strengthening of Aged Al-Li-Cu alloys, Acta metal , (1988), Vol. 36, No.11, 2995-3006,

John V. B.**:** Introduction to Engineering materials. Second edition, (1983), pp.178-183.

John W. Martin**:** Aluminum–Lithium alloys, Ann, Rev. Nat. Sci., Vol. 18, (1988), P.101.

Josef Betten **:** Creep Mechanics , 2nd Edition ,Library of congress.C.N.2004116203.Springer Berlin Heidelberg New York, ,(2005) .pp.49-75.

K. Hono, M. Murayama & L.Reich**:** Clustering and Segregation of Mg and Ag atoms during the precipitation processes in Al(-Li)-Cu-Mg-Ag alloys, National research Institute for Matels, 1-2-1 Sengen, Tsukuba 305, Jopan.

K. Hono, T. Satoh & Hirano**:** Evidence of multi-layer GP zones in Al-1.7 at % Cu alloy. Philos. Mag. 53A: 495-504 (1986).

Karl B. Rundman**:** Metal Casting.(Ref.Book for MY4130). Dep.of Materials Science and Engineering.Michigan Tech.University.

Karlik M. & Jouffrey B.**:** High resolution electron microscopy of Guinier-Preston (GPI) zones in Al-Cu based alloys. Acta Mater. 45: 2351-3263 (1997).

L. P Troeger., M. S. Domack & J. A Wagner.**:** Microstructural and mechanical characterization of shear formed Aluminum alloys for Airframe and space applications, NRC/ NASA, L.R.Center, (2000), 7icaa, ltp..l.p.troeger@larc.nasa.gov.

Larson F. R. & Miller J. **:** A time temperature relationship for rupture and creep stresses. ASME74, 765-775. (1952).

Lattice resolution measurement of strain fields at Guinier-Preston zones in Al-3% Cu. Acta Metall . 21: 219-228 (1973).

Lavernia E. J. & Grant N. J.**:** J. Mater. Sci, 22, 1521. (1987).

Lavernia E. J., Strivatstan T. S., & Mohamed F. A.:J. Mater, Sci. 25, 1137.(1990).

: Light Alloys From Traditional Alloys to Nanocrystals forth edition, (2005).

Lloyd D. J. **:**Precipitation Hardening. Proc. 7th Inter Conf. on Strength of Metals . McQueen,H. J. et al. Eds,. Pergamon Press. Toronto, 3. 1745. 1985.

M. J. Starink & J. L. Yan**:** Precipitation hardening in Al-Cu-Mg alloys: analysis of precipitates, modeling of kinetics, strength predictions, Materials Science Forum. Vol.519-521, (2006), 251-258.

M. J. Starink, A. J.Hobson, I.Sinclair & P. J. Gregson**:** Embrittlment of Al-Li-Cu-Mg alloys at slightly elevated temperatures: micro structural mechanisms of hardening, Mater. Sci. Eng. A, (2000), vol. 289, pp. 130-142.

M. J. Starink, P. Wang, I. Sinclair & P. J. Gregson**:** Microstructure and strengthening of Al-Li-Cu-Mg alloys and MMCs: II. Modeling of yield strength , Acta mater, vol. 47, (1999), pp. 3855-3868.

M. S. Yaghmace & G. Kaptay**:** On the stability range of SiC in ternary liquid Al-Si-Mg alloy.Faculity of Materials & Metallurgi Engineering,Un.of,Miskolc,(2002), www.unimiskolc.hu/~fkmsahba. (Temporary Address).

Matsubara E. and Cohen J. B.**:**Local atomic arrangements in the solid solution of Al-1.7 at % Cu at 793K, Acta Metal 31: 2129-2135 (1983).

Meyers Marc Andre' & Chawla Krishan Kuumar. **:**Mechanical behavior of materials. Prentice-Hall, New Jersey. ISBN 0-13-262817-1. (1999). 540-580.

Mishra R.S. & Pandey. A.B **:** High temperature creep behavior of 6061, Metallurgical Transaction A,21A.(1990) ,PP.2089-2090.

Mondolfo L.F..**:** Aluminum Alloys-Structures and Properties. (Butterworth, London). 554. (1976).

Monkman F.C. and Grant N.J.**:** An empirical relationship between rupture life and minimum creep rate in creep-rupture tests, Proc, ASTM 56: (1956) , 593-620.

Mukherjee A.K, Bird J.E, and Dorn J.E, Trans. ASM,62 (1964),155.

Murayame M.& Hono K.**:** Pre-precipitation clusters and precipitation processes in Al-Mg-Si alloys, acte mater 47 (1999), PP. 1537-1548.

Murray J. L.**:** The Al-Cu system. Int. Met. .Rev . 30: 211-233. (1985).

N. GaO, L. Davin, S. Wang, A. Cerezo & M. J. Starink**:** Precipitation in stretched Al-Cu-Mg alloys with reduced alloying content studied by DSC, TEM and atom probe, Materials Science Forum, (2002), vol. 396-402, pp 923-28.

Nicholson R. B., Thomas G., & Nutting J.**:** Electron microscopic studies of precipitation in aluminum alloys. J. Inst. Met. 87: 429-438 (1958-59).

Nicholson R. B.**:**- The interaction between point defects and solute atoms In aluminum alloys. In Intl.Conf. on Electron Difraction and the nature of Defects in Crystals,August 16-21, 1965, Australian Academy of Science, Intl . Union of Crystallog. and Intl. Union of Pure and Appel. Phys., Australian Aca-d. Sci., Melbourne, II N-2 (1965).

Noble B.& Thompson G. E.**:** J. Met. Sci. 5, 114. (1971).

Nong Gao, Marco J. Starink, Minoru Furukawa, Zenji Horita, Cheng Xu & Terence G. Langdon: Evolution of microstructure and precipitation in heat-treatable aluminum alloys during ECA pressing and subsequent heat treatment, Materials Science Forum, 503-504 (2006) , 275-280.

Orowan E**:** the Creep of Metals ,west of Scotland Iron and steel Institute ,P.45 (1947).

Orr R.L., Sherby O.D. and Dorn,Trans.ASM,46 (1954) 113.

Osamura K., Murakami Y., Sato T., Takagashi T., Abe T.& Hirano K.**::** Structure of GP zones in an Al-1.7 at % Cu alloy aged for 14 years at room temperature, Acta Metall , 31: 1669-1673 (1983).

Palmer I.G., Miller W. S., Lioyd D. J., & Bull M. J**.:** Aluminum-Lithium Alloys II, edited by sanders Jr. T. H. and Starke Jr. E. A. Warren dale , Metallurgy Society of AIME), 137. (1984).

Park J. K. and Ardell A. J. **:** Microstructures of the commercial 7075 Al alloy in the T651 and T& tempers. Metall Trans. 14A: 1957-1965, (1983).

peng X. Q. and Cao J.**:** " Numerical Determination of Mechanical Elastic Constant of Textile Composite ". Northwestern Univ-ersity USA.

Perlitz H.and Westgren A.**:** The crystal structure of Al_2CuMg. Arkiv. Kemi. Mineral. Geol. 16B, (1943).

Peters M.& Winkler P. J.editer**:** Aluminum Lithium Alloy VI(DJGM, Oberusel, Germany). (1992).

Phillips F. C.**:** An Introduction to Crystallography, Longmans, New York (1960).

Phillips V. A.**:** High resolution electron microscope observations on precipitation in Al-3%Cu alloy. Acta Metall. 23: 751-767 (1973).

Pickens J. R., Heubaum F. H., Langan T. J. & Kramer L. S.**:** Al-Cu-Li-Mg-Ag-Zr alloy Weldalite^{TM} 049. In Proc. 5th Conf. Al-Li alloys.Williams burg, A, March 1989, Materials and Component Engineering. Publications Ltd., Birmingham, UK. PP:1397.(1989).

Polmear Ian. J. & Chester R. J.**:** Abnormal age hardening in an Al-Cu-Mg alloy containing silver and lithium. Script Metall. 23: 1213-1217 (1989).

Polmear Ian. J. and Couper M.**:** Design and development of an experimental wrought aluminum alloy for use at elevated temperatures. Metal Trans. 19A: 1027-1035 (1988).

Polmear Ian. J.**:** Light Alloys From Traditional Alloys to Nanocrystals. Fourth Edition, ISBN-13: 978-0-7506-6371-7. (2006).

: Control of Precipitation Processes and Properties in Aged Aluminum Alloy by Trace Element Additions. Proc.6th Intl Conf on Al-alloys, The Japan Inst.of Light Metals, (1998), Tokyo, Japan, pp.75-86.

Preston G. D.: Nature 142: 570 (1938).

Quist W. E. & Narayahan G. H.**:** Aluminum alloys Contemporary Research and Applications. Treatise on Mate. Sci. Technol., 31, 219. , (1989).

R. K. Bird, D. L. Dicus, J. N. Fridlyander & V. S. Sandler **:**Al-Li alloy 1441 for fuselage applications, r.k.bird@Iarc.nasa.gov.

Ratchev P. ,Verlinden B.,De Smet P. & Van P.Houtte **:**Precipitation hard-ening of an Al-4.2 wt.% Mg 0.6 wt.% Cu alloy. Acta Ma-ter. 46: 3523-3533 (1998).

Read-Hill R. E.**:** Physical Metallurgy Principles. Boston. PWS. Eng engineering. Second edition. (1973) PP 827-887.

Reich L., Murayama M. & Hono K.**:** Evolution of Ω phase in an Al-Cu-Mg-Ag alloy –A three dimensional atom probe study. Acta Mater. 46: 6033-6062 (1998).

Ringer S. P., Hono K., Polmear I. J., and Sakurai T.**:** Nucleation of precipitates in aged Al-Cu-Mg- (Ag) alloys with high Cu-Mg ratios. Acta. Mater. 44: 1883-1898 (1996).

-: Cluster hardening in Al-Cu-Mg alloys. Scripta Mater. 36: 517-521 (1997).

-: Precipitation processes during the early stages of aging in Al-Cu-Mg alloys. Appl.Surface Sci.94/95:253-260(1996).

Ringer S. P., Caraher S. K. & Polmear I. J. **:**Response to comments on Cluster hardening by Zahra et al. Scirpta Mater. 39: 1559-1567. (1998).

Ringer S. P., Hono K.and Polmear I. J. **:** On the origins of hardening in Al-Cu-Mg-(Ag) alloys. Actta Mater. 45: 3731-3744 (1997)

Rioja R. J. & Laughlin D. E.**:** The early stages of GP zone formation in naturally aged Al-4wt. % Cu alloys. Metall . Trans. 8A: 1257-1261 (1977).

Robert A. Edahl & Marcia S. Domack**:** Effect of Thermal Exposure on The Tensile Properties of Aluminum Alloys for Elevated Temperature Service, NASA/ TP, (2004), 212988.

Roberto Cocomozzi**:** High temperature mechanical characterization of Aluminum,based,particulate,reinforced,composites.Depar tment of Aerospace Engineering,University of Bologna-(1999). robertococomazzi@libero.it

Rometsch P. A., *et al.***:** The effect of homogenizing on the quench sensitivity,(2002), materials science forum, PP. 396-402.

Ross C. T**.:** Finite Element in Engineering Science" FLLis Horwood. USA, (1985).

Rudman P. S. & Averbach B. L.: X-ray measurements of local atomic arrangements in aluminum –zinc and in aluminum-silver solid solutions. Acta Metall. 2: 576-582 (1954).

S. C. Wang & M. J. Starink**:** Two Types of S Phase Precipitates in Al-Cu-Mg alloys, Axta Material, 55 (2007), 933-941.

S.C.Wang, Z. Zhu & M. J. Starink**:** Estimation of dislocation densities in cold rolled Al-Mg-Cu-Mn alloys by combination of yield strength data, EBSD and strength models. Journal of Microscopy, 217 (2005) 174-178.

Sainfort P., and Dubost B.**:** Aluminum-Lithium IV, edited by G. champier, Dubost, D. Miannay, and L. Sabetay. (Fran.ce: Les Editions De Physique), 407(1987).

Sanders T. H. and Starke E.A.**:** editer, the 4th international Conference on Aluminum Alloys. Their physical and Mechanical Properties (The Georgia Institute of Technology, Atlanta, GA USA). : (1994).

Sanders T. H.,, Jr. and, Storke Jr E. A.**:** Aluminum –Lithium Alloys, V. edited by Sanders T. H. Jr. and E. A Starke E. A. Jr. (MCE, Birmingham, UK.), I(1989).

Sanders T.H., , Jr. and Starke E. A., , Jr., Acta Metall, 30, 927.

Sherby O.D. & Burke P. M**.:** Mechanical behavioral crystalline solids at elevated temperature .Washington, (1969), (NASA) Technical Reporter SC-NGR-05-020 -084,(1982).

Sherby O.D. and Miller ,A.K,J.Eng.Mater.Technol., 101 (1979) 387.

Silcock J. M.**:** Inst. Met., 88, 357(1959-1960).

Silcock J. M., Heal T. J. & Hardy H. K.**:** Structural ageing characteristics of binary aluminum copper alloys. J. Inst. Met. 82: 239-248 (1953-54).

Silcock J. M.**:** The structural ageing characteristics of Al-Cu-Mg alloys with copper: magnesium weight ratios of 7:1 and 2.2:1. J.Inst. Met. 89: 203-210 (1960-61).

Smallman R. E. & Bishop R. J.**:** Modern physical Metallurgy and Materials Engineering. Butterworth. (1999).

Smith A. F. , Vasudevan A. K. & Howell P. R.**:** Structure and properties of Al-Li-Cu-Mg-Zr alloy AA2091 in sheet form, Mat. Sci, & Tech., Vol.5, (1989), P.533.

Srivatsan T. S., Coyne E. J. & Starke E. A**.:** Micro structural characterizeation of two Li-containing Al-alloys, J. Mat. Sci., Vol.21, (1985), P.1553.

Starka E. A. & Lin F. S.**:** The influence of grain structure on the ductility of the Al-Cu-Li-Mn-Cd alloy 2020, Metall. Trans. A, Vol.13A, (1982), P.2259.

Starke E. A., Jr., Sanders, T. H. Jr. and Plamer, I. G:, J. Met., 24(1981).

Stephen J. Hales & Robert A. Hafley**:** Structure-Property correlations in Al-Li alloys integrally stiffened extrusions. NASA/ L. R. Center, Hampton,Virginia/ TP- (2001)- 210839.

T. Balakrishna Bhat & V. S. Arunachalan**:** Dislocation creep in particle-strengthened systems. Journal of materials science 12 (1977). 2241-2245.

Terence G. Langdon & Parviz Yavari**:** An investigation of harper-dorn creep – II the flow process, Acta metal, vol. 30, 881-887, (1982).

-: The ageing characteristics of ternary aluminum copper alloys with cadmium, Indium or tin, J. Inst. Met. 80: 483-492 (1951-52).

V. Yamakoy, E. Saether, D. Phillips & E. H. Glaessgen**:** Stress distribution during deformation of polycrystalline Aluminum by molecular-dynamics and finite-element modeling, NASA L. R. Center, Hampton,VA23681, USA/AIAA/ASME/ASCE/AHS/ASC-(2004)-1700.

Van Vlack L. H.**:** Materials Science for Engineering Library of congress card number.74.91151, 15BN, .Addision-wesiley, comp-any, Inc, (1970), pp. 453-456.

Vasudevan A. K. and Doherty R. D.**:** Aluminum Alloy-Contemporary Research and Applications, Treatise on Mater. Sci. Technol., 31 (Academic Press Inc.) (1989).

Vaughan D.and Silcock J. M.**:** The orientation and shape of θ precipitates formed in an Al-Cu alloy. Phys. Stat. Sol. 20: 725-736 (1967).

VietzJ. T. and Polmear I. J.**:** The Influence of Small addition of silver on The Ageing of Al-alloys:Observations on Al-Cu-Mg alloys. J. Inst. Met. 94:410-419 (1966).

W. F. Miao & D. E. Laughlin**:** Effect of Cu content and preaging on precipitation characteristics in Aluminum alloy 6022,

Metallurgical and materials transactions, vol.31A,, (2000) , 361.

W.M. Johnston, W. D. Pollock & D. S. Dawicke**:** Biaxial testing of 2195 Aluminum Lithium alloy using cruciform specimens, NASA/ CR-(2002)-211942.

Willams D. B. and Howell P. R.**:** Aluminum Alloy Contemporary Research and Applications, Treatise on Mater. Sci. Technol., 31, 365(1989).

William D. B.**:** Aluminum-Lithium alloys, edited by Sanders T. H. Jr. and E. A. Stark E. A. Jr (TMS-AIME), 324. (1980).

Wilson R. N. and Partridge P. g.**:** The nucleation and growth of S' precip-itates in an Al-2.5 Cu-1.2Mg alloy. Acta Metal. 13:1321-1327, (1965).

William F. Smith**:** Structure and properties at Engineering Alloys. Mc Graw-Hill Publishing Co. Courtesy of Aluminum Company of America.(1981).
www.uni-miskolc.hu/~fkmsahba.

Yao D. P, Znang Li Y. Z, Y. Y. & Shi, C. X.**:** The formation and growth of PFZ et grain boundary in Al-11. 9at % Li alloy, Soripta Metall., Vol.23, 1989, P.537.

Yic C. Y., Challer R,& Jaquerrod C.**:** High lamping capacity after precipita-teon on some commercial Al alloy, Material science and Engineering, 252 (1998), PP.78-84.

Yoshide H., Hashimoto H., Yokota Y.& Ajika N.**:** High resolution lattice images of GP zones in an Al-3.97 wt, % Cu alloy. Trans . Jpn. Inst. Met. 24: 378-385 (1983).

Zahra A. M., Zahra C. Y. Alfonso C. & charai A.**:** comments on cluster hardening in an aged Al-Cu-Mg alloy. Scripta Mater. 39: 1553-1558, (1998)